COLLOIDAL FORCE INTERACTIONS IN FILTRATION PROCESSES

By

RONALD CHARLES SABO, JR.

A DISSERTATION PRESENTED TO THE GRADUATE SCHOOL OF THE
UNIVERSITY OF FLORIDA IN PARTIAL FULFILLMENT OF THE
REQUIREMENTS FOR THE DEGREE OF
DOCTOR OF PHILOSOPHY

UNIVERSITY OF FLORIDA

2001

To my kid brother and sister and to all the children of the world not as blessed with opportunity as I…May God be with them all.

ACKNOWLEDGEMENTS

First I would like to thank my academic adviser, Dr. Chang-Won Park, for his immeasurable support and advice and for patiently guiding me to be a confident, independent researcher. The work ethics and philosophies Dr. Park shared with me will remain important to me throughout my career and personal life. I would also like to express my gratitude to my dissertation advisory committee members, Drs. Spyros Svoronos, Richard Dickinson and Ben Koopman, for providing valuable insight, advice and assistance in completing this work and for patiently accommodating me throughout the graduation process. I am also grateful for support from chemical engineering chairperson Dr. Tim Anderson and from the National Science Foundation-Engineering Research Center grant and for the guidance of ERC faculty members, Drs. Brij Moudgil, Hassan El-Shall, Sam Farrah, Ron Baney, Kevin Powers and Anne Donnelly. In addition, I appreciate the assistance of many chemical engineering and ERC staff members, including Shirley Kelley, Nancy Krell, Sophie Leone and Nancy Sorkin.

The help of fellow graduate students Josh Adler, Steve Truesdail, Kathy Shaw, Aaron Clapp, Jonah Klein, Troy Scott, Alina Ruta and Peter Kang proved invaluable in conducting this work. In addition, undergraduate students Melissa Sullivan, Lucas Barosso-Giachetti, Daniel Neumann and Steven Walker, as well as ERC technicians Gill Brubaker, Gary Scheiffele and John Henderson provided much assistance in preparing and performing many of the experiments in this dissertation. I would also be remiss to

not acknowledge Kenneth Kerr, Keisha Wilson, Kuide Qin, James Kanicky, Kerry Allahar, Jonghoon Lee and Yongcheng Li for the many enlightening discussions we had.

Finally, and probably most importantly, I thank God for affording me all the privileges that I too often take for granted and my mom for her unwavering confidence, support and love that have been a source of inspiration throughout my life.

TABLE OF CONTENTS

page

ACKNOWLEDGEMENTS iii

LIST OF SYMBOLS viii

ABSTRACT xii

CHAPTERS

1 INTRODUCTION 1

1-1 General Purpose 1
1-2 Accomplishments 2
1-3 Dissertation Organization 3

2 BACKGROUND AND LITERATURE REVIEW 5

2-1 Colloidal Interactions 5
2-1-1 DLVO-Type Interactions 5
2-1-2 Hydrophobic Interactions 8
2-1-3 Hydration Forces 9
2-1-4 Polymeric Forces 9
2-1-5 Specific Interactions 10
2-2 Hydrodynamics 10
2-2-1 Flow between Parallel Plates 10
2-2-2 Filtration Models 11
2-2-2-1 Capillary, Happel and Kuwabara models 12
2-2-2-2 Effective medium approximation 13
2-2-3 Sedimentation 16
2-3 Colloidal Transport 18
2-3-1 General Approaches 18
2-3-2 Convective-Diffusion 18
2-3-2-1 Brownian diffusion 19
2-3-2-2 Smoluchowski-Levich solution 21
2-3-2-3 Interaction force boundary layer approximation ... 22
2-3-3 Particle Collection by Filtration 24
2-3-3-1 Coefficient definitions 24

2-3-3-2 Theoretical collection rates 25
2-4 Literature Review of Deposition Experiments and Models... 27

3 COLLOIDAL DEPOSITION IN A PARALLEL PLATE FLOW CELL 32

3-1 Interaction Boundary Layer Approximation Requirements 32
3-2 Model for Deposition in a Parallel Plate Flow Cell 38
3-2-1 Model Development 39
3-2-1-1 Bulk region 40
3-2-1-2 Diffusion boundary layer 41
3-2-1-3 Surface force region 41
3-2-1-4 Matched, leading-order problem 43
3-2-2 Model Predictions 43
3-2-2-1 Convective-diffusion limit 43
3-2-2-2 Surface interaction controlled deposition 49
3-2-2-3 Effect of hydrodynamic retardation 52
3-3 Experimental Results 55
3-3-1 Concentration Effect..... 55
3-3-2 Flow Rate Effect..... 57
3-3-3 Position-Dependent Flux 58
3-3-4 Dependence on pH..... 60

4 VERIFICATION OF FILTRATION MODEL 62

4-1 Predictions from Effective Medium Approximation 62
4-2 Experimental Results 65
4-3 Verification of Effective Medium Approximation 69

5 MATERIALS, METHODS, AND CHARACTERIZATION 71

5-1 Filtration Experiments 71
5-1-1 Filter Configuration 71
5-1-2 Filtration Procedure 72
5-1-3 Granular Media 74
5-2 Parallel Plate Flow Cell Experiments 75
5-2-1 Equipment 76
5-2-2 Experimental Procedure 77
5-3 Preparation and Counting of Particle Dispersions 79
5-3-1 Dispersion Preparation 79
5-3-2 Counting Techniques 80
5-3-2-1 Direct particle counts 80
5-3-2-2 Indirect particle counts 80
5-4 Surface Modification 82
5-4-1 Metal Hydroxide Coating 82
5-4-2 Quaternary Ammonium Siloxane Coatings 82
5-4-2-1 Suhara coating 83

5-4-2-2 AEM 5700 85
5-5 Characterization Techniques 86
5-5-1 Electrokinetic Measurements 87
5-5-1-1 Unmodified media 89
5-5-1-2 Modified media 91
5-5-2 Hydrophobicity 92
5-5-3 Coating Stability 93
5-6 Numerical Methods 96

6 FILTRATION AND INACTIVATION OF MICROORGANISMS 98

6-1 Materials Used for Microbe Adsorption Studies 99
6-2 Batch Inactivation of Bacteria and Viruses 100
6-3 Column Filtration of Viruses 104
6-4 Economic Feasibility of Metal Hydroxide Coated Filter Media 106

REFERENCE LIST 110

BIOGRAPHICAL SKETCH 118

LIST OF SYMBOLS

A,B,C,D	Constants in EMA model
A_{sp}	Specific surface area of filter
A_v	Hamaker constant
a_c	Collector radius
a_p	Particle radius
b	Gap height in PPFC
c	Particle concentration
c_0	Bulk particle concentration
D	Diffusion coefficient
D_∞	Bulk diffusion coefficient
Da	$Da = k' a_c / D_\infty$
e	Elementary charge of an electron, 1.602×10^{-19} C
$f_1(r)$	Radial dependence of stream function in effective medium
$f_2(r)$	Radial dependence of stream function in fluid envelope
F(h)	Position-dependent drag force
F_{st}	Drag force using Stokes Law
g	Acceleration of gravity, 9.8 m/s^2
h	Minimum separation between particle and surface

J	Particle surface flux
k_B	Boltzmann constant, 1.381×10^{-23} J/K
k'	Dimensional deposition rate constant
k	$k = k'\kappa^{-1}/D_\infty$
k_m	Mass transfer coefficient
k_p	Permeability
l	Depth of packed-bed filter
L	Length of PPFC
n_i	Number concentration of ion i
p_1 & p_2	Dimensionless pressure in effective medium & fluid envelope, respectively
Pe	Peclet number Ub/D_∞ or Ua_c/D_∞
ΔP	Pressure drop across porous media
Q	Volumetric flow rate
Q_1	Dimensionless EMA parameter defined by (2.21)
r	Dimensionless radial coordinate
R	Dimensionless fluid envelope radius
T	Temperature
U	Average fluid velocity
u	Fluid velocity
U_s	Particle settling velocity
U_g	Dimensionless gravity term, $U_g = \frac{U_s}{U} Pe^{2/3}$
u_r, u_θ	Radial and circumferential velocities

U_{max}	Maximum velocity at channel centerline
V	Particle volume
w	Width of PPFC
x	Coordinate parallel to flat plate
y	Coordinate normal to flat plate
z	Depth coordinate in a packed-bed filter
z_i	Valency of ion i

Greek characters

α	Correction factor to Stokes drag, $F(h)/F_{St}$
β_s & β_c	Dimensionless filtration parameter for spherical & cylindrical collectors
δ_D	Diffusion boundary layer scale
ε	Packed bed porosity
ε_0	Permittivity of vacuum, 8.854×10^{-12} Nm^2/C^2
ε_r	Dielectric constant of the medium
ε	Permittivity of medium, $\varepsilon_0\varepsilon_r$
γ	$\cosh^{-1}(1+h/a_p)$
γ_s & γ_c	Integral function for spherical & cylindrical collectors, respectively
η	Filtration efficiency
κ	Reciprocal of the Debye length
λ	Filter coefficient

λ_p	$a_c/\sqrt{k_p}$
μ	Fluid viscosity
ϑ	Circumferential coordinate
ρ_f	Fluid density
ρ_p	Particle density
τ_s	Surface shear rate
ψ_{01},ψ_{02}	Potential at surfaces one and two, respectively
Ψ	Stream function
ζ	Zeta potential

Subscripts and over bars

~	Indicates dimensionless bulk region variable
*	Indicates dimensionless diffusion boundary layer variable
_	Indicates dimensionless surface force region variable

Abstract of Dissertation Presented to the Graduate School
of the University of Florida in Partial Fulfillment of the
Requirements for the Degree of Doctor of Philosophy

COLLOIDAL INTERACTIONS IN FILTRATION PROCESSES

By

Ronald Charles Sabo, Jr.

December 2001

Chair: Chang-Won Park
Major Department: Chemical Engineering

A recently developed filtration model based on an effective medium approximation has been verified for Brownian particles in the presence and absence of an energy barrier. Previously, good agreement between filtration models and experiments was seen only in the absence of significant electrostatic repulsion, i.e., when the deposition was transport-controlled. The inability to predict filtration rates when electrostatic repulsion is significant is due to the lack of an adequate understanding or description of colloidal interactions. Therefore, an independent method of accounting for colloidal interactions has been employed in this research by directly measuring deposition kinetics in a well-defined geometry. Computerized video microscopy, coupled with an appropriate transport model, was used to extract deposition rate constants between colloidal silica and glass substrates in a parallel plate flow cell. In addition, good agreement was seen between the measured and predicted deposition behavior in the parallel plate flow cell for a variety of physicochemical conditions. So

the predictions of the filtration model based on an effective medium approximation for the capture of 0.5 μm-diameter silica spheres in a packed-bed were verified by incorporating independently measured deposition rate constants. In addition, the filtration of bacteria and viruses was enhanced via surface modification of granular filter media. However, the removal rates of microorganisms in a packed-bed could not be reliably predicted, thus illustrating the need for better understanding of colloidal interactions in filtration processes.

CHAPTER 1
INTRODUCTION

1-1 General Purpose

The deposition and dispersion of colloidal particles are of fundamental interest for a wide variety of applications including drug delivery, printing inks and municipal water treatment as well as the processing and manufacturing of microelectronic devices, minerals, cosmetics and biomaterials. In particular, granular and fibrous filtration is of practical interest for removing microorganisms and other contaminants from municipal and industrial water supplies and from conditioned air as well as for improving the transport of minerals in soils for agricultural purposes. Therefore, an adequate understanding of filtration processes has significant social, public health and economic implications.

Ultimately a methodology for predicting filtration behavior based on measurable system properties is desired. Unfortunately, however, filtration rates for most natural systems of practical interest cannot be reliably predicted based on current theories. Filtration efficiencies can be predicted for some simple systems but not for more practically relevant problems such as the removal of poliovirus in a packed-bed filter. Therefore, this work was aimed at verifying a recently developed filtration model under conditions, which have previously shown poor agreement between experiments and models.

In addition, novel surface coatings for granular filter media were investigated to enhance the removal of bacteria and viruses in a packed-bed filter. These coatings were often shown to improve removal rates of microorganisms by orders of magnitude. Therefore, advancement in the technology and understanding of such processes can have significant societal impacts including the preservation of human life.

1-2 Accomplishments

A filtration based on an effective medium approximation was verified in a packed-bed filter for a range of physicochemical conditions using a novel method, which eliminated the need of an explicit expression for colloidal interactions. By employing the interaction force boundary layer approximation, colloidal interaction terms in the transport equations were reduced to a single parameter in the boundary condition at the surface. This parameter, which is termed the deposition rate constant, was then independently measured under well-defined flow conditions in a system with properties nearly identical to those used in packed-bed filtration experiments. The measured deposition rate constant was subsequently used in conjunction with the effective medium approximation to adequately predict filtration rates for a variety of physicochemical conditions.

The transport equations, with the gravity terms retained, were appropriately scaled and solved using a finite difference method to model colloidal deposition in a parallel plate flow cell. The predictions of this model were then compared to measured deposition behavior of colloidal silica in a flow cell observed using computerized video microscopy. Good agreement was seen between predicted and measured collection rates of 0.5 and 1.0 μm-diameter silica particles on glass plates when deposition was transport-

controlled. For the cases in which deposition was controlled by repulsive electrostatic interactions, collection rates were much greater than predicted using the interaction force boundary layer approximation in conjunction with DLVO-theory. Deposition rate constants were then extracted for the systems of interest and used as a parameter to predict filtration rates using the effective medium approximation. The system was also characterized for other necessary parameters to predict filtration rates entirely based on existing theories.

In addition, coatings were applied to granular filter media and colloidal silica to enhance the inactivation or removal of microorganisms. Metal hydroxides and quaternary ammonium siloxane coatings were used to impart a positive charge on filter media to aid in the capture of negatively charged bacteria and viruses. Both of these coatings were promising in their ability to enhance microbe capture, but the filtration rates could not be reliably predicted.

1-3 Dissertation Organization

This communication presents research done to verify a filtration model and to enhance filtration rates of microorganisms. Chapter 2 gives a short review of models and experiments found in the literature which are pertinent to this research, including colloidal interactions and transport in a packed-bed. Chapter 3 is devoted to the modeling and experimental efforts for colloidal transport in a parallel plate flow cell. Here good agreement is demonstrated between experimentally measured and theoretically predicted deposition rates. Chapter 4 is dedicated to the work done for verifying the filtration model based on the effective medium approximation. Chapter 5 describes all the critical materials, procedures and characterization results pertinent to

deposition experiments in a flow cell and a packed-bed. Finally, Chapter 6 discusses the efficacy of coatings to filter or inactivate bacteria and viruses. An economic feasibility study of aluminum and ferric hydroxide coatings is also presented here.

CHAPTER 2
BACKGROUND AND LITERATURE REVIEW

Predicting colloidal deposition or aggregation requires a description of the interaction and external forces, hydrodynamics and the physical and chemical characteristics of the suspension. Much work has been done to understand and mathematically describe colloidal interactions and hydrodynamics, so a review of relevant literature is given below.

2-1 Colloidal Interactions

Colloidal particles, which roughly range from as small as ten angstrom (10^{-9}m) to about one micrometer (10^{-6}m) in diameter (Hiemenez and Rajagopalan, 1997), in suspensions have astounding properties due to the dominance of interparticle forces (Russel et al., 1989). Colloidal forces control many aspects of colloidal suspensions including their rheological and optical properties (Russel et al., 1989). Subtle changes in physical properties can lead to large changes in colloidal interactions and thus physical properties. Colloidal interactions have been divided into several types including electrostatic, van der Waals, hydrophobic, hydration and steric contributions.

2-1-1 DLVO-Type Interactions

The only widely accepted explicit formulation of these interactions comes from the widely accepted theory of Derjaguin-Landau-Verwey-Overbeek (DLVO), which considers the total interaction to be a superposition of electrostatic and van der Waals

interactions (Hiemenez and Rajagopalan, 1997; Adamson, 1990). Independent developments made by Derjaguin and Landau (1941) and by Verwey and Overbeek (1948) form the basis of the so-called DLVO theory, which has since been modified and adapted by many researchers including Hogg et al. (1966) and Gregory (1981). Several of these models can be found in Rajagopalan and Kim (1981), Elimelech et al. (1995) and Li (1998). In addition, a great deal of experimental work has been devoted to measuring or confirming expressions that describe electrostatic and van der Waals interactions (Clapp and Dickinson, 2001; Ducker et al., 1994; Meagher, 1992; Israelachvili and Adams, 1978). For simplicity, only one model is used in this work to describe DLVO theory, as described below. For constant surface potential, $|\psi| < 50\text{mV}$ and $\kappa a_p > 5$, the electrostatic interaction between a sphere and plate is given as (Hogg et al., 1966)

$$\phi_e = 2\pi a_p \varepsilon(\psi_{01}^2 + \psi_{02}^2)\left[\frac{\psi_{01}\psi_{02}}{(\psi_{01}^2 + \psi_{02}^2)}\ln\left(\frac{1+\exp(-\kappa h)}{1-\exp(-\kappa h)}\right) + \ln(1-\exp(-2\kappa h))\right] \qquad (2.1)$$

Here h is the minimum separation distance between the spherical particle and plate, a_p is the particle radius, ε is the dielectric constant of the medium, ψ_{0i} is the potential of surface i, and κ is the reciprocal Debye-length defined as

$$\kappa^2 = \frac{e^2}{\varepsilon k_B T}\sum_i n_i z_i^2 \,. \qquad (2.2)$$

The unretarded van der Waals interaction for a sphere and a plate is given by

$$\phi_v = -\frac{A_v}{6}\left[\frac{2a_p(h+a_p)}{h(h+2a_p)} + \ln\left(\frac{h}{h+2a_p}\right)\right] \qquad (2.3)$$

where A_v is the Hamaker constant (Hamaker, 1937). Figure 2-1 shows four typical DLVO interaction profiles. A comparison of models by Rajagopalan and Kim (1981)

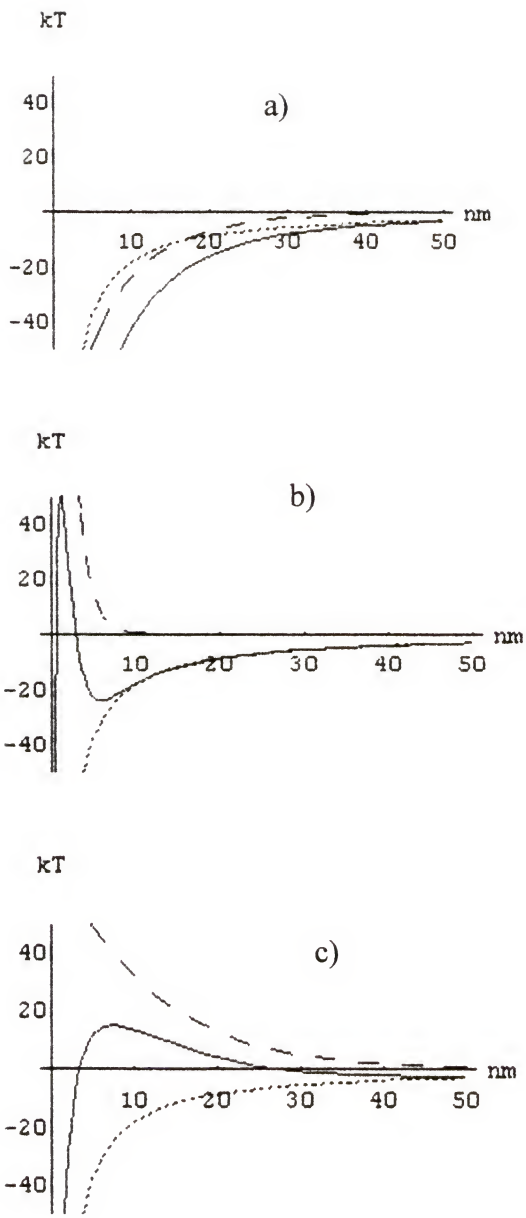

Figure 2-1. Typical DLVO profiles sphere-plate interactions calculated using a constant-potential model for electrostatic interactions, which is represented by dashed (— — —) lines and an unretarded van der Waals model, which is represented by dotted (----------) lines. Solid lines represent the superposition of electrostatic and van der Waals interactions. Part a) represents an overall attraction, b) shows the case of a large secondary minimum, and c) represents the case in which a barrier to deposition exists. A is the Hamaker constant, a_p is the particle radius, c is the salt concentration and ϕ represents the zeta potential of the sphere or plate.

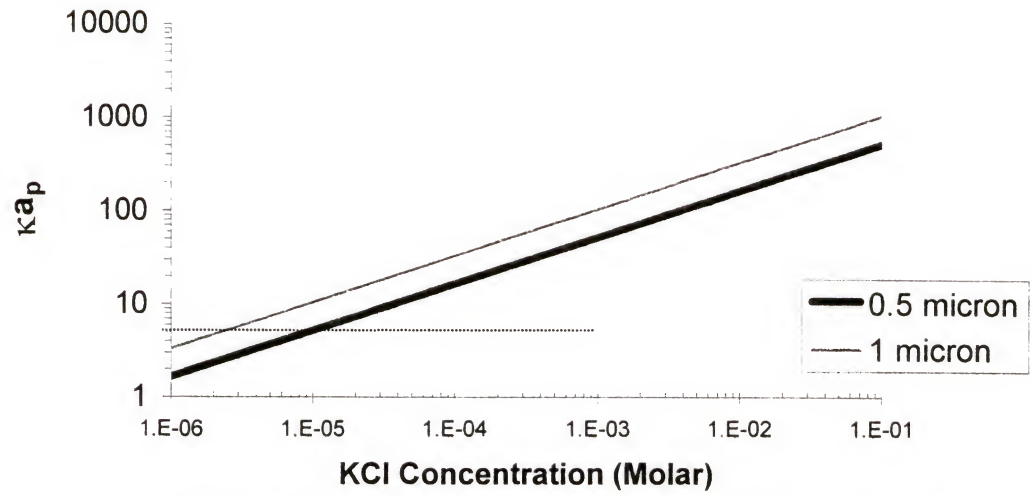

Figure 2-2. The effect of potassium chloride concentration of the ratio of particle size to Debye length for 0.5 and 1.0 μm-diameter particles.

suggests that these expressions are as likely as any others to be sufficient in describing deposition phenomena. Also, the requirement that $\kappa a_p > 5$ holds in the limit of large particles and small double layers, and Figure 2-2 shows the requirement for 0.5 and 1.0 μm particles used in this experiment is met at and above potassium chloride concentrations of 10^{-5} M.

2-1-2 Hydrophobic Forces

When non-polar molecules are introduced into an aqueous suspension, an energetically unfavorable disruption in the orientation of water molecules will occur. The system will tend towards a more favorable configuration, which can result in the aggregation of the non-polar substrates (Hiemenez and Rajagopalan, 1997; Elimelech et al., 1995). The most common example of this behavior is the demixing of water and oil. Many other implications of hydrophobic forces have been noted and studied in recent years (Israelachvili, 1992; Farrah et al., 1981; Kokkoli, 1998). Claesson and Christenson

(1998) used a surface force apparatus (SFA) to measure hydrophobic forces at separation distances up to 80 nm and found this interaction exceeded van der Waals interaction by two orders of magnitude. Rabinovich and Yoon (1994) used an atomic force microscope (AFM) to measure hydrophobic forces and discovered the attractive force sharply increased for surfaces with advancing contact angles greater than 95°. Hydrophobic forces are known to play a crucial role in colloidal deposition in biological systems, mineral flotation, food processing, etc. and is one interest of this study.

2-1-3 Hydration Forces

For two surfaces to make true contact in an aqueous solution, all water adsorbed at the point of contacts must be removed, thereby increasing the amount of energy required to bring the surfaces into contact. This additional force required for deposition is known as hydration forces in water, and decays exponentially with a decay length of a few nanometers (van de Ven, 1989). While these forces are ever present in colloidal suspension, no quantitative representation exists, so they will not be included in any calculations in this work.

2-1-4 Polymeric Forces

When polymers are added to colloidal suspensions, surface properties and particle interactions can be significantly altered via a variety of mechanisms. Steric stabilization occurs when adsorbed layers of polymers shield attractive interactions and also prevent overlap of the polymer layers. Bridging can occur when large molecular weight polymers adsorb to more than one particle forming an aggregate. Ionic polymers can also be used to induce a certain charge on a substrate thereby changing colloidal interactions. Polymeric forces are quite important for a number of applications yet little is know about

their origin (Hiemenz and Rajagopalan, 1997; Elimelech et al., 1995), and they will not be studied in this work.

2-1-5 Specific Interactions

Forces such as electrostatic and van der Waals are ubiquitous in aqueous, colloidal suspensions, but other forces such as receptor-ligand interactions are specialized to certain molecules. Specific forces are expected to play a significant role in the adhesion of microbiological particles and could account for the large discrepancy between theoretical deposition rates and experimental observations (Bell et al., 1984). Much effort is being devoted to identifying, measuring, modeling and predicting such specific forces (e.g., Dickinson, 1997; Bell et al., 1984), but they will not be explicitly considered in this study.

2-2 Hydrodynamics

The fluid velocity fields required to solve the convective-diffusion equation (2.24) are obtained by solving the equations of motion for the appropriate geometry. Due to the spatial complexity of a packed-bed filter, geometrical approximations, such as those discussed in 2-3-2, are necessary to estimate the flow field around granular collectors. The velocity field obtained for the effective medium approximation for granular filtration, as well as for flow between two plates, is presented in this section.

2-2-1 Flow between Parallel Plates

The two-dimensional velocity profile (2.5) for flow between parallel plates is readily obtained by solving a momentum balance equation with no-slip boundary conditions (2.4a-c) (Bird et al., 1960).

$$\frac{\partial^2 u}{\partial y^2} = \frac{1}{\mu}\frac{\partial P}{\partial x} \qquad (2.4a)$$

$$u = 0 \text{ at } y = 0 \text{ and } y = b \qquad (2.4b,c)$$

$$u = \frac{b^2}{2\mu}\frac{\Delta P}{L}\left[\left(\frac{y}{b}\right)-\left(\frac{y}{b}\right)^2\right] \qquad (2.5)$$

The volumetric flow rate, Q, and the average velocity, U, are found by

$$Q = \int_0^b wu(y)dy = wbU = \frac{wb^3\Delta P}{12\mu L}. \qquad (2.6)$$

Also, it is often more convenient to speak in terms of shear rates rather than velocity profiles, so the shear rate at the surface is given as

$$\tau_s = \left.\frac{\partial u}{\partial y}\right|_{y=0} = \frac{6Q}{wb^2}. \qquad (2.7)$$

2-2-2 Filtration Models

An adequate model of the fluid flow in a packed bed should describe the velocity field around the collectors and the pressure drop through the bed in a realistic way. Obtaining the true flow field in a packed bed is virtually impossible due to the complexity and irregularity of its geometry, so geometric models have been applied to approximate the velocity and pressure fields. The capillary tube model provides reasonable prediction for pressure gradients but not for the velocity field, while the spherical cell models proposed by Happel (1958) or Kuwabara (1959) provide reasonably good predictions for both pressure and velocity fields, although they are not without some ambiguities (Tien,1989; Li, 1998). Also, these cell models are theoretically limited to the case in which porosity is above about 0.6 (Li, 1998; Happel and Brenner, 1965), and the non-uniformity of collector particles can not be rigorously taken into consideration (Li and Park, 2000; Spielman, 1977). Li and Park (2000) proposed a filtration model based on the effective medium approximation that divides the flow into two regions; the

spherical fluid envelope region near the collector is described by creeping flow, and the outer or effective medium region is described by Brinkman's equation to account for the presence of other collectors. The effective medium approximation for filtration was found to be in better agreement to experimental permeability measurements and to numerical transport calculations than other models (Li and Park, 2000).

2-2-2-1 Capillary, Hapel and Kuwabara models

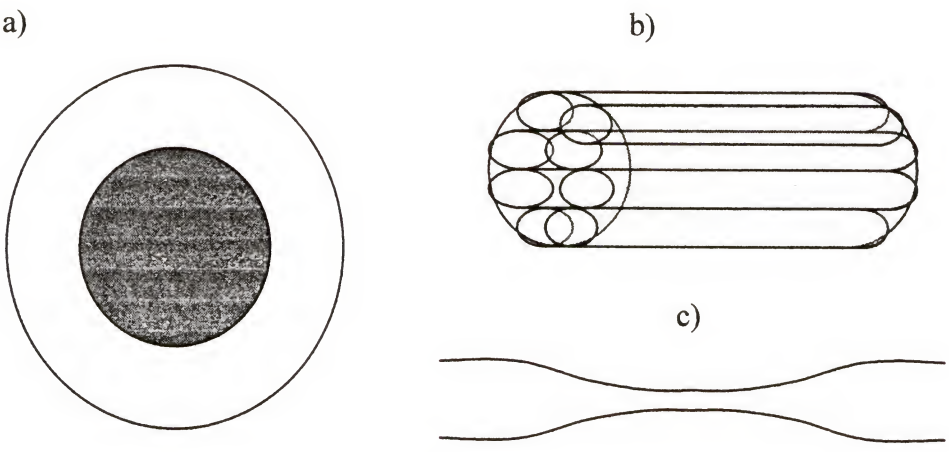

Figure 2-5. Some typical geometrical representations of granular packed-bed filters: a) spherical cell model; b) capillary tube model; and c) constricted tube models.

Capillary and cell models, such as those developed by Happel (1958) and Kuwabara (1959), have been extensively used in the literature to describe flow phenomena in a packed-bed filter. Figure 2-5 gives a schematic representation of these types of geometrical approximations. Capillary tube models essentially represent a granular packed-bed as a bundle of these tubes. Capillary models have been successfully

used to predict pressure drops across porous media, but they do not provide a realistic representation of flow fields inside these porous media (Tien, 1989; Li, 1998). The cell models depicted in Figure 2-5, which are expected to give more representative flow fields around a granular collector, consist of a solid collector element surrounded by a fluid envelope. Some ambiguity to the boundary condition exists as either a stress-free or vorticity-free boundary condition can be applied at the outer edge of the fluid envelope, corresponding to the Happel or Kuwabar models, respectively. To address this ambiguity, Li and Park (2000) modified the cell models for filtration by employing an effective medium approximation as discussed in 2-2-2-2. Only predictions from the effective medium approximation for filtration will be sought here, but due to the popularity of these models they are worth mentioning.

2-2-2-2 Effective medium approximation

The effective medium approximation assumes a liquid envelope, whose dimension is found from the porosity of the bed, and which immediately surrounds the spherical collector as in the Hapel and Kuwabara models. This envelope is then surrounded by a so-called effective medium, which takes into account the presence of surrounding collectors as shown in Figure 2-6. Stokes' equation is solved inside the fluid envelope, while Brinkman's equation is solved in the effective medium region, which extends to infinity. The dimensionless forms of these equations, in which pressure p is scaled by $\mu U/a_c$, velocity u is scaled by U and the radial coordinate r is scaled by the collector radius a_c, are given by equations (2.8) and (2.9):

$$\nabla p = \nabla^2 \mathbf{u}, \qquad 1 < r < R \tag{2.8}$$

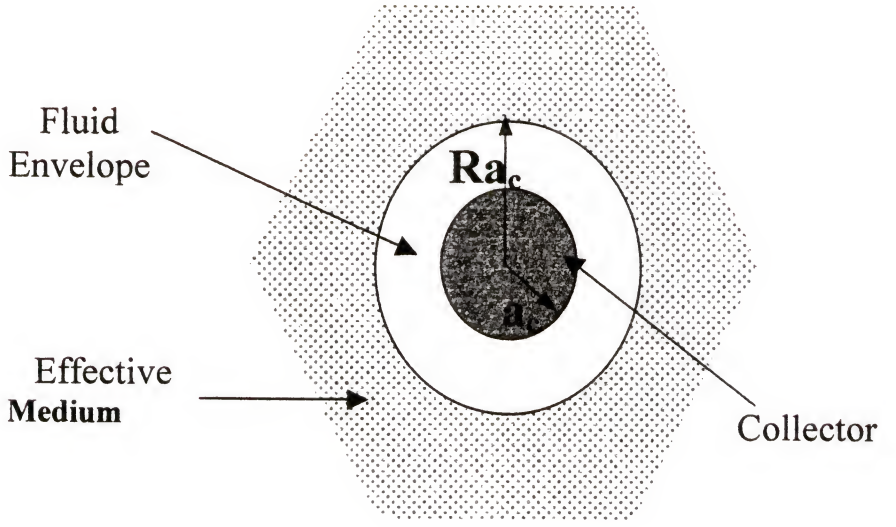

Figure 2-6. Schematic representation of filtration model based on the effective medium approximation.

$$\nabla p = \nabla^2 \mathbf{u} - \lambda_p^2 \mathbf{u}, \qquad r > R \tag{2.9}$$

Here, $\lambda_p^2 = a_c^{\,2}/k_p$, where k_p is the permeability of the packed-bed. The boundary conditions imposed are the no-slip condition at r=1, the continuity of velocity, stress and pressure at r=R and the velocity far from the collector must approach that of uniform flow in the packed-bed.

An analytical solution can be obtained for this problem by using a stream function, Ψ, which is defined as follows:

$$u_r = -\frac{1}{r^2 \sin\vartheta}\frac{\partial \Psi}{\partial \vartheta} \tag{2.10}$$

$$u_\vartheta = \frac{1}{r \sin\vartheta}\frac{\partial \Psi}{\partial r} \tag{2.11}$$

$$\Psi = f(r)\sin^2\vartheta . \tag{2.12}$$

By applying the condition that the velocity must approach the uniform velocity far from the sphere, f(r) in the outer region becomes

$$f_1(r) = -\frac{1}{\lambda_p^2 r}A + \left(\lambda_p + \frac{1}{r}\right)e^{-\lambda_p r}B - \frac{r^2}{2}. \tag{2.13}$$

From the no-slip boundary condition, f(r) is given in the inner region as

$$f_2(r) = \left(-\frac{r^4}{20} + \frac{r^2}{12} - \frac{1}{30r}\right)C + \left(\frac{r^2}{3} - \frac{r}{2} + \frac{1}{6r}\right)D. \tag{2.14}$$

In addition, the pressure in these regions can be expressed as follows:

$$p_1 = \left(-\lambda_p^2 r + \frac{1}{r^2}A\right)\cos\vartheta \tag{2.15}$$

$$p_2 = \left(rC + \frac{1}{r^2}D\right)\cos\vartheta \tag{2.16}$$

A, B, C and D are obtained by matching the velocity and stress at the junction of these two regions (r=R) and are described by the following four equations (2.17a-d):

$$-\frac{1}{\lambda_p^2 R}A + \left(\lambda_p + \frac{1}{R}\right)e^{-\lambda_p R}B + \left(\frac{R^4}{20} - \frac{R^2}{12} + \frac{1}{30R}\right)C - \left(\frac{R^2}{3} - \frac{R}{2} + \frac{1}{6R}\right)D = \frac{R^2}{2}$$

$$\frac{1}{\lambda_p^2 R^2}A - \left(\lambda_p^2 + \frac{\lambda_p}{R} + \frac{1}{R^2}\right)e^{-\lambda_p R}B + \left(\frac{R^3}{5} - \frac{R}{6} - \frac{1}{30R^2}\right)C - \left(\frac{2R}{3} - \frac{1}{2} - \frac{1}{6R^2}\right)D = R$$

$$\left(-\frac{1}{R^2} + \frac{12}{\lambda_p^2 R^4}\right)A - \left(\frac{4\lambda_p^2}{R^2} + \frac{12\lambda_p}{R^3} + \frac{12}{R^4}\right)e^{-\lambda_p R}B + \left(\frac{7R}{5} - \frac{2}{5R^4}\right)C + \left(-\frac{1}{R^2} + \frac{2}{R^4}\right)D = -\lambda_p^2 R$$

$$-\frac{6}{\lambda_p^2 R^4}A + \left(\frac{\lambda_p^3}{R} + \frac{3\lambda_p^2}{R^2} + \frac{6\lambda_p}{R^3} + \frac{6}{R^4}\right)e^{-\lambda_p R}B + \left(\frac{3R}{10} + \frac{1}{5R^4}\right)C - \frac{1}{R^4}D = 0$$

By matching the overall porosity to the size of the fluid envelope for a collector size distribution density of $P(a_c)$, we determine the thickness of the fluid envelope δ_e by

$$1-\varepsilon = \frac{\int_0^\infty a_c P(a_c)da_c}{\int_0^\infty (a_c+\delta_e)^3 P(a_c)da_c} \tag{2.18}$$

Evidence suggests that R should be taken as $1.028(a_c + \delta_e)/ a_c$, where 1.028 has been found empirically (Li, 1998). Finally, the permeability can be written as

$$\lambda_p^2 = \frac{a_c^2}{k_p} = \frac{3(1-\varepsilon)a_c^2}{\int_0^\infty a_c^3 P(a_c)da_c} \int_0^\infty a_c D(R,\lambda_p)P(a_c)da_c\,, \tag{2.19}$$

where D is found to be

$$D(R,\lambda_p) = -\frac{6}{Q_1}\left[6R^6\lambda_p^3 + 21R^5\lambda_p^2 - 5R^4\lambda_p^3 + 45R^4\lambda_p - 5R^3\lambda_p^2 + 45R^3 - R\lambda_p^3 - \lambda_p^2\right], \tag{2.20}$$

$$\begin{aligned} Q_1 = {} & 180R^3 + 24R^5\lambda_p^2 - 45R^4\lambda_p^2 - 9\lambda_p^2 + 4\lambda_p^3 + 180R^4\lambda_p + 4R^6\lambda_p^3 \\ & + 10R^3\lambda_p^3 - 9R\lambda_p^3 - 9R^5\lambda_p^3 + 30R^2\lambda_p^2 - 180R^3\lambda_p \end{aligned} \tag{2.21}$$

Thus, a complete description of the permeability and fluid velocity in a packed-bed of spherical collectors is achieved (Li and Park, 2000).

2-2-3 Sedimentation

The effect of gravity on colloidal transport can be considered by first writing the net buoyancy force as

$$F_g = \Delta\rho V g\,, \tag{2.22}$$

where $\Delta\rho$ represents the difference in fluid and particle densities, V the particle volume and g is the acceleration due to gravity. The settling velocity U_s of the particle is

obtained by balancing the gravitational force with the drag force F_d exerted by the fluid on a spherical particle

$$U_s = \frac{2g(\rho_p - \rho_f)a_p^2}{9\mu\alpha}. \qquad (2.23)$$

Wilson (2000) proposed a method of determining the bulk-settling rate of particles by measuring the absorption at two different heights of a colloidal suspension with an UV-visible spectrophotometer during settling. Basically, the ratio of the height-interval to the time-interval between inflection points of the two absorption-time curves gives the average settling rate as depicted in Figure 2-4. Wilson (2000) measured the settling rate of the same 1 μm-diameter silica particles used in this work to be 10^{-4} cm/s, while the rate estimated from (2.23) was about $5x10^{-5}$ cm/s. The theoretical rates calculated from equation (2.23) were used in obtaining concentration profiles using the model discussed in 3-2.

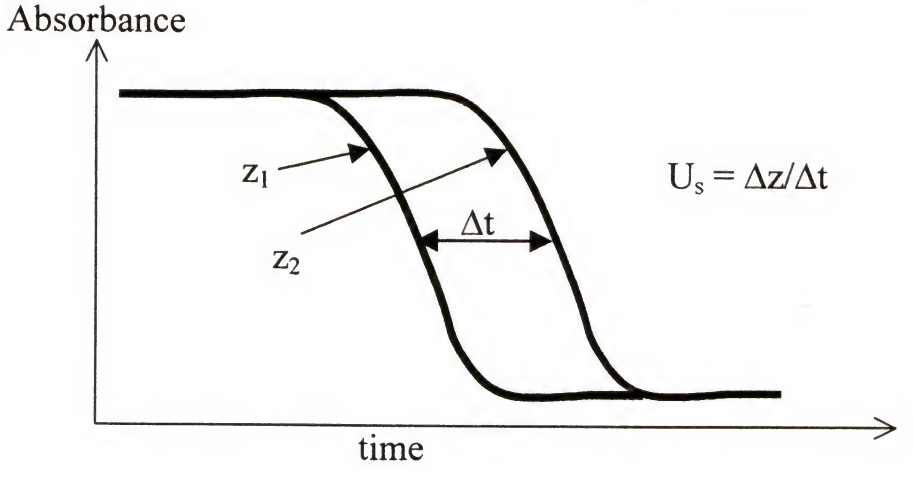

Figure 2-4. Schematic of uv-visible spectrophotometer experiments to determine the bulk settling rate of colloidal particles in suspension (Wilson 2000)

2-3 Colloidal Transport

2-3-1 General Approaches

Colloidal transport can be modeled either by following the particle trajectory using a Lagrangian viewpoint or by describing the probability densities of particles from a fixed or Eularian viewpoint (Adamczyk et al., 1983; Elimelech et al., 1995) . The Lagrangian description is advantageous in that the finite-size of the particles is considered, whereas the Eularian description treats particles as point-masses, which is the main deficiency of continuum theory (Adamczyk et al., 1983). The Eularian perspective for the transport of Brownian particles can offer analytical solutions, which can be extended to heat transfer problems, whereas the trajectory analysis approach for colloidal transport requires extensive computation time due to the stochastic nature of Brownian motion. In this work, colloidal transport will only be modeled using the convective-diffusion equation, which evolves from a Eularian description, yet the results of models formulated from the Lagrangian viewpoint will be discussed in 2-4.

2-3-2 Convective-Diffusion

A colloidal particle in solution is subject to many forces including Brownian motion, convection, gravity and colloidal interactions, all of which are described by the convective-diffusion equation. By assuming the particles will always tend toward a Maxwellian distribution of velocities on an appropriate time-scale, the Fokker-Plank equation was formulated which describes the probability distribution of particles (Chandrasekhar, 1943). Equation 2.4 is the well known convective-diffusion equation, including the contribution of external and surface forces K, and can be deduced from the

Fokker-Plank equation for colloidal dispersions in which particle inertia is negligible (Adamczyk et al., 1983; Chandrasekhar, 1943).

$$\frac{\partial c}{\partial t} + u \cdot \nabla c = \nabla \cdot \left[D\nabla c - D\frac{K}{k_B T} c \right] \tag{2.24}$$

Here c is particle concentration, which is analogous to a probability distribution, u is taken as the fluid velocity, D is the diffusion coefficient, k_B is the Boltzmann constant, T is temperature, and t is time. The Stokes number N_{St} can provide information about the importance of inertial impact, even though no exact criteria exist. The Stokes number for packed beds is given by

$$N_{St} = \frac{2\rho_p U a_p^2}{9\mu a_c}, \tag{2.25}$$

where ρ_p is the particle density. Deposition by inertial impaction drastically decreases for Stokes numbers below about 0.1 (Tien, 1989). A typical Stokes number for systems in this study is about 0.04, thus justifying the omission of inertia and the use of the convective-diffusion equation (2.24). Difficulty in solving the convective-diffusion equation arises due to the lack of understanding of colloidal interactions and because of the drastically different length-scales associated with colloidal transport. A method of accounting for the varying length-scales, i.e., the interaction force boundary layer approximation, is discussed in 2-3-2-2, 3-1 and 3-2-1.

2-3-2-1 Brownian diffusion

Brownian motion is described by the diffusion coefficient, which is found by balancing thermal fluctuations with the drag exerted on the particle by the fluid. Einstein (1920) first formulated the diffusion coefficient based on Stokes' law for the drag on a sphere of radius a_p:

$$F_{st} = 6\pi\mu a_p U, \tag{2.26}$$

where μ and U are the fluid viscosity and average velocity, respectively. The resulting equation for the diffusion coefficient is known as the Stokes-Einstein equation:

$$D = \frac{kT}{6\pi\mu a_p}. \tag{2.27}$$

However, Stokes' law was developed for the drag on a particle in a fluid media that extends to infinity, which is an inherent violation in the deposition process. Brenner (1961) developed a correction factor to the Stokes-Einstein equation that accounts for the effects of hydrodynamic retardation for a sphere moving towards or away from a surface. This correction for a rigid surface is

$$\alpha = \frac{F(h)}{F_{st}} = \frac{D_\infty}{D(h)} = \tag{2.28}$$

$$\frac{4}{3}\sinh\gamma\sum_{n=1}^{\infty}\frac{n(n+1)}{(2n-1)(2n+3)}\left[\frac{2\sinh(2n+1)\gamma+(2n+1)\sinh 2\gamma}{4\sinh^2(n+\frac{1}{2})\gamma-(2n+1)^2\sinh^2\gamma}-1\right],$$

where h is the separation between particle and surface and

$$\gamma = \cosh^{-1}\left(\frac{h+a_p}{a_p}\right). \tag{2.29}$$

Figure 2-3 shows the hydrodynamic retardation correction factor as a function of particle-wall separation distance for a 1-micron particle. Employing optical trapping experiments, Clapp and Dickinson (2001) and Frej and Prieve (1993) have shown that Brenner's correction (Eqs. 2.28 and 2.29) for the position-dependent diffusion coefficient of Brownian particles near a wall is quite reasonable, especially at separation distances large than the Debye length. Goldman et al. (1967a and 1967b) also formulated a correction for the motion of a sphere tangentially to the surface, but this correction will

be omitted from the current investigation since diffusion tangentially to the surface has been found negligible when considering the appropriate length-scale in that direction.

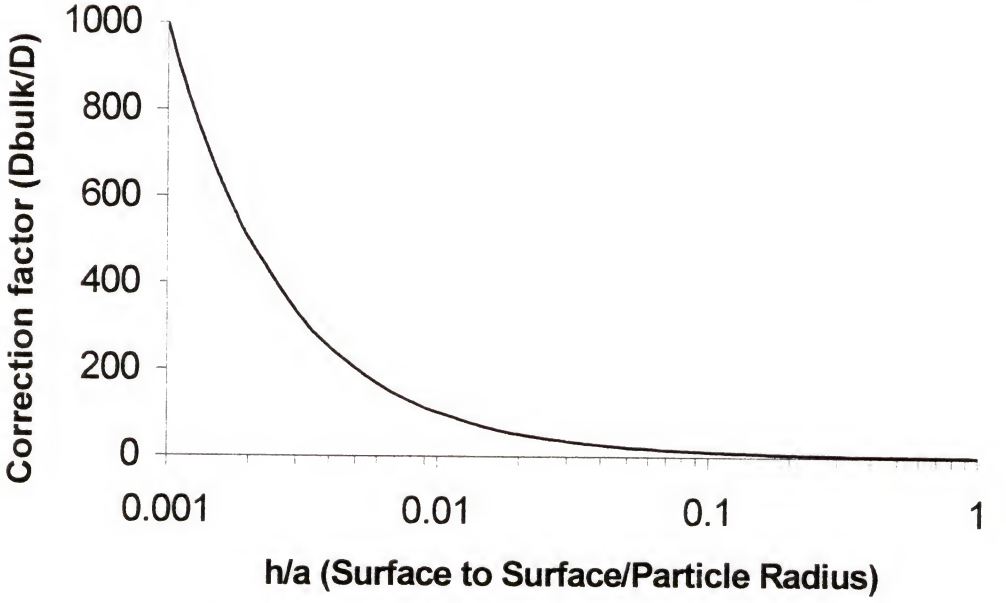

Figure 2-3. Hydrodynamic correction factor for sphere moving towards a plane surface (Brenner 1961).

2-3-2-1 Smoluchowski-Levich solution

The convective-diffusion equation has been solved for a variety of geometries and under a variety of simplifying assumptions. One such solution for purely convective-diffusion controlled transport of molecular-sized solutes in the absence of gravity, hydrodynamic retardation and surface forces is attributed to Levich (1962).

$$D_\infty \nabla^2 c = u \cdot \nabla c \qquad (2.30)$$

Under these assumptions, equation 2.10, along with perfect sink and uniform bulk concentration boundary conditions, Levich (1962) found the surface flux for flow in a

channel to be

$$j_{\perp} = \frac{D_{\infty} c_0}{\int_0^{\infty} \exp[-\eta^3] d\eta} \left(\frac{2U}{bD_{\infty} x} \right)^{1/3} \tag{2.31}$$

b is the channel gap and x is the downstream distance (Levich, 1962). The dimensionless flux or Sherwood number Sh, defined by the following equation, is dependent on downstream distance (Adamczyk et al. 1983; van de Ven 1989):

$$Sh = \frac{a_p}{D_{\infty} c_0} j_{\perp} \tag{2.32}$$

The average Sherwood number over the length of the channel L is often used in the literature for comparing deposition rates. This so-called Smoluchowski-Levich solution corresponds to the diffusion-limited case of particle deposition in the absence of gravity, colloidal forces and hydrodynamic interactions and is equivalent to the interaction force boundary layer solution in the limit of a large deposition rate constant.

2-3-2-2 Interaction force boundary layer approximation

Convective-diffusion equations are readily written to predict particle concentration profiles in the deposition process, but solving these equations with gravity, surface forces, and hydrodynamic retardation effects included becomes quite difficult even numerically because of the drastically different length-scales associated with transport and deposition. An approximate solution can be obtained by dividing the problem into appropriately scaled regions and matching the solutions at adjacent boundaries. Using such an approach, Spielman and Friedlander (1974) introduced the so-called interaction force boundary layer approximation in which surface force terms collapse into an apparent first-order reaction boundary condition at the surface:

$$J = k'c\,, \tag{2.33}$$

$$k' = D_\infty / \int_0^\infty \{\exp(\phi) - 1\} dy \tag{2.34}$$

The underlying assumption to this model is that the surface force layer is much smaller than the diffusion boundary layer, which in turn is much smaller than the characteristic length-scale for the bulk flow domain (e.g. the gap-width between plates for flow in a channel). The scaling arguments as well as the development of the interaction force boundary layer approximation (IFBLA) for flow between parallel plates is presented in Chapter 3.

Prieve and Ruckenstein (1976) later determined that the interaction force boundary layer approximation originally obtained by Ruckenstein and Prive (1973) and Spielman and Friedlander (1974) is only valid in the presence of a repulsive interaction between particle and collector, and that in the absence of an energy barrier, full transport equations should be solved. Using a more mathematically rigorous matched asymptotic expansion scheme, Shapiro et al. (1990) reiterated that the IFBLA is only valid in the presence of short-ranged repulsive colloidal interactions. In addition, Prieve and Ruckenstein (1976) noted that hydrodynamic retardation of a particle near a wall should not be neglected as it can reduce the deposition rate constant by orders of magnitude. Adamczyk and van de Ven (1981) also suggest that the IFBLA is not appropriate in the presence of a significant secondary minimum. Therefore, salt concentrations of colloidal suspension were kept high enough to expect short double layers but low enough that large secondary minima were not expected.

The interaction force boundary layer approximation model described and used in this work assumes that a clean, smooth, heterogeneous surface is available for the

deposition of non-aggregated particles and that blocking, detachment and aging effects are negligible. Arguably, these assumptions hold for the non-biological experiments in this research, in which particle concentrations in solution and on the surfaces are low and in which glass slides have a root-mean-square roughness as low as a few nanometers (Truesdail, 1999). Although the effects of blocking, coagulation, aging and detachment are neglected here, a discussion of other work considering these effects can be found in section 2-4.

2-3-3 Particle Collection by Filtration

2-3-3-1 Coefficient definitions

The collection of particles in a packed-bed is usually expressed in terms of a filter coefficient, filter filtration efficiency, mass transfer coefficient or Sherwood number, so definitions of these terms is in order. As usual, the flux J of particles to a collector is given as the number of particles deposited per unit area per time, and the Sherwood number is

$$Sh = J\frac{a_c}{D_\infty c_0} = \frac{k_m a_c}{D}. \qquad (2.35)$$

These terms are useful in measuring the local deposition rate, but the filter coefficient λ or efficiency η better describe the performance of the filter. Assuming the deposition rate is first order with respect to particle concentration, a balance of particles entering and leaving a differential volume of the column can be written as

$$-U\frac{dc}{dz} = JA_{sp}. \qquad (2.36)$$

Here z is the depth-coordinate in the packed-bed, and the solution of this equation yields the concentration profile along the length of the filter:

$$c(z) = c_0 e^{\frac{-A_{sp} k_m}{U} z}. \quad (2.37)$$

The filter coefficient, which is independent of bed depth, is

$$\lambda = \frac{A_{sp}\, k_m}{U}. \quad (2.38)$$

Finally, the filtration efficiency, which is dependent on bed depth l, is expressed as

$$\eta = \frac{c_{in} - c_{eff}}{c_{in}} = 1 - e^{-\lambda l}, \quad (2.39)$$

where c_{in} and c_{eff} are the inlet and effluent concentrations. Experimentally, the filter coefficient is found by measuring the concentration at a minimum of two depths in the bed, and equations 2.37 and 2.38 are solved or fitted to find the filter coefficient.

2-3-3-2 Theoretical collection rates

For the case in which Brownian diffusion, convection and colloidal interactions are significant, and in which gravity, hydrodynamic retardation and interception are negligible, Spielman and Friedlander (1974) developed a semi-analytical solution for the deposition rate of particles onto cylindrical and spherical particles using the interaction force boundary layer approximation. For spherical collectors they (Spielman and Friedlander, 1974; Li and Park, 2000) determined the Sherwood number to be

$$Sh = 0.635 A_s^{1/3} Pe^{1/3} \gamma_s(\beta_s), \quad (2.40)$$

where

$$\beta_s = 1.125 A_s^{-1/3} Pe^{-1/3} Da, \quad (2.41)$$

and for cylindrical collectors, the Sherwood number was found to be

$$Sh = 0.731 A_s^{1/3} Pe^{1/3} \gamma_s(\beta_s), \quad (2.42)$$

where

$$\beta_s = 1.022 A_c^{-1/3} Pe^{-1/3} Da . \qquad (2.43)$$

Determining γ_s and γ_c requires a numerical solution to a Volterra integral. Spielman and Friedlander (1974), therefore tabulated results to the integral, and a summary of these results is shown in Table 2-1. The flow parameters As and Ac depend on the model used to estimate the flow field around a collector element, and they are summarized for various models in Table 2-2.

Table 2-1. Values converted from the Volterra integral solution by (Spielmand and Friedlander, 1974)

βs or βc	γ_s	γ_c
0	0	0
0.01	0.01404	0.013198
0.02	0.02772	0.026078
0.05	0.06669	0.062857
0.1	0.12545	0.118709
0.2	0.22410	0.213217
0.5	0.42303	0.407133
1	0.59840	0.58220
2	0.75180	0.73887
5	0.88508	0.87783
10	0.93945	0.93536
20	0.96895	0.96667
50	0.98735	0.98637
100	0.99366	0.99307
∞	1	1

Table 2-2. Expressions for the flow field parameter A_s for different cell models. Expressions taken from (Li 1998; Spielman and Friedlander 1974).

Spherical Cell Model	A_s
Happel	$A_s = \frac{1-(1-\varepsilon)^{5/3}}{1-(1-\varepsilon)^2 - \frac{3}{2}(1-\varepsilon)^{1/3} + \frac{3}{2}(1-\varepsilon)^{5/3}}$
Brinkman's	$A_s = 1 + \lambda_p$
Effective Medium Approximation	$A_s = \frac{2}{Q_1}\left[30R(4-R^2) + 10\lambda_p R(-8+12R+5R^3) + 3\lambda_p^2(1-5R^2 - 10R^3 + 14R^5) + 3\lambda_p^3 R(1+5R^2-10R^3+4R^5)\right]$ where $Q_1 = 180R^3 + 24R^5\lambda_p^2 - 45R^4\lambda_p^2 - 9\lambda_p^2 + 4\lambda_p^3 + 180R^4\lambda_p + 4R^6\lambda_p^3 + 10R^3\lambda_p^3 - 9R\lambda_p^3 - 9R^5\lambda_p^3 + 30R^2\lambda_p^2 - 180R^3\lambda_p$

2-4 Literature Review of Deposition Experiments

An extensive amount of research has been performed to understand various effects on colloidal deposition in a number of different geometries including packed-beds, rotating discs and parallel plate flow channels. Studies on the influence of physical (e.g. particle size and flow rate) and chemical (e.g. salt concentration and pH) parameters on particle attachment and detachment rates, blocking effects, aging phenomena, etc. can be found throughout the literature. Unfortunately, most of the efforts to model such effects seem to be parametric and non-predictive. However, some of the results of modeling and experimental work on colloidal deposition is presented below, and good reviews of deposition models and experiments can be found in Elimelech et al. (1995), Tien (1989) and Adamczyk et al. (1983).

In general, when particles and collectors are oppositely charged, fairly good agreement has been repeatedly observed experimental deposition data and theoretical calculations (Bowen and Epstein, 1979; Fitzpatrick and Spielman, 1973; Adamczyk and van de Ven, 1981; Fitzpatrick, 1972; van de Ven, 1998; Adamcz et al., 1986). This theoretical and experimental agreement for the collection of colloidal particles in the presence of attractive double layers has been noted for a number of geometrical systems including packed-bed filters (Fitzpatrick and Spielman, 1973; van de Ven, 1998), parallel plate flow channels (Bowen and Epstein, 1979; Adamcz and van de Ven, 1981), impinging jet stagnation-point flows (Adamczyk et al., 1986) and rotating discs (Hull and Kitchener, 1969). However, as the size of the particle being collected in a packed-bed is increased beyond approximately a couple of microns in diameter, the agreement between theoretical predictions and experimental data was seen to become poor for even for oppositely charged particles and collectors (Elimelech, 1994; Tien, 1989).

Conversely, when collectors and particles are similarly charged, experimental collection rates of colloidal particles often differ from theoretical predictions by orders of magnitudes (Marshall and Kitchener, 1966; Hull and Kitchener, 1969; Tobiason and O'Melia, 1988; Bowen and Epstein, 1979; Sjollema and Busscher, 1990a). In such experiments the dependence of particle deposition on pH or salt concentration could not be predicted in the presence of double layer repulsion. Typically, the dependence on pH was experimentally seen to be much more gradual than predicted by including DLVO-type expressions for colloidal interactions in models for particle collection in both packed-bed (Tobiason and O'Melia, 1988; Tobiason, 1987; Fitzpatrick, 1972; Elimelech, 1991) and flat plate systems (Sjollema and Busscher, 1989 and 1990a). Therefore, the

predicted deposition rates are sometimes orders of magnitudes different from experimentally observed deposition rates (Adamczyk et al., 1983; Elimelech et al., 1995). It should also be noted that Chang and Whang (1997 and 1998) recently used the Kuwabara cell model along with a trajectory analysis approach to predict adequately predict filtration rates of Brownian particles in the presence of repulsive double layer interactions. However, the results of these simulations when deposition was transport-controlled provided poorer agreement than previous models.

Nearly every communication noting poor agreement between modeling and experiments seems to cite heterogeneity of surface charge or roughness as the source of the discrepancy. Some models have been developed to account for heterogeneity of charge, surface structure or particle size distribution (Song et al., 1994; Vaidyanathan, 1986; Vaidyanathan and Tien, 1991; Tien, 1989; Czarnecki and Warszynski, 1987), but little work has been done to verify heterogeneity as the source of the observed disagreement. Typically, these models show that heterogeneity can account for experimental and discrepancies by assuming surfaces have patch-wise charges or protrusions. While these models are usually parametric, they prove that the heterogeneity explanation, which pervades the deposition literature, is plausible. Other such explanations include hydrodynamic and electrokinetic coupling, surface charge regulation and polymeric configurations, but no sufficient model exists to predict deposition or detachment a priori (van de Ven, 1998).

Generally when no barrier to deposition is present, the process is considered to be transport-controlled, and the deposition rates can usually be predicted by the convective-diffusion equation. However, when attractive colloidal interactions are long-ranged,

collection rates in a packed-bed or in a stagnation point-flow system were experimentally and theoretically seen to be significantly higher than predicted by the convective-diffusion limit (Chari and Rajagopalan, 1985; Adamczyk et al., 1989; Elimelech, 1991). For oppositely charged particles and collectors, the filtration rates were seen to increase dramatically as the salt concentrations were decreased (Elimelech, 1991; Adamczyk et al., 1989), which is opposite to the trend seen for similarly charged materials.

Direct observations of colloidal deposition in well-defined geometries have also elucidated that blocking effects, bond aging and cleaning methods can play a significant role in the deposition rates. Meinders and Busscher (1993) concluded that interaction forces between polystyrene particles and glass slides changed over time by studying the resident-time dependence of desorption in a parallel plate flow cell. Statistical analysis of the distribution of deposited particles has revealed that a particle on the collector surface significantly affects the deposition of other particles (Dabros and van de Ven, 1982 and 1983; Meinders et al., 1992; Sjollema and Busscher, 1990b). The deposited particles are reported to inhibit deposition in regions ranging from about 3 particle diameters away (Sjollema and Busscher, 1990b) up to 675 geometrical cross sections (Meinders et al., 1992). Dabros and van de Ven (1983) also note that the type of acid used to clean glass slides can appreciably affect deposition rates onto the slides even though the measured zeta potentials were similar for all the treatments. Finally, Luthi et al. (1998) concluded that the sites available for adsorption are transient after observing that immediately after desorption of latex particles, the surface lost its ability to adsorb particles for hours. While these blocking and aging effects can be substantial and should not be ignored, the experiments in this research were designed to minimize such effects. Namely, particle

concentrations in the bulk and on the surface were maintained low to minimize blocking or coagulation effects, and salt concentrations used were moderate to minimize the likelihood of significant secondary minima (and thus detachment) and to satisfy the interaction force boundary layer requirement of small double layers.

CHAPTER 3
COLLOIDAL DEPOSITION IN A PARALLEL PLATE FLOW CELL

3-1 Interaction Force Boundary Layer Approximation Requirements

Throughout this work, the interaction force boundary layer approximation (IFBLA), introduced in 2-2-3, will be used to model colloidal deposition, thus the validity of this approximation is shown here. The primary assumption of the IFBLA is that the surfaces forces act over a region much smaller than the size of the diffusion boundary layer, which in turn is much smaller than some characteristic bulk length-scale. The appropriate length-scale for the surface force and bulk regions are taken to be the Debye length (Eq. 2.2) and collector size for filtration or gap width for flow cell problems, respectively. The length scale for the diffusion boundary layer, which is not readily apparent, is found by matching the convective and diffusive terms of the convective-diffusion equation in that layer, as described in section 3-2-1 and by Levich (1962). Experimental conditions must be chosen to satisfy these assumptions, so the applicable range of operation conditions for filtration and flow cell experiments are discussed below.

First, the validity of the scaling assumption for flow between two plates, as shown in Figure 3-1 and Equation (3.1), is discussed.

$$\kappa^{-1} << \delta_D << b \qquad (3.1)$$

For systems in which electrostatic and van der Waals forces are predominate, the Debye length, which depends mostly on the type and concentration of electrolyte present, can be

used as an appropriate length-scale for the surface force region. The diffusion boundary layer length-scale, which is found by matching convective and diffusive terms, is determined in section 3-2-1 to scale as

$$\delta_D \sim \mathrm{bPe}^{-1/3}, \tag{3.2}$$

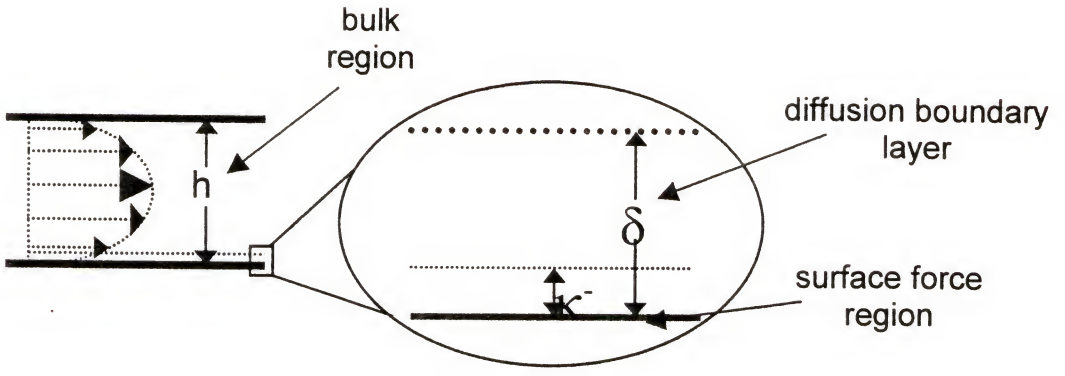

Figure 3-1. Schematic of the three distinct regions in a parallel plate flow cell.

where b is the gap-width in the flow cell, and the Peclet number is

$$\mathrm{Pe} = \mathrm{Ub/D}, \tag{3.3}$$

where U is the average fluid velocity and D is the bulk diffusion coefficient. Thus, the IFBLA requirement, in terms of measurable variables becomes

$$\frac{\kappa^{-1}}{b} << \left(\frac{Ub}{D_\infty}\right)^{-1/3} << 1 \tag{3.4}$$

Also, it should be noted that δ_D is simply a length-scale and is in no way indicative of the exact size of the boundary layer, but it is sometimes referred to as the boundary layer thickness.

Figure 3-2 shows that the ratio of boundary layer thickness to gap-width is small over a wide range of flow rates and particle sizes, as required. Silica particles of 0.5 and 1.0 μm diameters were chosen for deposition experiments since they are large enough to be observed microscopically but small enough to exhibit Brownian motion. Figures 3-3 and 3-4 show the effects of potassium chloride concentration and flow rate on the ratio of Debye length to diffusion boundary layer thickness for 0.5 and 1.0 μm-diameter particles, respectively. For potassium chloride concentrations above about 10^{-4} M, the ratio

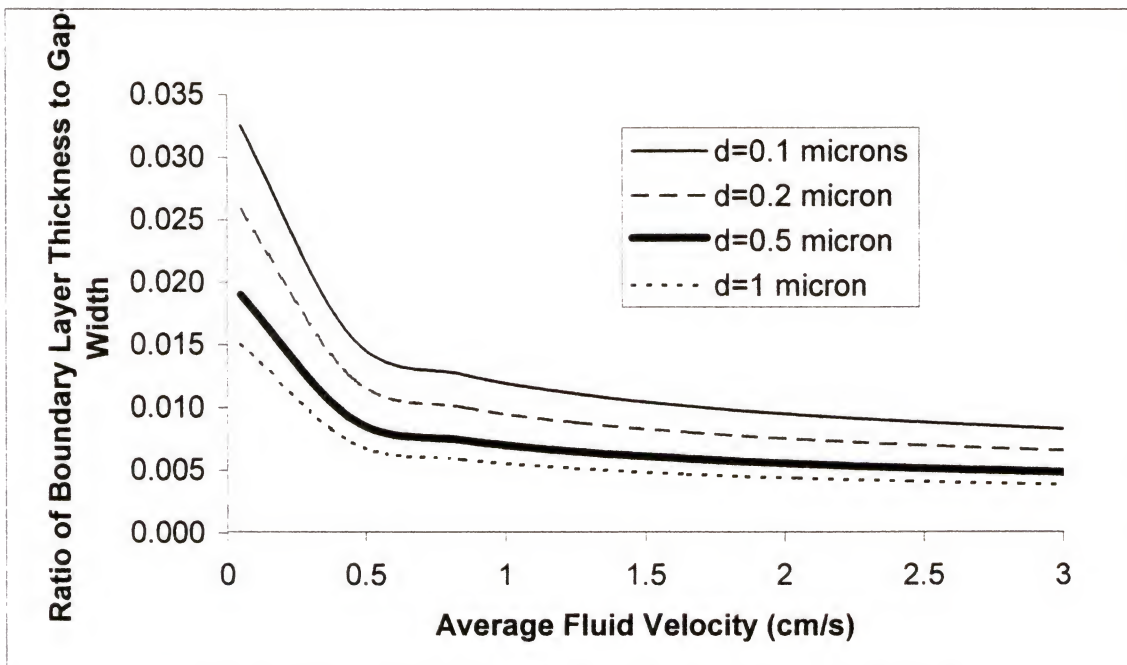

Figure 3-2. Effect of particle size and flow rate on the relative diffusion boundary layer thickness.

becomes very small for both 0.5 and 1.0 μm-diameter particles. Salt concentrations of about 1 mM were used in most experiments to satisfy this requirement and to minimize changes in conductivity when adjusting pH with the addition of acid or base. So the assumptions of the interaction force boundary layer assumption for the deposition of 0.5 and 1.0 μm silica particles are met for a wide range of flow rates and for potassium chloride concentrations at or above 0.1 mM.

Similarly, the operating conditions in a packed-bed were examined to meet the boundary layer scaling requirements. For flow in a packed-bed with collector radii a_c, the Peclet number is given as

$$Pe = Ua_c/D, \qquad (3.5)$$

and the diffusion boundary layer length-scale is taken to be

$$\delta_D \sim bPe^{-1/3} \qquad (3.6)$$

Figure 3-5 shows that the ratio of boundary layer thickness to collector radius, $Pe^{-1/3}$, is much less than one for collector radii as small as 100 microns and for superficial velocities as small as 0.05 cm/s. In addition, in Figures 3-6 and 3-7, the Debye length is seen to be much smaller than the diffusion boundary layer thickness for potassium chloride concentrations of 10^{-4} M and higher. Therefore, the scaling assumptions of the interaction force boundary layer approximation are met for a wide range of experimental conditions employed in this work.

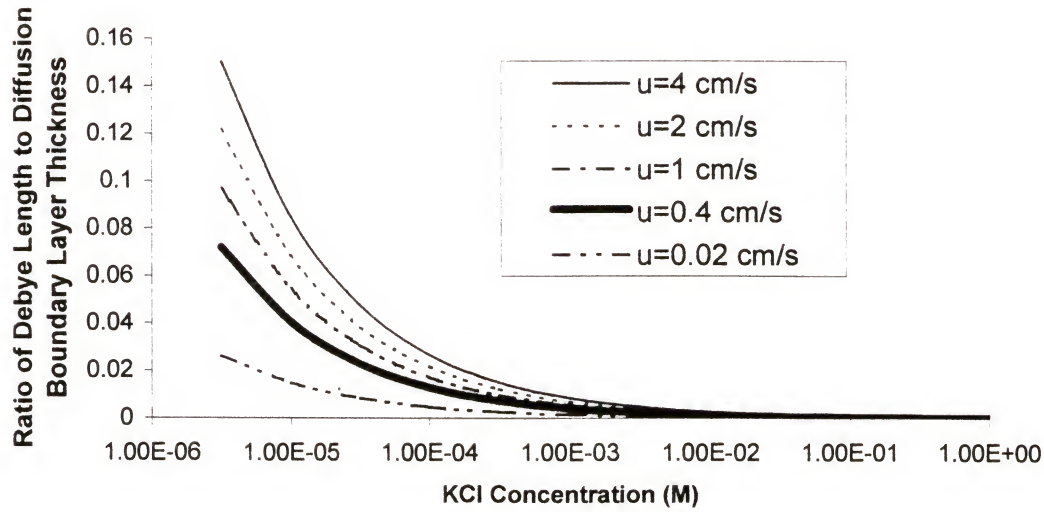

Figure 3-3. Ratio of Debye length to diffusion boundary layer thickness for 0.5 μm particles in a parallel plate flow cell.

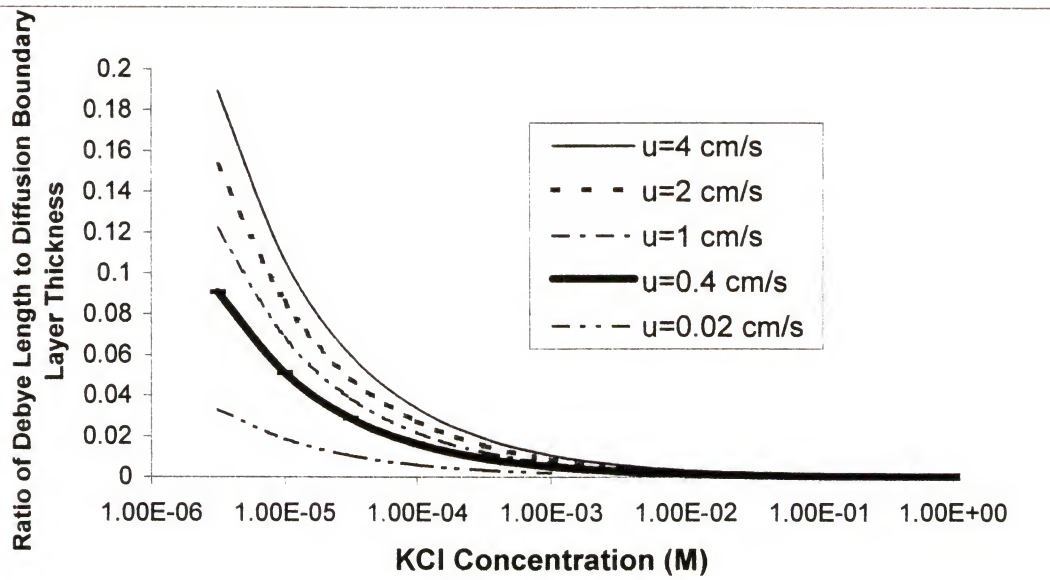

Figure 3-4. Ratio of Debye length to diffusion boundary layer thickness for 1.0 μm particles in a parallel plate flow cell.

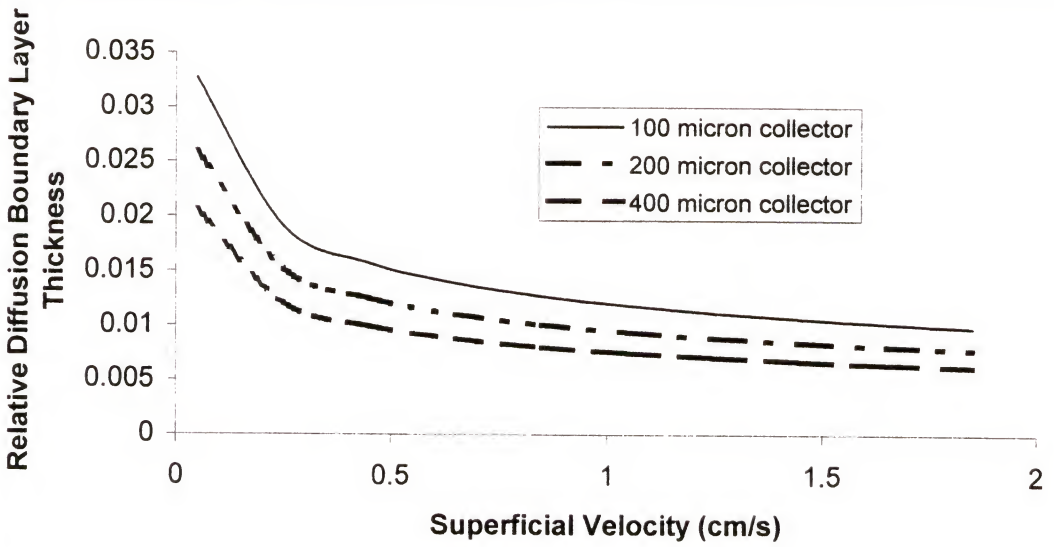

Figure 3-5. Effect of collector size and velocity on the relative diffusion boundary layer thickness for a 0.5 μm particle in a packed-bed

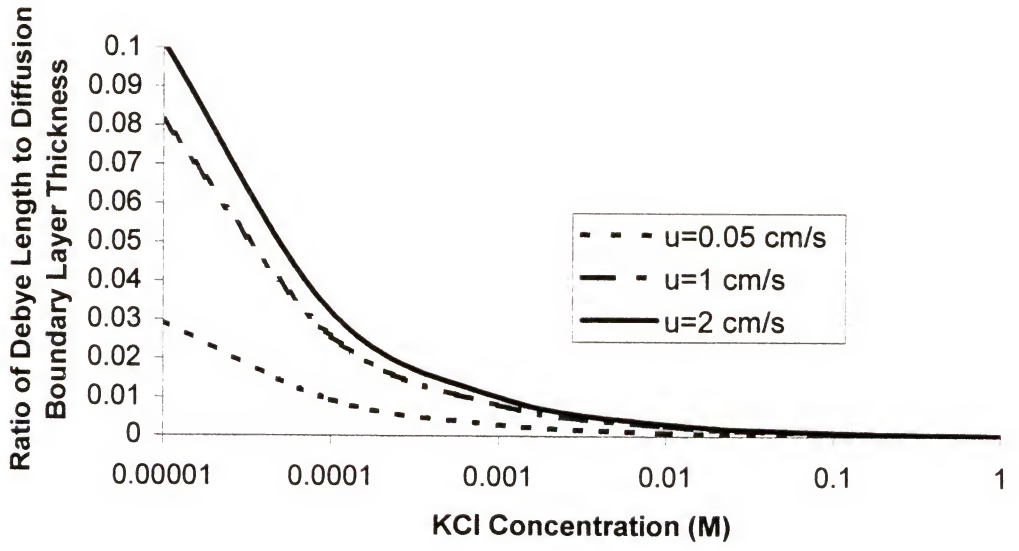

Figure 3-6. Ratio of Debye length to diffusion boundary layer thickness for a collector radius of 0.1 mm in a packed-bed

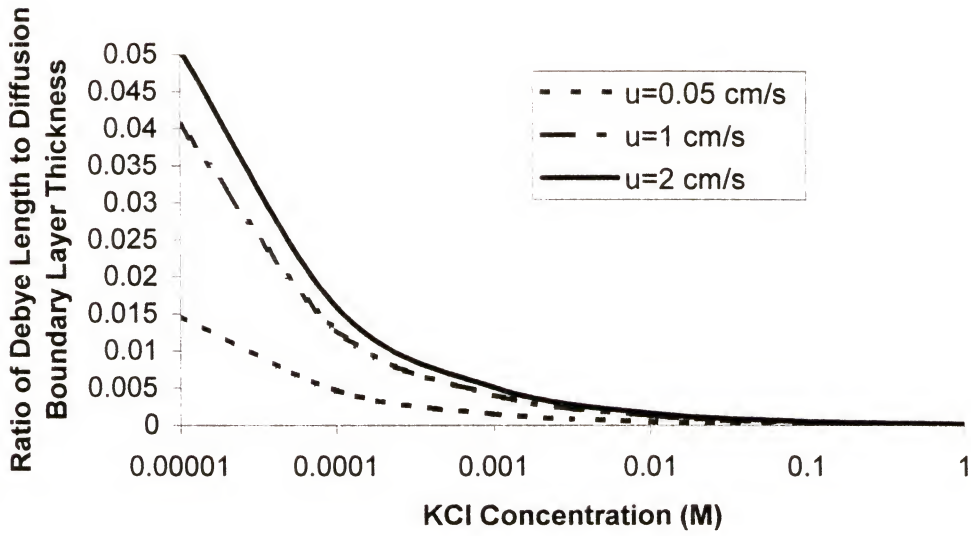

Figure 3-7. Ratio of Debye length to diffusion boundary layer thickness for a collector radius of 0.4 mm in a packed-bed

3-2 Model for Deposition in a Parallel Plate Flow Cell

Since the interaction force boundary layer approximation (IFBLA) appears valid for nearly all cases of interest in this work, a solution to this approximation is sought. As shown in section 2-3-3-2, a semi-analytical solution to the IFBLA can be obtained for a variety of geometries when gravity and hydrodynamic retardation are neglected. However, for large or dense particles gravity should not be disregarded, and the inclusion of hydrodynamic retardation in the interaction force boundary layer approximation may reduce the calculated deposition rate constant by orders of magnitude (Prieve and Ruckenstein 1976). Therefore, gravity and position-dependent diffusion coefficient will be considered in the scaling and solution to the deposition problem between flat plates.

3-2-1 Model Development

As mentioned, the distance over which surface forces act is typically much smaller than the bulk and diffusion length-scales, which creates difficulty in adequately solving for particle flux and concentration profiles. Therefore, dividing the problem into multiple length scales, and matching concentrations or fluxes at adjacent regions is appropriate. So the method of matched asymptotic expansion is employed here to solve the steady-state convective-diffusion equation (2.24) in a parallel plate flow cell.

Variables of the convective-diffusion equation are made non-dimensional by defining scales appropriate for each corresponding region, and a summary of the dimensionless variables is listed in Table 3-1. In all regions, the particle concentration is scaled by the bulk concentration c_0, and interaction potential ϕ is scaled by k_BT, and the coordinate in the direction of flow is scaled by the gap-width b. The natural length-scale for the coordinate normal to the surface is taken to be the gap-width b in the bulk region and the Debye length κ^{-1} in the surface force region. The normal-coordinate length-scale δ_D in the diffusion boundary layer is found by matching convective and diffusive terms in that region. The fluid velocity in each region is scaled by the average velocity and by the length-scale in the particular layer relative to the gap-width as shown in Table 3-1. Then by inspecting the dimensionless convective-diffusion equations for each region, leading-order terms are retained, and terms with smaller coefficients are eliminated as demonstrated in the following sections.

Table 3-1: List of dimensionless variables scaled for each of the three regions.

Region I: Bulk	Region II: Diffusion Boundary Layer	Region III: Surface Force Interaction Layer
$\tilde{y} = y/b$	$y^* = y/\delta_D$	$\bar{y} = y/\kappa^{-1}$
$\tilde{x} = x/b$	$x^* = x/b$	$\bar{x} = x/b$
$\tilde{u} = u/U$	$u^* = \frac{ub}{U\delta_D}$	$\bar{u} = \frac{ub}{U\kappa^{-1}}$
$\tilde{c} = c/c_0$	$c^* = c/c_0$	$\bar{c} = c/c_0$
$\tilde{\phi} = \phi/k_B T$	$\phi^* = \phi/k_B T$	$\bar{\phi} = \phi/k_B T$
	$\frac{\delta_D}{b} \sim Pe^{-1/3} = \left(\frac{Ub}{D_\infty}\right)^{-1/3}$	

3-2-1-1 Bulk region

Convection can be reasoned to be the dominant mechanism for particle transport in the bulk region for the case of large Peclet numbers. Usually, a uniform particle concentration is considered at the inlet of the flow cell:

$$\tilde{c} = 1 \qquad \text{at} \qquad \tilde{x} = 0 \tag{3.7}$$

The appropriate variable transformation of the convective-diffusion equation (2.24) yields the following dimensionless equation for two-dimensional, steady-state flow in the bulk region:

$$\tilde{u}\frac{\partial \tilde{c}}{\partial \tilde{x}} = \frac{1}{Pe}\left(\frac{\partial^2 \tilde{c}}{\partial \tilde{x}^2} + \frac{\partial^2 \tilde{c}}{\partial \tilde{y}^2}\right) + \frac{1}{Pe}\left(\frac{\partial \tilde{c}}{\partial \tilde{y}}\frac{\partial \tilde{\phi}}{\partial \tilde{y}} + \tilde{c}\frac{\partial^2 \tilde{\phi}}{\partial \tilde{y}^2}\right) + \frac{U_s}{U}\frac{\partial \tilde{c}}{\partial \tilde{y}} \tag{3.8}$$

Because Pe>>1, (3.8) can be reduced to

$$\tilde{u}\frac{\partial \tilde{c}}{\partial \tilde{x}} = 0 + O\left(Pe^{-2/3}; \frac{U_s}{U}\right) \tag{3.9}$$

Also, since the velocity $\tilde{u}$ is not uniquely zero, (3.9) implies that the concentration is uniform in the bulk:

$$\tilde{c} \approx 1 \tag{3.10}$$

3-2-1-2 Diffusion boundary layer

Similarly, properly scaling (2.24) for the diffusion boundary layer yields

$$u^* \frac{\partial c^*}{\partial x^*} = \frac{\partial^2 c^*}{\partial y^{*2}} + \frac{\partial c^*}{\partial y^*}\frac{\partial \phi^*}{\partial y^*} + c^* \frac{\partial^2 \phi^*}{\partial y^{*2}} + U_g \frac{\partial c^*}{\partial y^*}, \tag{3.11}$$

where $U_g = \frac{U_s}{U} Pe^{2/3}$. Also, since the interaction force layer is assumed to be small compared to the diffusion boundary layer, the interaction potential is neglected in the diffusion boundary layer. Thus, (3.11) is reduced to

$$u^* \frac{\partial c^*}{\partial x^*} = \frac{\partial^2 c^*}{\partial y^{*2}} + U_g \frac{\partial c^*}{\partial y^*}. \tag{3.12}$$

In (3.12) the gravity settling term U_g may or may not be negligible depending on the relative magnitue of the settling velocity U_s, which can be readily calculated from (2.23), to the average fluid velocity U in the bulk. In the present analyis, $\frac{U_s}{U}$ is determined to be approximately $O(Pe^{-2/3})$ for 1 μm-diameter silica particles, so the gravity term is retained.

3-2-1-3 Surface force region

Finally, the convective-diffusion equation, along with the boundary conditions at the inlet and at the surface in the surface force region can be recast in dimensionless form as

$$\bar{u}\frac{\partial \bar{c}}{\partial \bar{x}} = \left(\frac{b}{\kappa^{-1}}\right)^3 \frac{1}{Pe}\left[\frac{\partial^2 \bar{c}}{\partial \bar{y}^2} + \frac{\partial}{\partial \bar{y}}\left(c\frac{\partial \bar{\phi}}{\partial \bar{y}}\right)\right] + \frac{U_s}{U}\left(\frac{b}{\kappa^{-1}}\right)^2 \frac{\partial \bar{c}}{\partial \bar{y}}, \tag{3.13a}$$

$$\text{At } \bar{y} = 0, \qquad \bar{c} = 0 \tag{3.13b}$$

$$\text{At } \bar{x} = 0, \qquad \bar{c} = 1 \tag{3.13c}$$

Since the interaction force boundary layer approximation requires that $Pe^{-1/3} >> \frac{\kappa^{-1}}{b}$,

and since $\frac{U_s}{U} \sim O(Pe^{-2/3})$, (3.13a) simplifies to

$$\frac{\partial}{\partial \bar{y}}\left(\bar{c}\frac{\partial \bar{\phi}}{\partial \bar{y}} + \frac{\partial \bar{c}}{\partial \bar{y}}\right) = 0. \tag{3.14}$$

Equation (3.14), along with boundary condition (3.13b), is integrated to yield

$$\bar{c} = -\exp(-\bar{\phi})J(\bar{x})\left[\int_0^{\bar{y}} \exp(\bar{\phi})d\bar{y}'\right], \tag{3.15a}$$

which can also be written as

$$\bar{c} = -\exp(-\bar{\phi})J(\bar{x})\left[\int_0^{\bar{y}} (\exp(\bar{\phi}) - 1)d\bar{y}' + \bar{y}\right] \tag{3.15b}$$

For the outer region of the surface force region, i.e. as $\bar{y} \to \infty$,

$$\bar{c}(\bar{y} \to \infty) = -J(\bar{x})\left[\int_0^{\infty} (\exp(\bar{\phi}) - 1)d\bar{y}' + \bar{y}\right] \tag{3.16}$$

Now, the outer region of the surface force region is recognized as being matched with the inner region of the diffusion boundary layer such that (3.16) can be written as

$$c^*(y^* = 0) = -J^*(x^*)\left[\int_0^{\infty} (\exp(\bar{\phi}) - 1)d\bar{y}'\right] \tag{3.17}$$

3-2-1-4 Matched, leading-order problem

The resulting equations from each of the regions are now matched to yield one set of differential equations for the particle concentration in the diffusion boundary layer with the outer boundary condition coming from the bulk region and the surface boundary condition coming from the surface force region. Thus, the leading-order problem cast in terms of the diffusion boundary layer variables, in which the velocity profile has been linearized, is

$$6y^* \frac{\partial c^*}{\partial x^*} = \frac{\partial^2 c^*}{\partial y^{*2}} + U_g \frac{\partial c^*}{\partial y^*} \tag{3.18a}$$

$$\text{At } x^*=0, \qquad c^* = 1 \tag{3.18b}$$

$$\text{As } y^* \to \infty, \qquad c^* \to 1 \tag{3.18c}$$

$$\text{At } y^* = 0, \qquad \frac{\partial c^*}{\partial y^*} = c^*(k - U_g) \tag{3.18d}$$

where

$$k = 1/\int_0^\infty \{\exp(\bar{\phi}) - 1\} d\bar{y} . \tag{3.18e}$$

An analytical solution to this problem is not available, so a numerical solution was sought using the Crank-Nicolson finite difference method as described in 5-6 and by Hoffman (1989).

3-2-2 Model Predictions

3-2-2-1 Convective-diffusion limit

In the absence of repulsive colloidal interactions, the deposition process is transport-controlled, i.e. once a particle becomes sufficiently close to a surface such that attractive surfaces forces are significant, the particle will deposit. Such a case is

mathematically equivalent to a perfect sink boundary condition and to the condition of a large deposition rate constant in the interaction force boundary layer approximation. Figure 3-8 shows that the flux predicted by the IFBLA matches the flux predicted by the Smoluchowski-Levich solution (Eq. 2.31) as the deposition rate constant k approaches infinity when neglecting gravity and hydrodynamic retardation. The agreement shown in Figure 3-8 is not surprising, but it lends credibility to the numerical scheme used to solve equations (3.18a-e).

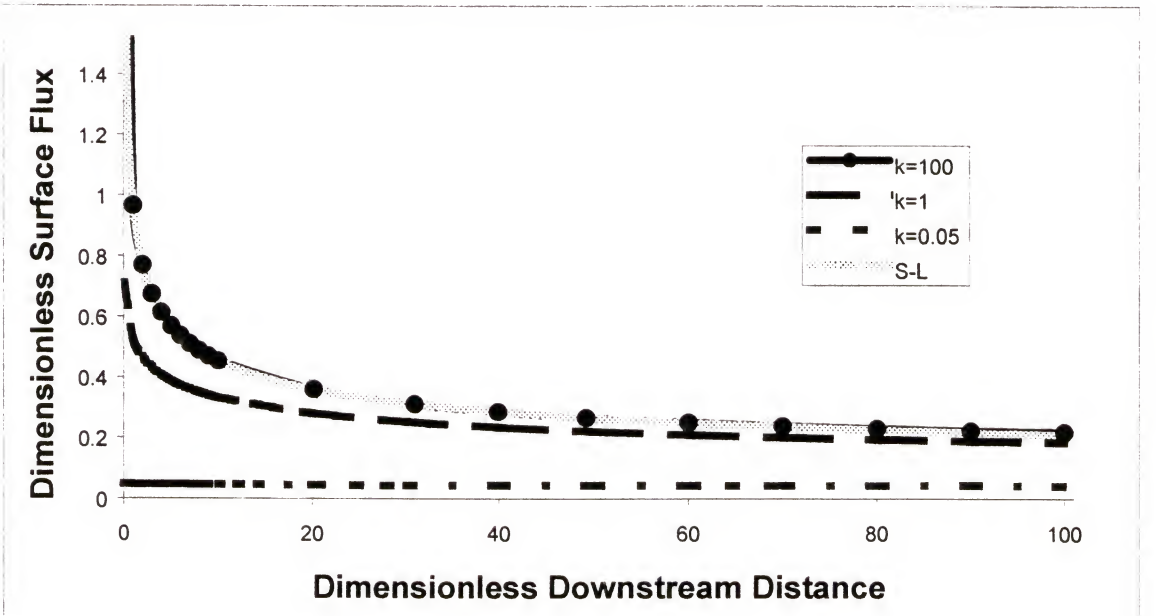

Figure 3-8. Particle surface flux in the absence of gravity is shown as a function of downstream distance in a parallel plate flow cell for several values of k. For large k, numerical results agree well with the analytical solution of the Smoluchowski-Levich solution (2.31).

Since the density of the silica particles used in this work is about twice that of the suspending electrolyte solution, the gravity term, which scales to the square of particle radius and to the negative one-third power of fluid velocity, should be considered. The

particle flux will decrease as the fluid velocity increases when gravity is significant, but for the case in which gravity is insignificant, the flow rate will not significantly affect the deposition rate to a flat plate, assuming the hydrodynamic force does not overwhelm the colloidal interactions. Figure 3-9 shows that the effect of fluid velocity is much more significant for 1 μm-diameter silica particles than for 0.5 μm particles. Flow an average fluid velocity above about 1 cm/s, the deposition rate of 0.5 μm silica particles is not affected by the flow rate. Such effects are likely to be observed in a packed-bed filter, so 0.5 μm silica particles will be used for filtration experiments to make use of the semi-analytical solution of Spielman and Friedlander (1976) in section 2-3-3.2, which neglects gravity.

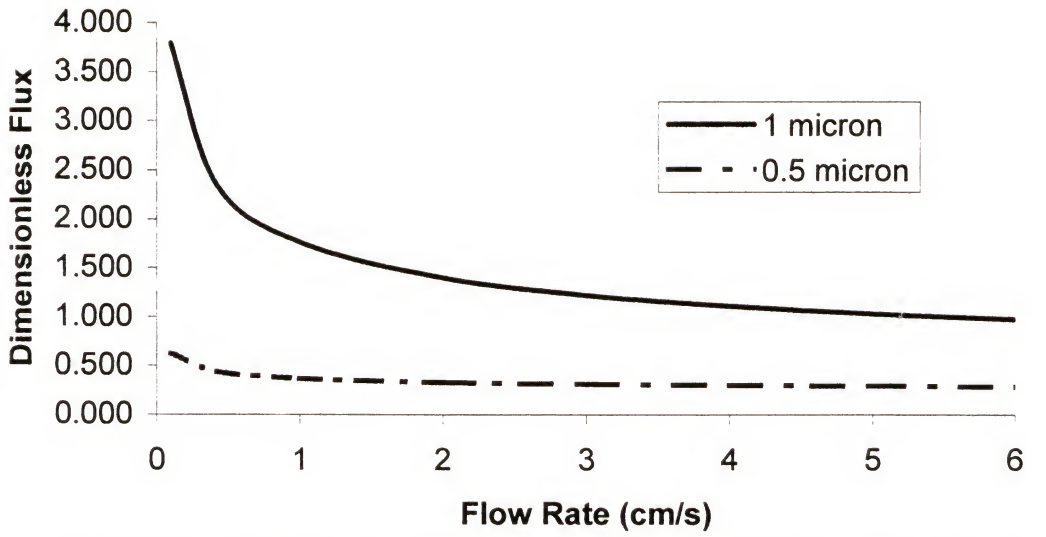

Figure 3-9. The influence of fluid velocity on dimensionless surface Flux in a parallel plate flow cell for 0.5 and 1.0 micron diameter silica particles in the transport-limited regime

The size of a colloidal particle drastically affects the deposition behavior in both the transport- and interaction-controlled regimes. Figure 3-10 shows the effect of particle radius on the flux of spherical particles with a specific gravity of 2.0 in a parallel plate flow cell when the deposition is controlled by transport, i.e. when no barrier to interaction is present and when the surface is considered a perfect sink. For small particles (e.g., a radius of 50 nm), diffusion is the dominating transport mechanism, whereas gravity is the controlling transport mechanism for larger particles (e.g., a radius of 0.5 μm). Figure 3-10 shows a minimum in the flux for particles with a radius of about 0.2 μm. No

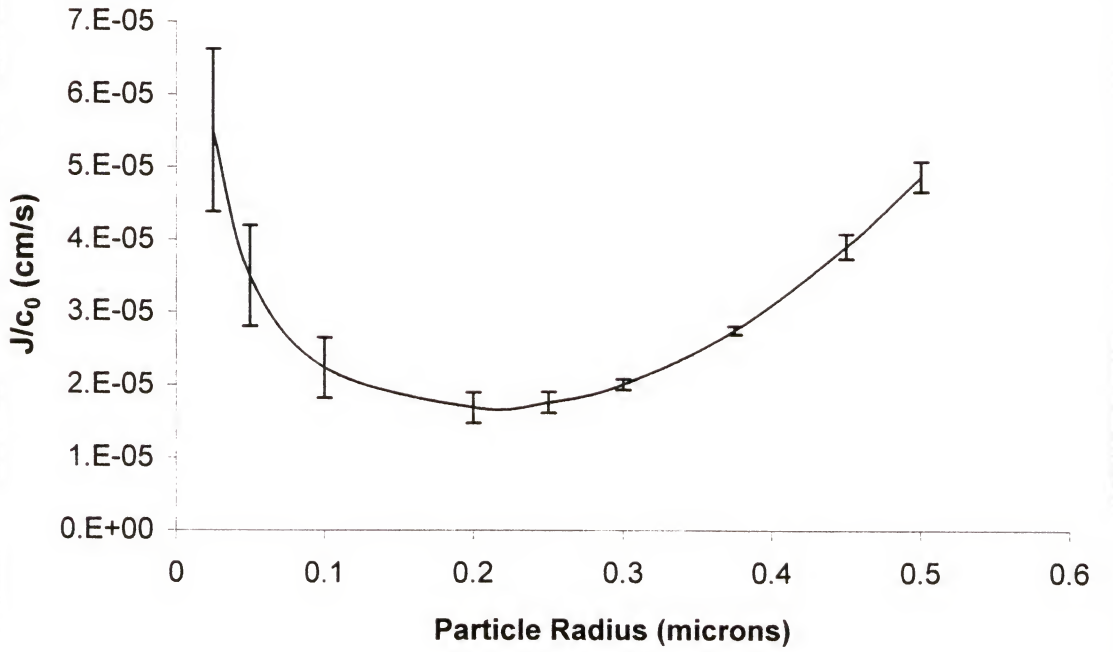

Figure 3-10. Effect of particle size on the flux of spherical particles with a specific gravity of two in a parallel plate flow cell.

minimum is observed for neutrally buoyant particles depositing to a flat plate, as illustrated in Figure 3-11. In a packed-bed, however, such minima are seen at a particle

diameter of about 1 μm even for neutrally buoyant particles (Elimelech et al. 1995). The reason for these minima is that as the particle size increases above about 1 μm, the inertia of the particle becomes significant, thus giving an increase in filtration rates. Therefore, error bars for several positions in each of these figures indicate standard deviations of the average fluxes. Since the particle flux is dependent on position, the average values shown in Figures 3-10 through 3-12 all have some error associated with them.

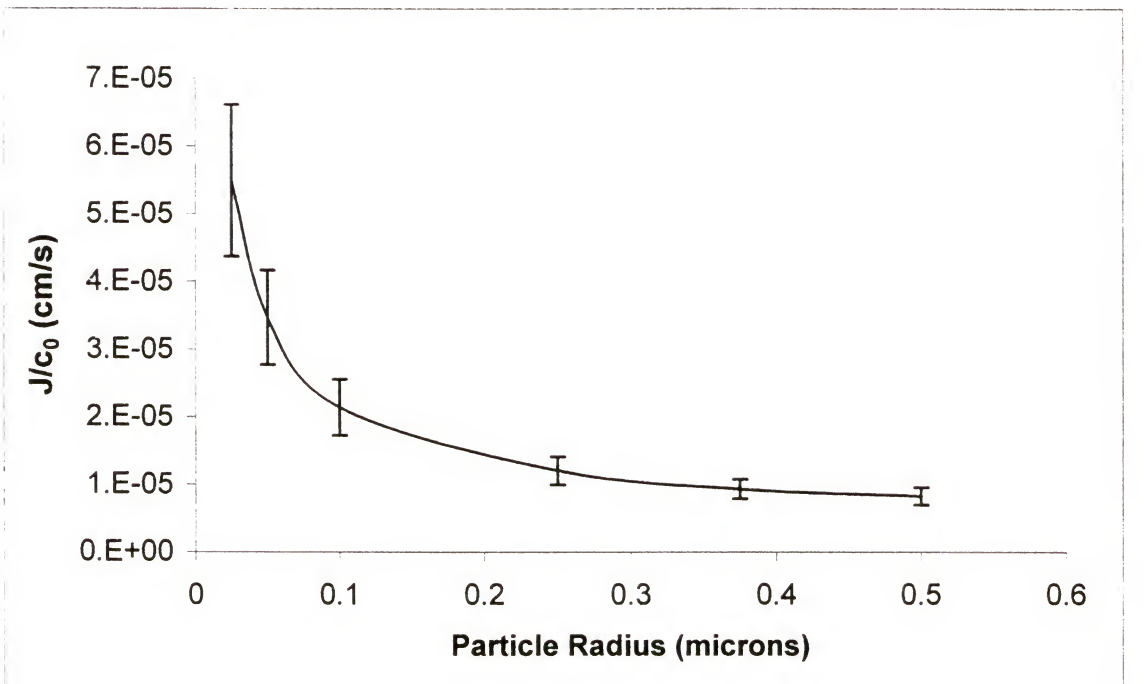

Figure 3-11. Effect of particle size on the flux of spherical particles in the absence of gravity.

Also, the divergence between the dimensional and dimensionless flux values is worth mentioning at this point. Because the diffusion boundary layer length scale contains the particle size and fluid velocity, the behavior depicted by the dimensionless flux can be misleading. For instance, in Figure 3-11, the dimensionless flux is plotted

against the particle radius for spherical particles with a specific gravity of 2.0, similar to Figure 3-10. However, no minimum is observed in the plot of dimensionless flux because the scaling factor contains the particle size. Therefore, one should be cautious in interpreting the results expressed in dimensionless quantities as phenomena observable in dimensional values.

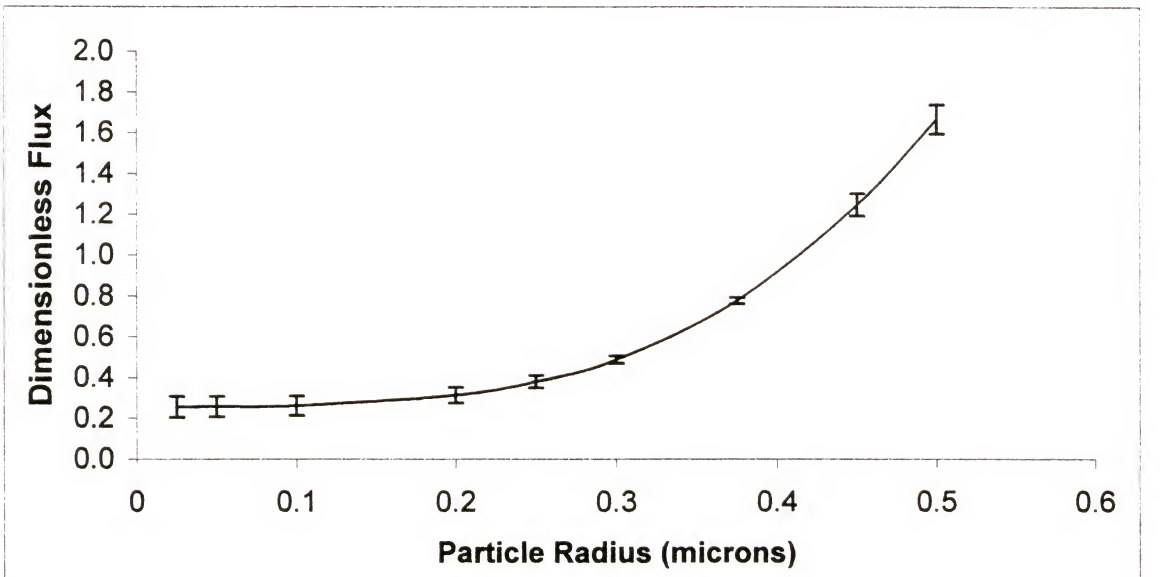

Figure 3-12. The dimensionless flux dependence on particle radius in the presence of gravity.

Particle concentration profiles in a parallel plate flow cell can be valuable in interpreting the influence of system parameters, such as gravity or the deposition rate constant, on deposition behavior. As such, Figures 3-13 and 3-16 compare the calculated concentration profiles obtained for 0.5 μm-diameter particles in the presence and absence of the gravitational settling term for a large and small deposition rate constant, respectively. Figure 3-13 reveals that there is a depletion of particles near the surface, as compared to the bulk, when the deposition is transport-controlled, whether or not gravity

is included. For particles that settle due to gravity, the depletion is less extreme; in other words, the gravitational force enhances the transport of particles to the surface.

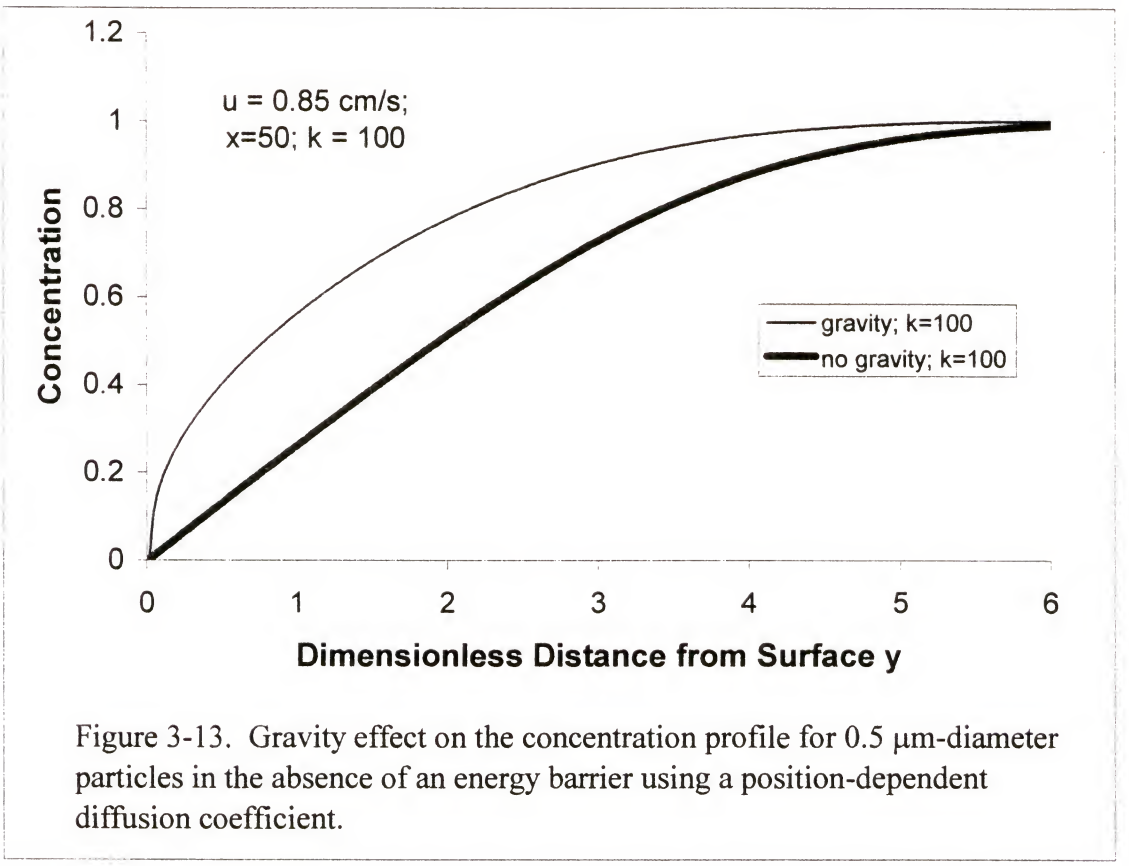

Figure 3-13. Gravity effect on the concentration profile for 0.5 μm-diameter particles in the absence of an energy barrier using a position-dependent diffusion coefficient.

3-2-2-2 Surface interaction controlled deposition

The flux of colloidal particles is reduced in the presence of a significant repulsive barrier. The deposition rate constant of the interaction force boundary layer approximation is indicative of the magnitude of the repulsive barrier. A large deposition rate constant corresponds to the lack of an energy barrier between particle and collector, and a small deposition rate constant corresponds to a large barrier to deposition. Figures 3-14 and 3-15 show the effect of the deposition rate constant on the flux of 1 μm and 0.5 μm-diameter silica particles, respectively.

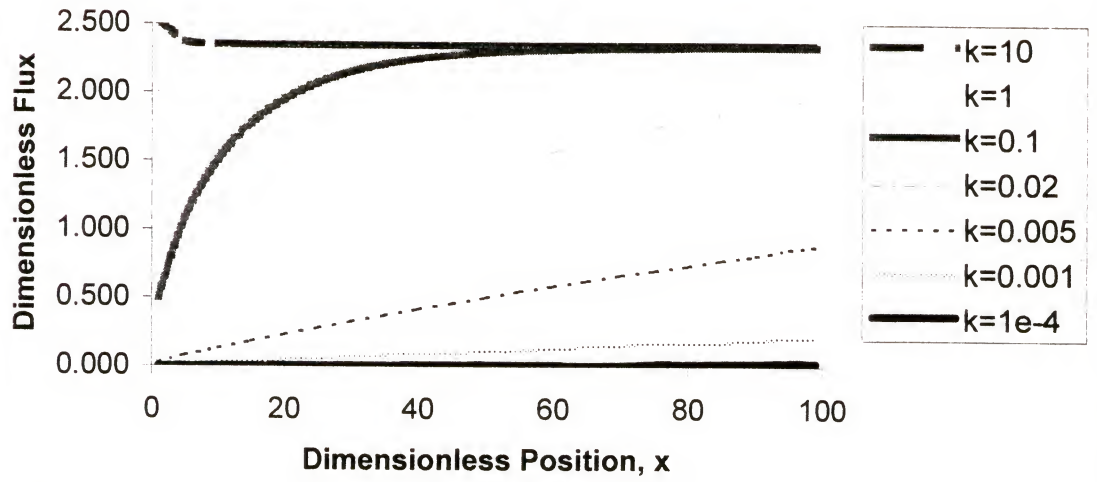

Figure 3-14. The calculated flux of 1.0 μm-diameter silica particles for a wide range of deposition rate constants in the absence of hydrodynamic retardation.

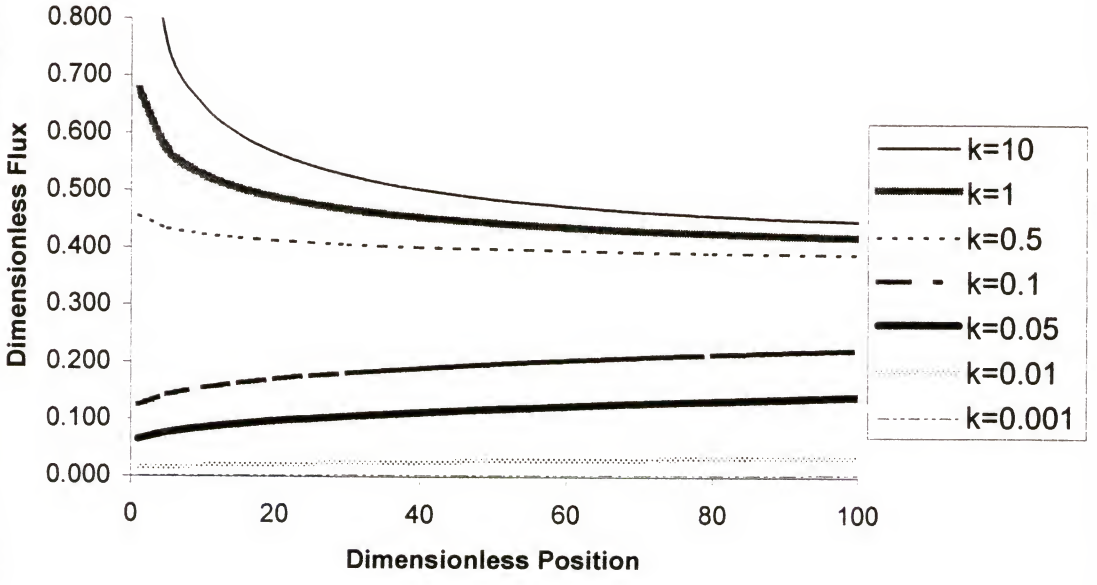

Figure 3-15. The calculated flux of 0.5 μm-diameter silica particles for a wide range of deposition rate constants in the absence of hydrodynamic retardation.

The calculated concentration profile for a case in which the deposition is controlled by repulsive colloidal interactions is depicted in Figure 3-16. Here, the accumulation of particles near the surface due to sedimentation can be seen. When gravity is neglected, however, only a very slight depletion near the surface as compared to the bulk is observed. Also, if the gravity term is equivalent to the deposition rate constant, the concentration profile is flat and the flux of particles towards the surface is determined by sedimentation.

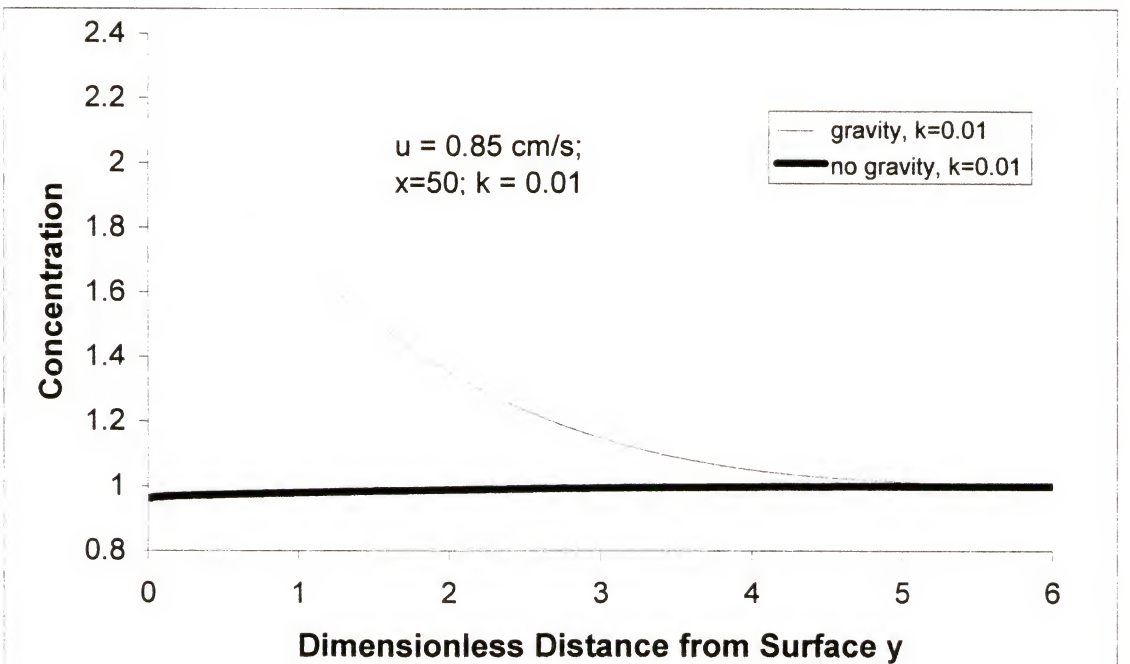

Figure 3-16. Gravity effect on the concentration profile for 0.5 μm-diameter particles in the presence of an energy barrier using a position-dependent diffusion coefficient.

The predicted flux of 0.5 μm-diameter silica particles midway downstream in the flow channel is shown in Figure 3-17 as a function of the deposition rate constant k. For deposition rate constants near ten, the flux is seen to be transport-controlled, and further

increase in the rate constant does not increase the flux. These results are compared to experimental deposition rates to extract deposition rate constants, which are used to predict filtration rates.

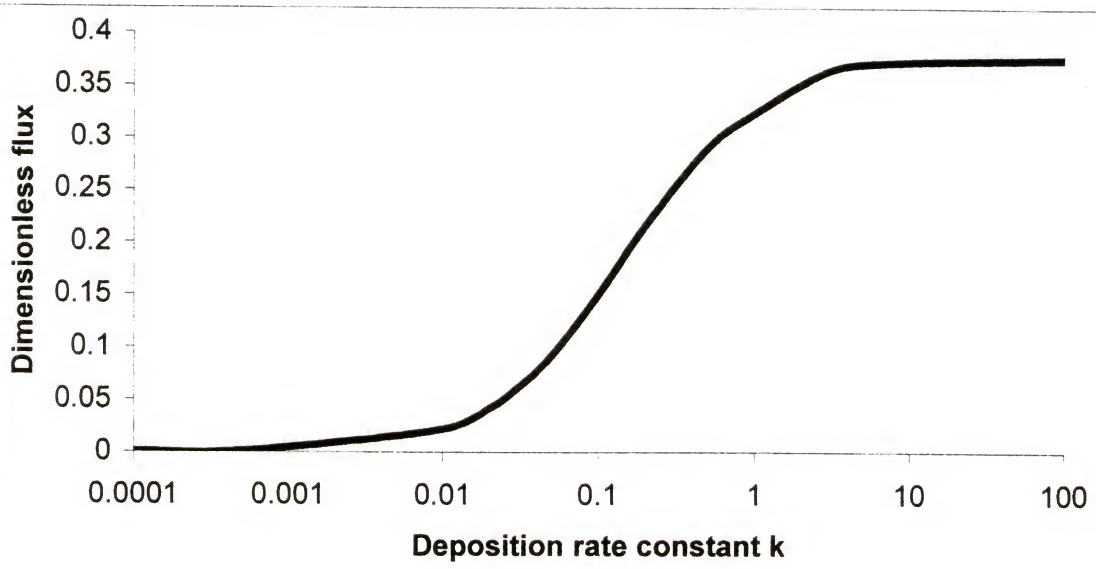

Figure 3-17. Predicted flux of 0.5 mm-diameter silica particles in the center of the parallel plate flow channel.

3-2-2-3 Effect of hydrodynamic retardation

Because diffusion is a dominant mechanism for the deposition of colloidal particles, hydrodynamic retardation near the surface is expected to affect the rate at which particles are collected. The solution for the position-dependent diffusion coefficient developed by Brenner (1961) predicts a diffusion coefficient of zero at the surface, but a particle needs only approach close enough to the surface such that colloidal forces dominate. Since the outer limits of the surface force region corresponds to the wall surface in the model, Brenner's correction should be adjusted such that the surface in the model corresponds to a non-zero diffusion coefficient or a finite drag force. Therefore,

the position used to calculate the correction factor to Stokes' law for drag should be offset from the position used in the model. Figure 3-18 shows the effect of the magnitude of this offset on the flux in a parallel plate flow cell. As the size of the offset decreases, so does the flux, which is expected since an offset of zero corresponds to the case of no diffusion at the surface and since a large offset corresponds to the case in which hydrodynamic retardation is disregarded. For purposes of comparing experimental and theoretical results, the Debye length is used as the offset, as in section 3-3.

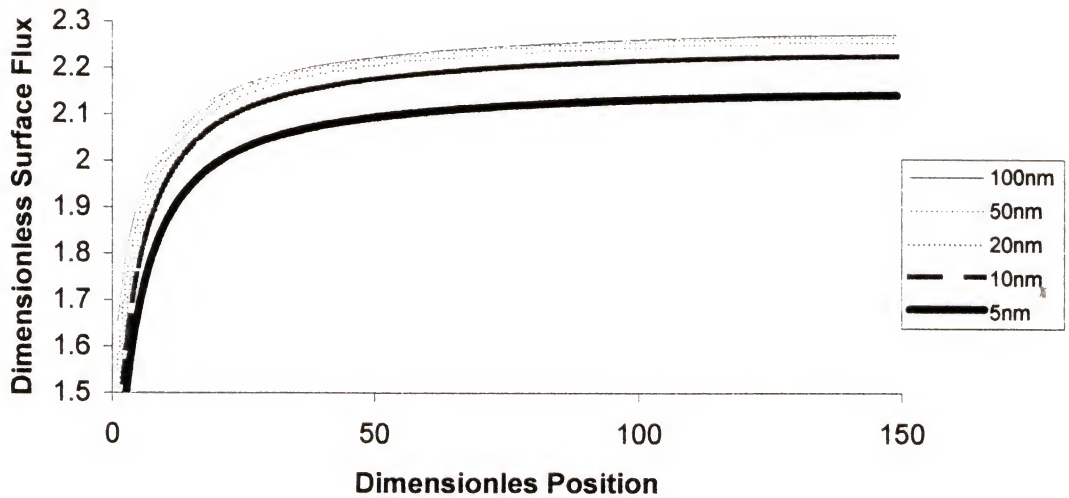

Figure 3-18. The transport-limited flux of 1 mm-diameter silica particles with and without the inclusion of hydrodynamic retardation for various offset value parameters.

A comparison of the calculated concentration profiles for constant and position-dependent diffusion coefficients is shown in Figure 3-19 for 1 μm-diameter silica particles in the absence of an energy barrier. For the case in which the diffusion coefficient is taken to be constant, the particle concentration is depleted near the surface and gradually increases to the bulk concentration some distance away from the surface.

However, when Brenner's correction to Stokes' law is considered, the particle concentration has a maximum a small distance from the surfaces, as shown in Figure 3-19. This maximum appears because hydrodynamic retardation causes the diffusion coefficient to become very small near the surface, resulting in a bottle-neck-type behavior. In other words, particles far from the surface in the diffusion boundary layer are able to diffuse towards the surface rather quickly but are slowed near the surface due to the increased drag.

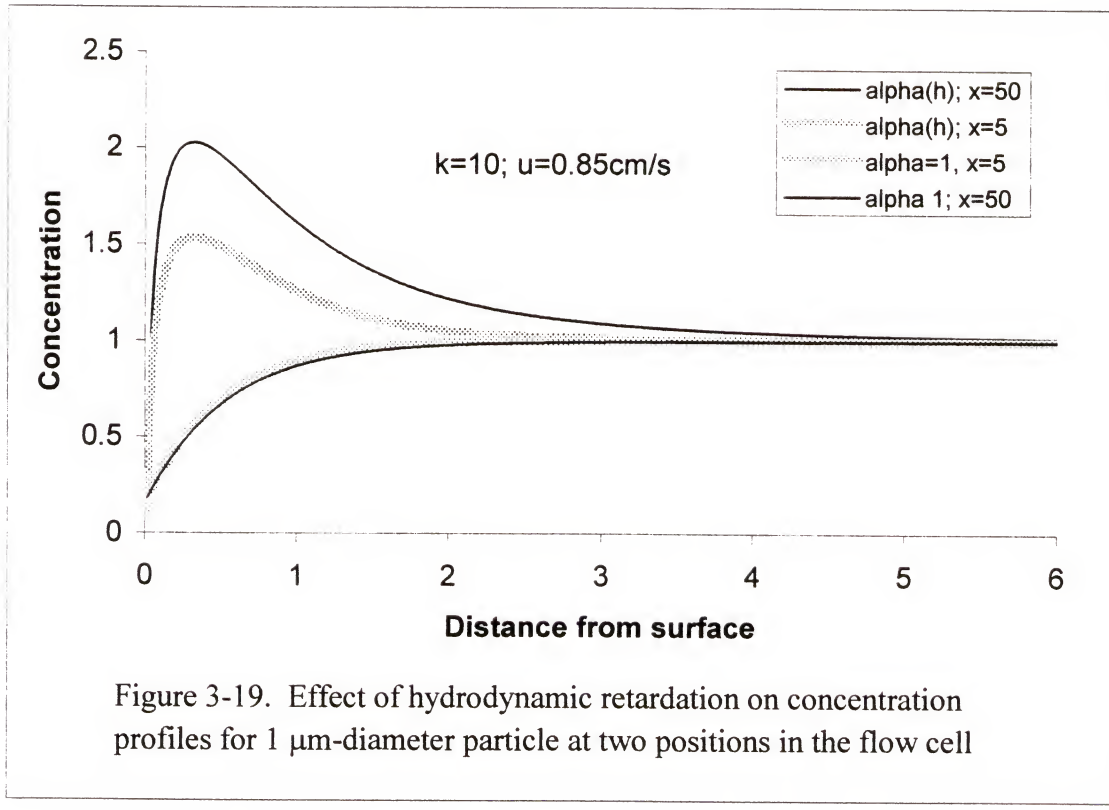

Figure 3-19. Effect of hydrodynamic retardation on concentration profiles for 1 μm-diameter particle at two positions in the flow cell

Because an analytical solution to the problem of particle collection in a packed-bed is desired, an equivalent, constant correction to Stokes' law is sought. The calculated flux profiles of 0.5 μm-diameter silica particles in a parallel plate flow cell are compared for various correction factors in Figure 3-20. While no constant correction factor gives

an exact profile match to Brenner's correction, choosing an alpha of 1.3 yields an average flux that is within two decimal places of the average calculated using the position-dependent correction. Therefore, the constant alpha value of 1.3 is used to calculate filter coefficients for 0.5 μm-diameter particles in a packed-bed.

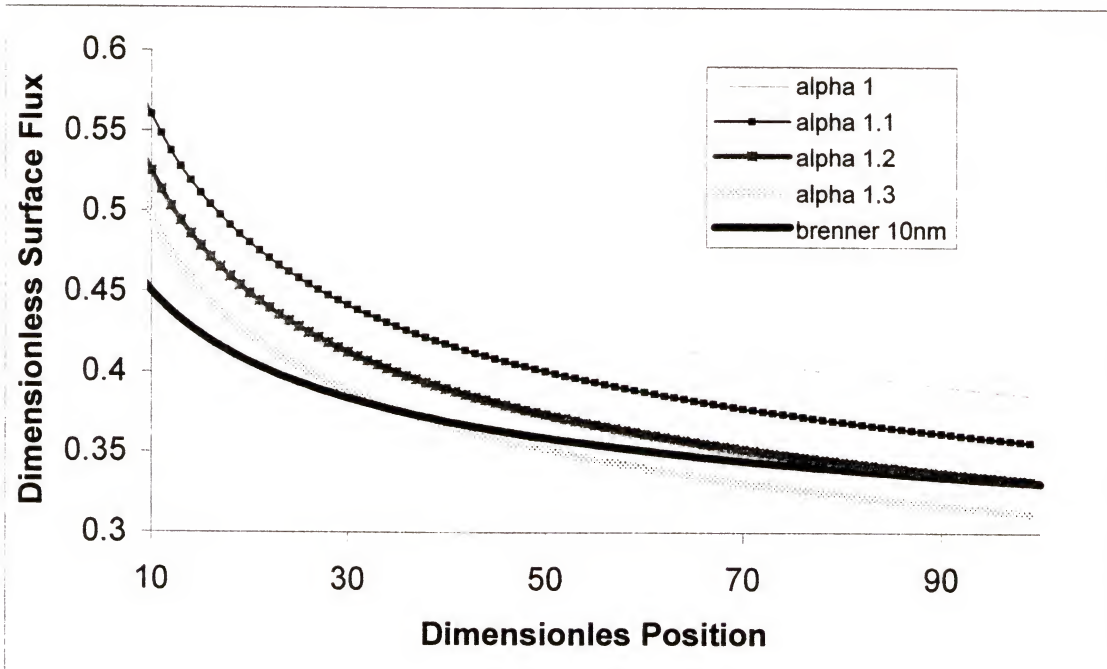

Figure 3-20. Comparison of calculated flux for 0.5 μm-diamter silica particles in a parallel plate flow cell for constant and position dependent corrections to Stokes' drag on a shpere.

3-3 Experimental Results

3-3-1 Concentration Effect

The flux of colloidal silica to a flat plate was seen to follow first-order deposition kinetics with respect to the bulk particle concentration. The deposition rate of 1 μm silica particles in a parallel plate flow channel was seen to have a linear dependence on particle concentration whether the rate was limited by transport or repulsive colloidal interactions.

Figure 3-21 shows the concentration dependence for the flux of 1 μm silica particles for two different concentrations of pH. The case of pH 2.7 represents the transport-limited regime since electrostatic repulsion is negligible near the isoelectric point, and the case of

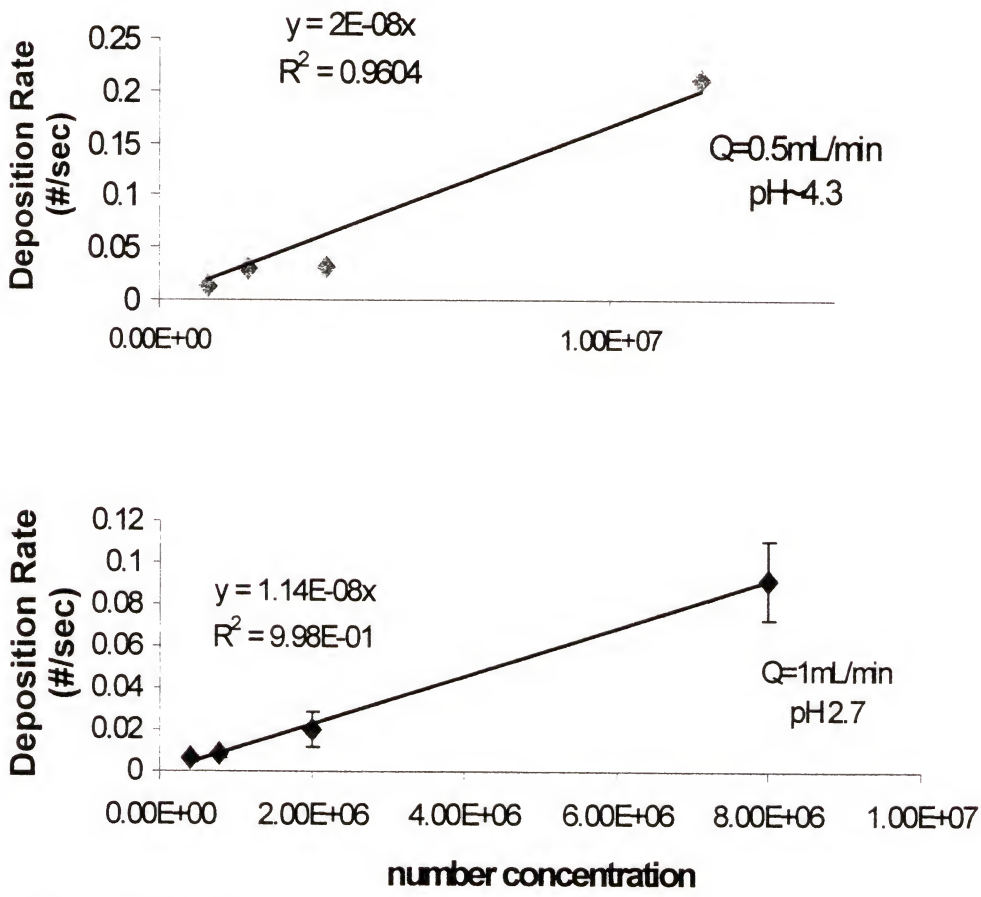

Figure 3-21. The deposition rate dependence on concentration: a)pH 4.3 is a colloidal-interaction limited case and b)pH 2.7 corresponds to a transport-limited regime.

pH 4.3 is an example in which electrostatic repulsion is significant. The linear dependence of particle flux on concentration seen in Figure 3-21 is an indication that the

deposition kinetics are first-order as described by the IFBLA and as assumed in filtration models.

3-3-2 Flow Rate Effect

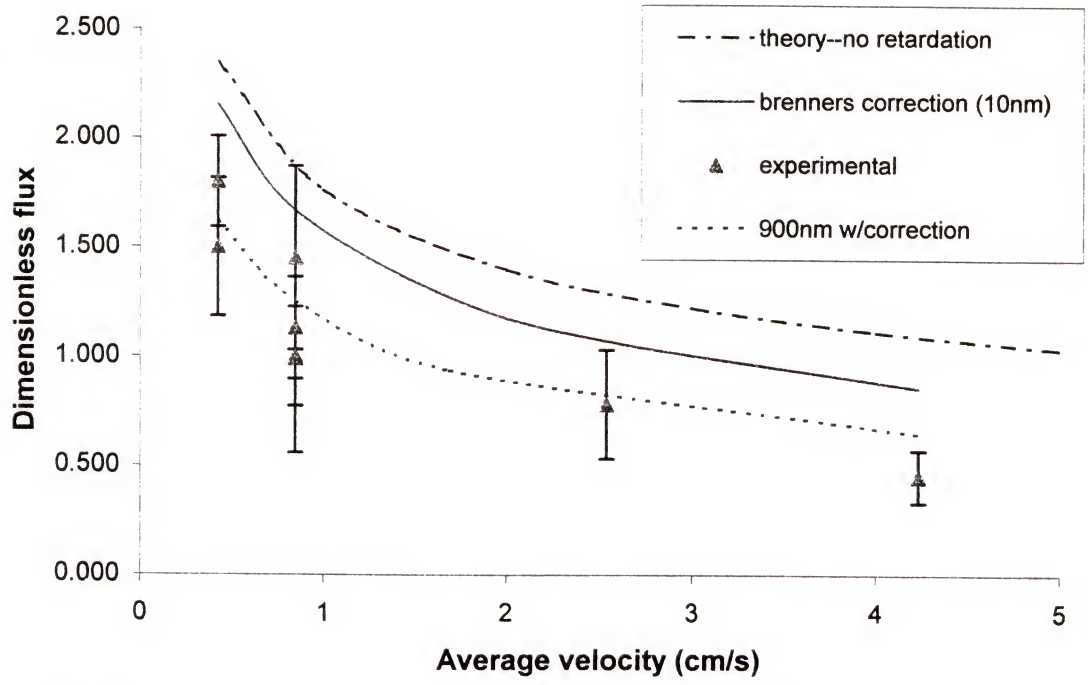

Figure 3-22. Comparison of experimental data to flux predicted using the interaction force boundary layer approximation.

The flux of 1 μm silica particles in a 1 mM potassium chloride solution at pH 2.7, which is close to the isoelectric point of silica particle and glass (see Figure 5-13), is shown in Figure 3-22. As predicted, an increase in flow rate was seen to result in the decrease of the flux of 1 μm silica particles. As previously mentioned, when electrostatic repulsion is negligible, as should be the case near the isoelectric point of the collector or particles, the deposition rate is expected to be transport-controlled. So, the data in Figure 3-22 is compared to the convective-diffusion limit for 1 μm particles with and without

the inclusion of hydrodynamic retardation. The data is also compared to the convective-diffusion limit for particles with a diameter of 0.9 μm, which is one standard deviation below the mean particle size. Clearly, the experimental data is in reasonable agreement with predictions based on the interaction force boundary layer approximation for a deposition rate constant of 10.

3-3-3 Position-Dependent Flux

As shown in Figure 3-14, the calculated flux of 1 μm-diameter silica particles is dependent on the position in the flow cell when a barrier to deposition is present but independent of position when the deposition is transport-controlled. In Figure 3-23, experimental measurements at various values of pH qualitatively verify these behaviors.

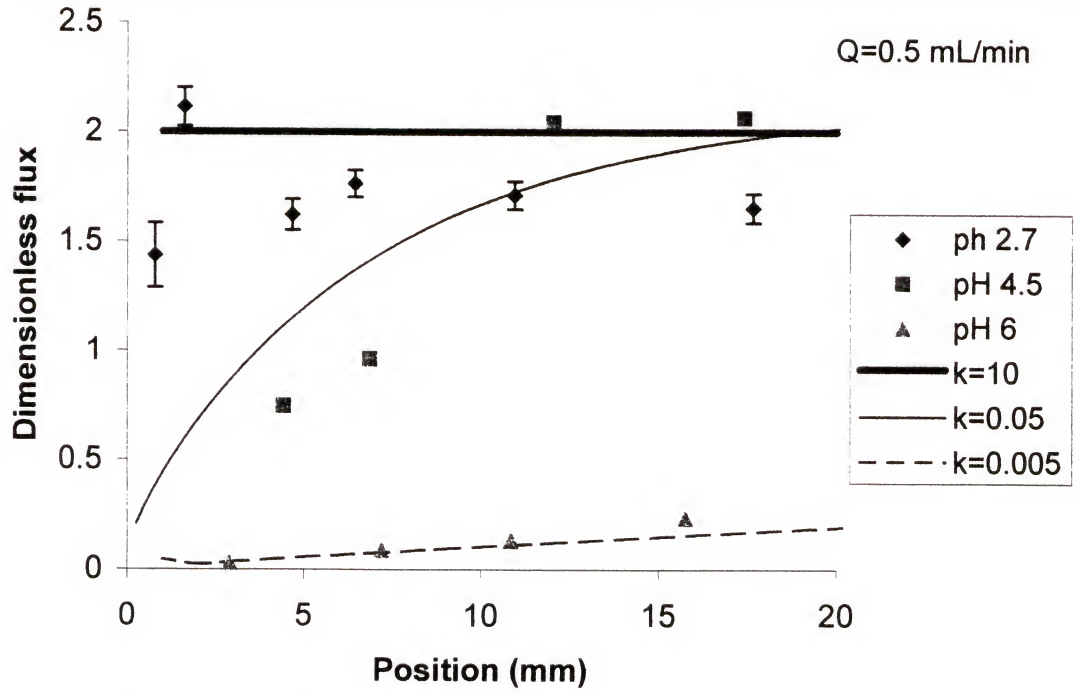

Figure 3-23. Comparison of experimentaly and calculated position-dependent behavior of 1 μm-diameter silica particles in a flow cell.

At pH 2.7, which is near the isoelectric point of the silicates, the flux is seen to be relatively independent of position. At pH 4.5 and 6, however, the particle flux shows a strong dependence on position. Theoretically, this behavior provides a good means of extracting deposition rate constants, but the scatter in the data is often too large to reliably do so.

As shown in Figure 3-14, the flux is not expected to vary with downstream position in the flow cell when deposition is transport controlled. In general, such behavior was observed experimentally, but a fairly large scatter in the data was seen. For

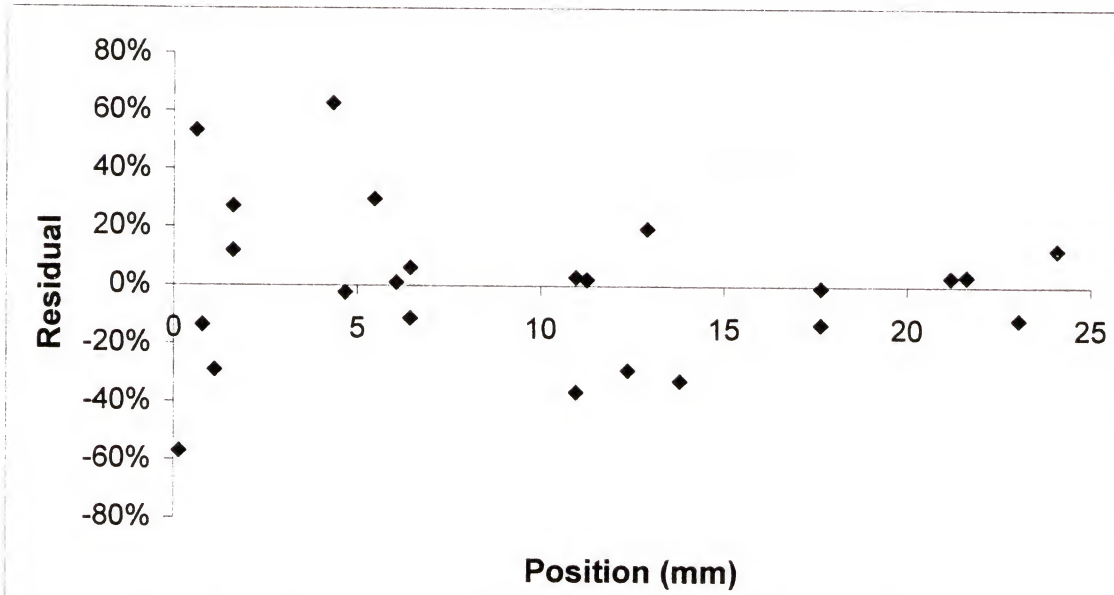

Figure 3-24. Position dependence of deviation from the average flux for the deposition of 1 μm-diameter silica particles at pH 2.7-2.8.

1 μm-diameter silica particles at pH 2.7-2.8, the deviation of individual flux measurements from the average of these measurements is shown in Figure 3-24. Here, the deviation or residual value is generally seen to be smaller downstream in the flow cell

than near the entrance. Also, the residuals are not seen to be either positively or negatively biased.

3-3-4 Dependence on pH

As the pH is increased from the isoelectric points of the colloidal particles and glass substrates, repulsive electrostatic barrier between the particle and substrate becomes increasingly significant. Therefore, the flux of silica particles is expected to decrease as pH is increased from the transport-limited case at low pH near the isoelectric point.

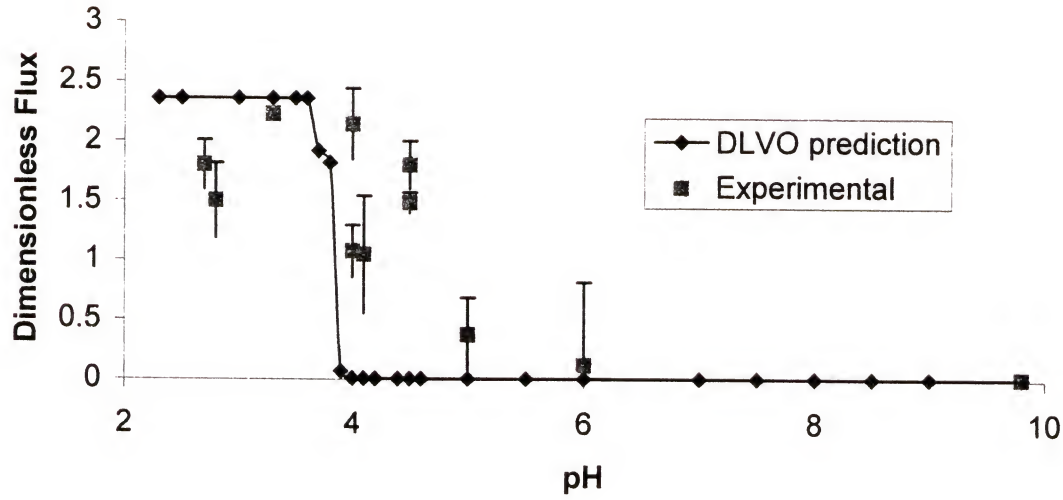

Figure 3-25. The flux of 1 mm-diameter silica particle averaged for several positions in a parallel plate flow cell. The experimental dependence on pH is much more gradual than that predicted by DLVO theory based on a fit of the

Figures 3-25 and 3-26 show that the experimentally measured particle flux in a parallel plate flow channel gradually decreases as the pH is increased for 1.0 and 0.5 μm-diameter silica particles, respectively. The gradual decrease is in contrast to the drastic reduction predicted by DLVO theory based on a fit of the measured zeta potentials, as seen in Figure 3-25. Figure 3-26 shows the effect of pH on the flux 0.5 μm-diameter

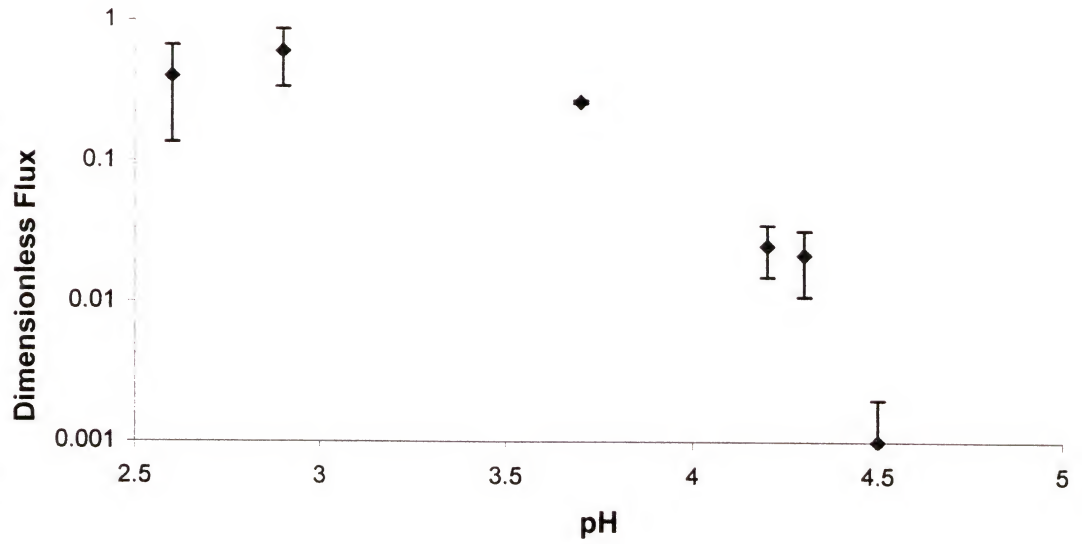

Figure 3-26. The effect of pH on the flux of 0.5 mm-diameter silica particles in a parallel plate flow cell.

silica particles in the center of the flow channel. As mentioned in 2-4, this is in keeping with the findings of other researchers for a wide variety of geometries. By comparing the results of Figure 3-26 to predicted deposition rates in Figure 3-17, deposition rate constants were extracted, and then these extracted rate constants were used to predict filtration rates with the effective medium approximation for comparison to experimental filter coefficients in section 4-3.

CHAPTER 4
VERIFICATION OF FILTRATION MODEL

The filtration of colloidal silica has been carried out in columns packed with spherical glass beads under a variety of physicochemical conditions. The filtration coefficients obtained from these experiments were compared to a filtration model based on the effective medium approximation, as described by Li and Park (2000) and in section 2-3-3. Good agreement was seen between predictions and experimental observations over a wide range of pH when independently measured deposition rate constants were applied to the effective medium approximation, as opposed to using deposition rate constants predicted by DLVO theory.

4-1 Predictions from Effective Medium Approximation

Filtration coefficients for various flow rates, collector sizes and deposition rate constants were calculated using the effective medium approximation model, Happel's model and Brinkman's model. Figure 4-1 shows the effect of collector size and deposition rate constant on the filter coefficient for 1 μm-diameter particles for all three models. As expected, smaller collector sizes correspond higher filtration rates, and a large deposition rate corresponds to a high filtration rate. Figure 4-1 also illustrates that once the deposition rate constant exceeds a certain value, filtration can not be enhanced with further increase in the rate constant. The predicted effect of superficial velocity on filtration rates is shown in Figure 4-2 for multiple values of the deposition rate constant. Figure 4-3 shows the effect of pH on filter coefficients for Happel's, Brinkman's and the

effective medium approximation models using DLVO theory to calculate deposition rate constants based on measured zeta potentials, which are shown in Figure 5-13. The predicted filtration rates in Figure 4-3 are seen to have a very sharp dependence on pH for all the filtration models, and the models can not be distinguished above about pH 3.9. A more detailed analysis of the effect of physicochemical parameters on predictions based on the effective medium approximation can be found in Li and Park (2000) and Li (1998).

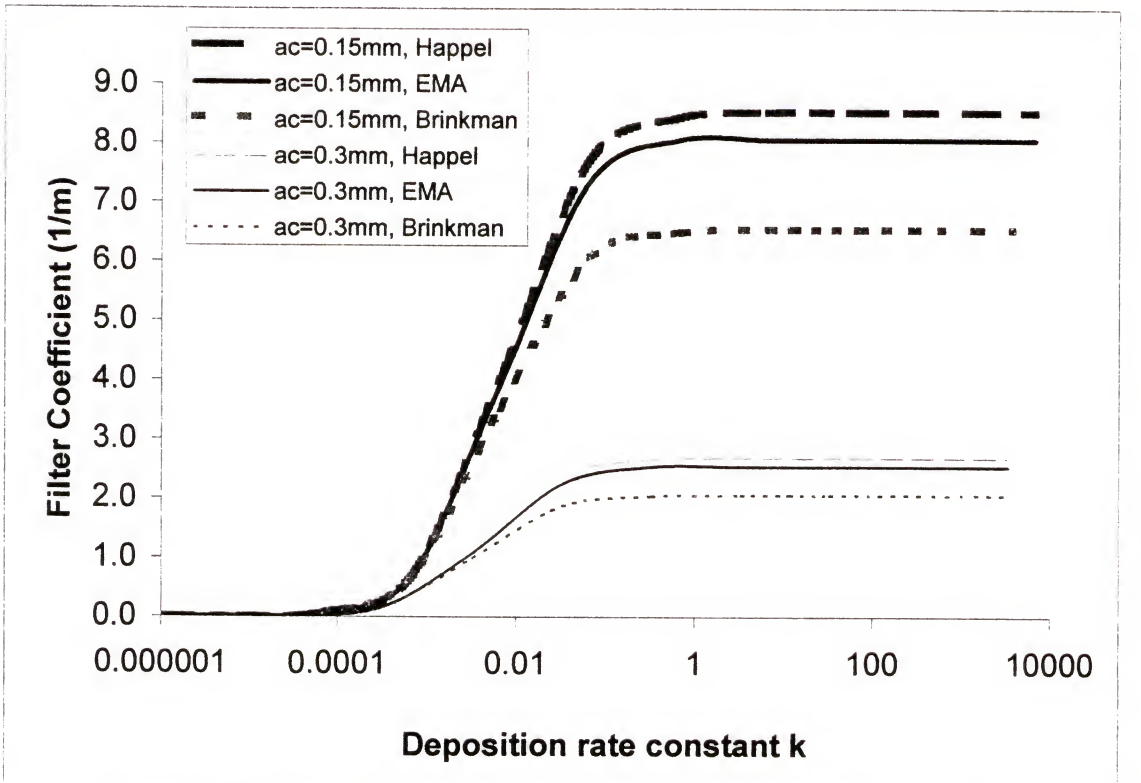

Figure 4-1. Effect of deposition rate constant on filter coefficient of 0.5 μm-diameter particles collected by both 0.15 and 0.3 mm-radius spheres in a packed bed at a superficial velocity of 1 mm/s.

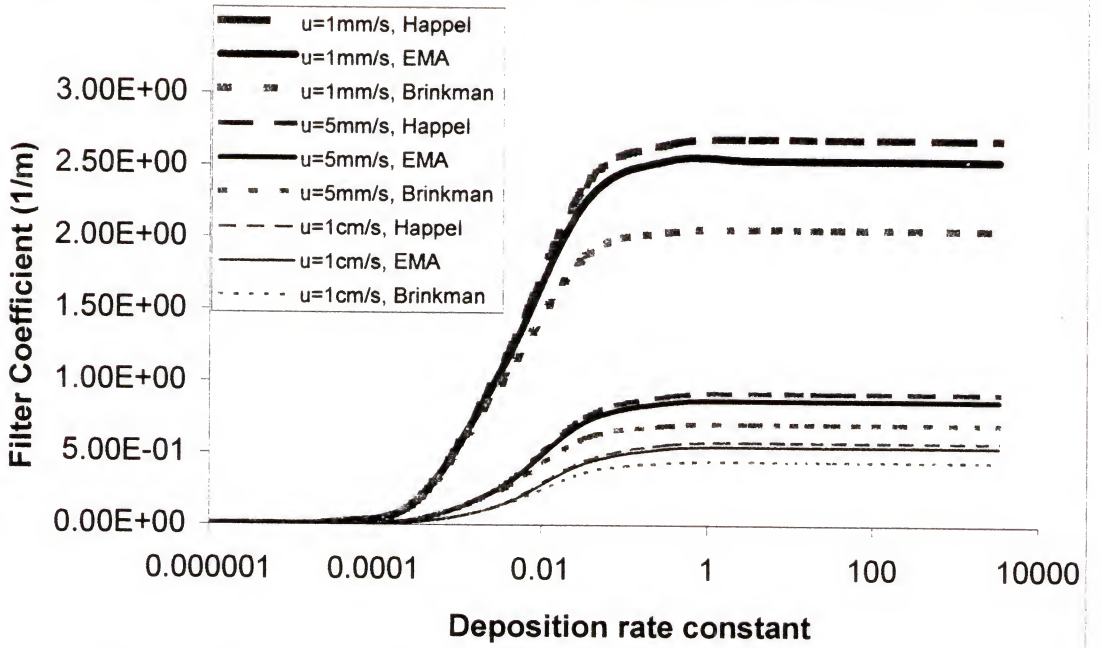

Figure 4-2. The effect of superficial velocity and deposition rate constant on filter coefficient for 0.5 mm-diameter particles in a packed-bed of 0.6 mm-diameter spherical collectors.

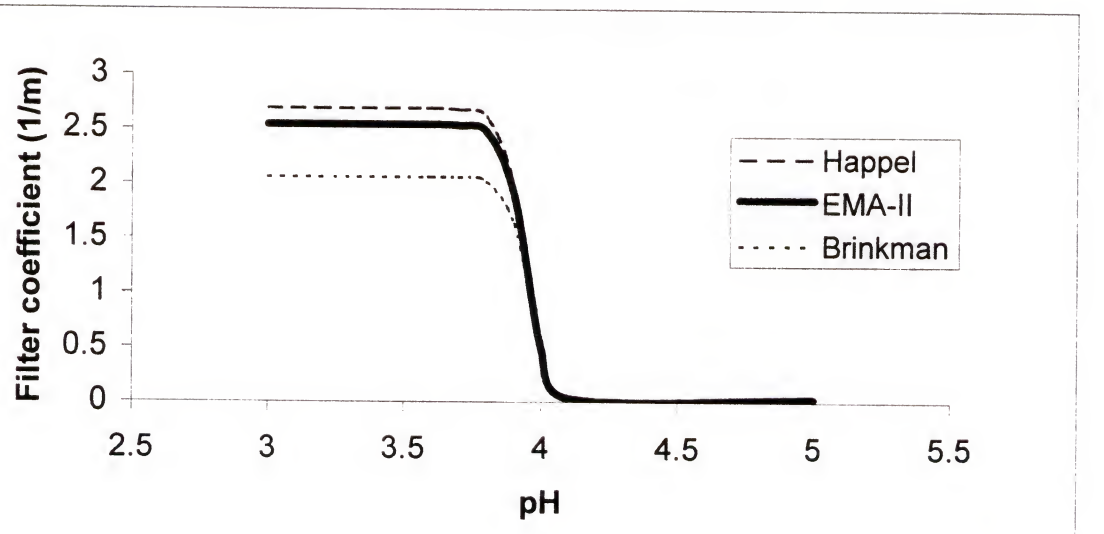

Figure 4-3. Effect of pH on filter coefficient of 0.5 μm particles in a packed-bed of 0.6 mm-diamter glass spheres using DLVO calculations based on measured zeta potentials.

4-2 Experimental Results

The filtration rates of 0.5 and 1.0 μm-diameter silica particles have been measured for a wide range of pH, as well as for multiple flow rates and potassium chloride concentrations. To obtain filtration coefficients, particle solutions were passed through a granular packed-bed as described in section 5-1, and the particle concentrations were measured at various column depths. The filter coefficient was found by fitting the particle concentration over the length of the column to an exponential decay, as shown in Figure 4-4. Figure 4-5 shows the effect of fluid velocity on filter coefficient for 1 μm-diameter silica particles in a packed-bed of 0.3 mm-diameter glass spheres. As expected from Figure 4-2, an increase in superficial velocity results in a decrease in filter coefficient.

The influence of salt concentration and pH on the filtration of colloidal silica in a packed-bed is shown in Figures 4-6, 4-7 and 4-8. Figures 4-6 and 4-7 show the effect of potassium chloride and pH, respectively, on the filter coefficient of 1 μm-diameter silica by 0.3 mm-diameter collectors. An increase in potassium chloride concentration results in a compression of the double layer, thus decreasing the range of electrostatic repulsion thereby causing van der Waals attraction to become dominant. Therefore, as shown in Figure 4-6, the filter coefficient increases as the salt concentration is increased. An increase in pH is seen (Figure 4-7) to cause a decrease in filter coefficient, since electrostatic repulsion dominates as the zeta potential of the particles and collectors becomes more negative. Similarly, the effect of pH on the filtration of 0.5 μm-diameter silica in a packed-bed of 0.6 mm-diameter collectors is seen in Figure 4-8. The increase of filtration coefficients with the increase in electrolyte concentration and with the

decrease in pH is expected, but the effects are much more gradual than predicted by DLVO theory. Since DLVO theory does not yield deposition rate constants that adequately predict filtration rates in the presence of electrostatic barriers, an independent method was devised to verify the effective medium approximation in the presence of energy barriers by independently measuring the deposition rate constants.

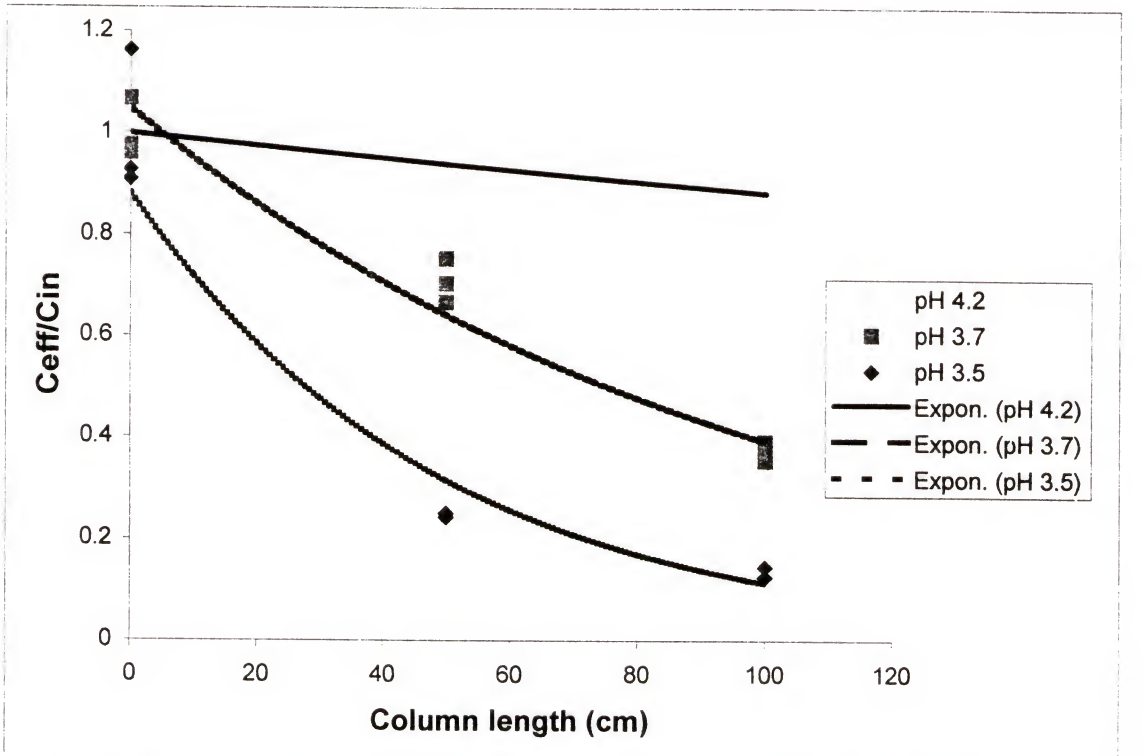

Figure 4-4. Silica concentrations relative to inlet concentration after passing through columns packed with 0.6 mm glass beads. Filter coefficients are determined from an exponential fit of the data.

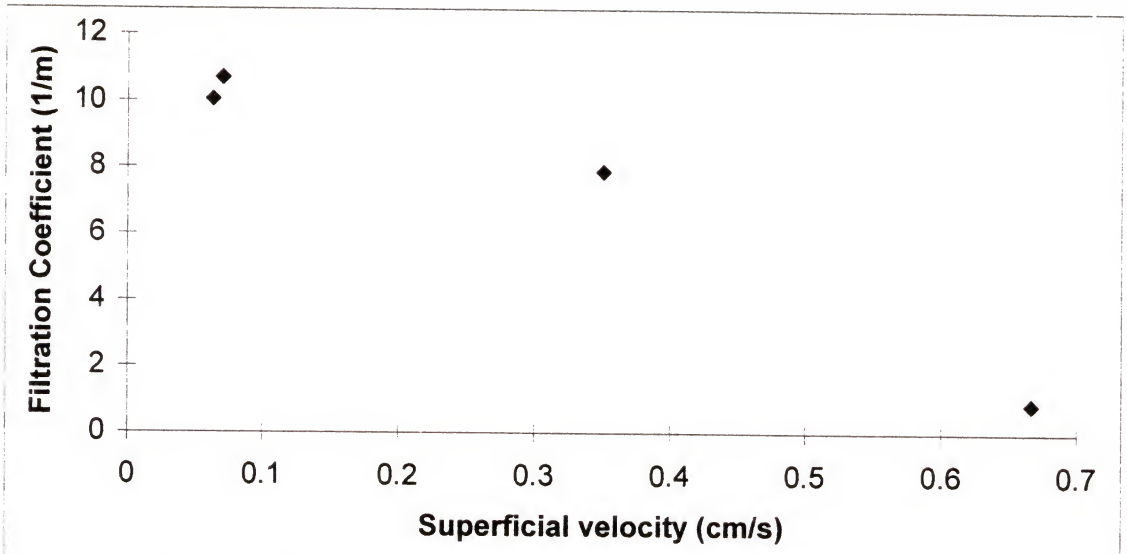

Figure 4-5. The effect of flow rate on the filter coefficient for the collection of 1.0 mm-diameter silica particles in a packed-bed of 0.3 mm-diameter glass spheres at pH 4 with a potassium chloride concentration of 0.1M.

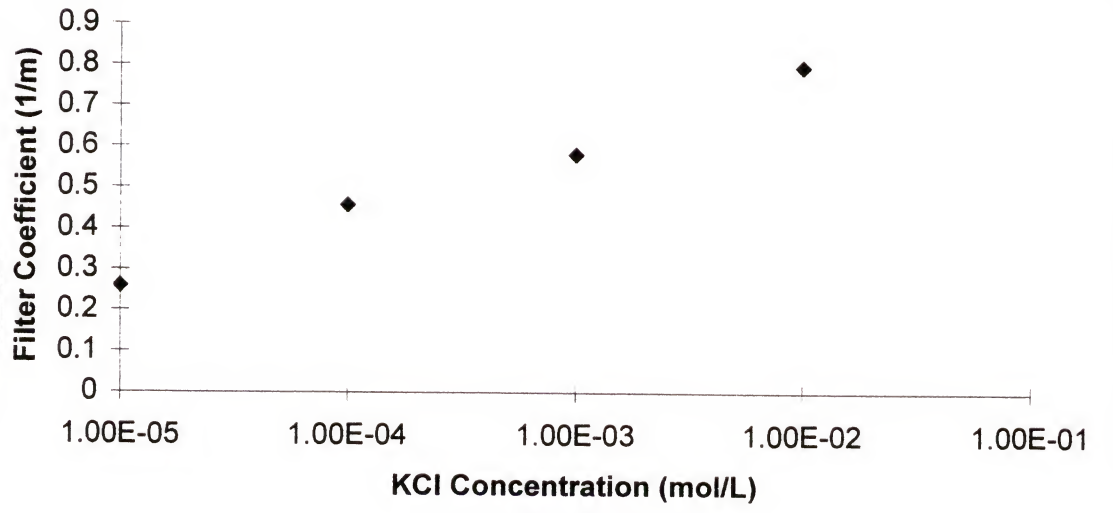

Figure 4-6. The effect of potassium chloride concentration on the filter coefficient for the collection of 1.0 μm-diameter silica particles in a packed-bed of 0.3 mm-diameter glass spheres at pH 7 and at a superficial velocity of 4 mm/s.

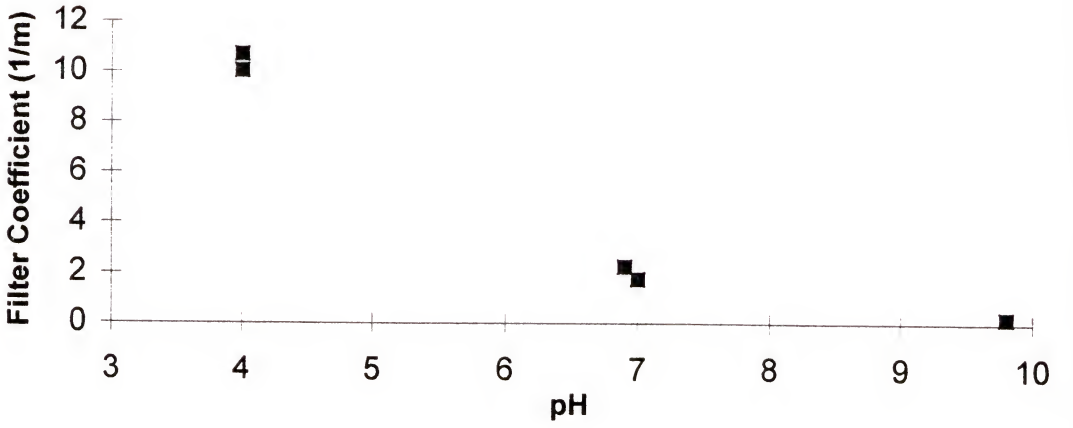

Figure 4-7. The effect of pH on the filter coefficient for the collection of 1.0 μm-diameter silica particles in a packed-bed of 0.3 mm-diameter glass spheres at a superficial velocity of 0.7 mm/s.

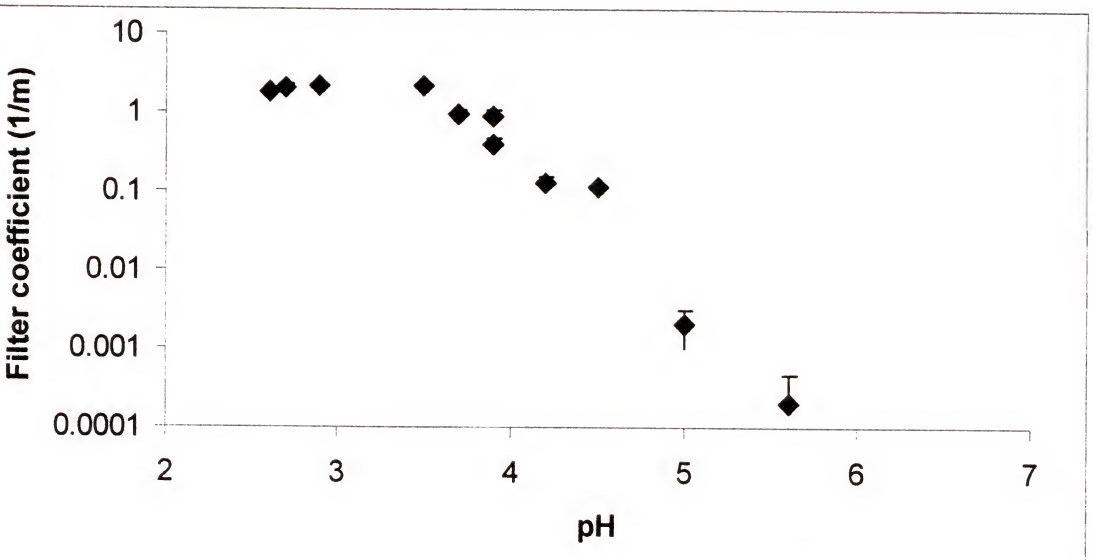

Figure 4-8. Experimental filtration coefficients for 0.5 μm-diameter silica particles in a packed-bed of 0.6 mm-diamter glass spheres at a superficial velocity of 0.1 mm/s.

4-3 Verification of the Effective Medium Approximation

By using video microscopy to directly measure the deposition rates of 0.5 μm-diameter silica particles to a flat glass slide, deposition rate constants were extracted with the aid of the model discussed in section 3-1. The deposition rate constants are expected to describe the interaction between the particle and surface and not depend on system parameters, such as geometry or flow rate. Therefore, the deposition rate constant measured between silica and glass in a flow cell are extended to predict filtration rates between colloidal silica and spherical glass collectors in a packed-bed.

The experimental deposition data from Figure 3-26, along with the theoretical predictions from Figure 3-17, produce deposition rate constants for 0.5 μm-diameter silica particles and glass at several pH values. Figure 4-9 compares experimental filtration rates to the predictions from the effective medium approximation model using both the measured and DLVO-predicted deposition rate constants. Clearly, using this independent measure of the deposition rate constant gives much better agreement between predicted and measured filter coefficients for silica in a packed-bed of glass spheres. Also, Figure 4-10 shows the ratio of experimental to theoretical filtration coefficients for 0.5 and 1.0 μm-diameter silica particles for several flow rates when deposition is expected to be transport-controlled. The effective medium approximation predicts the expected rates within about a factor of two, which is about as good as should be expected (Fitzpatrick 1972). Therefore, the filtration model based on the effective medium approximation is seen to be valid for the collection of colloidal particles in a packed-bed filter.

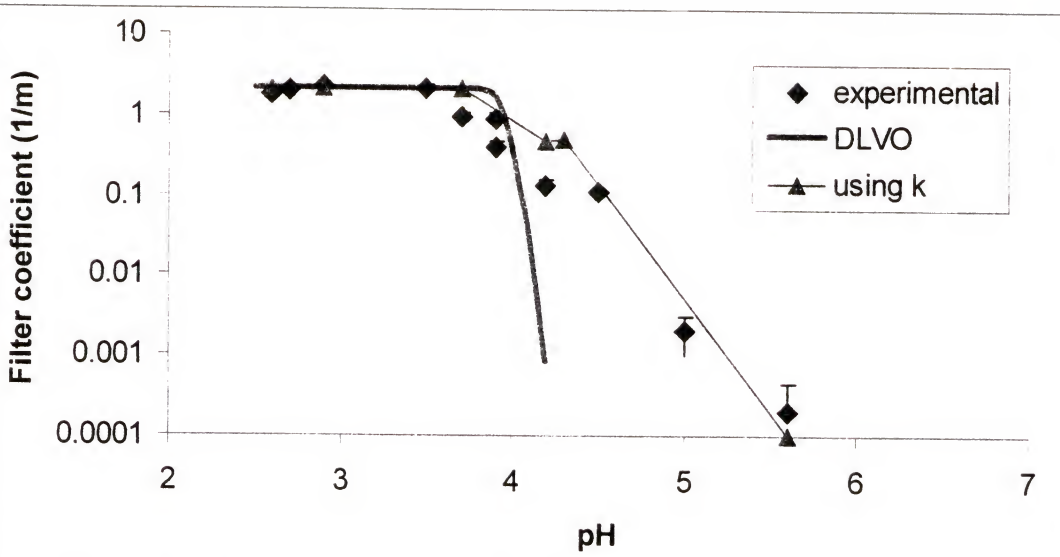

Figure 4-9. Comparison of experimental filtration rates to those predicted by DLVO-theory and by independently measured deposition rate constants for 0.5 μm-diameter silica particles in a packed-bed of 0.6 mm-diamter glass spheres.

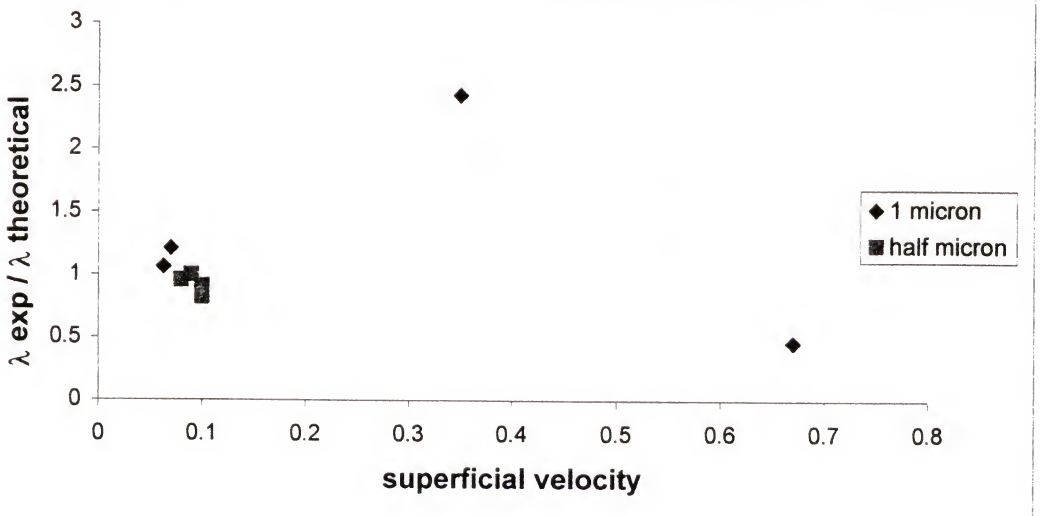

Figure 4-10. The ratio of experimental and theoretical filtration coefficients based on the effective medium approximation for conditions that are expected to be transport-controlled.

CHAPTER 5
MATERIALS, METHODS AND CHARACTERIZATION

Video microscopy has been used to measure particle deposition in a parallel plate flow cell to verify a filtration model and to investigate colloidal interactions. Colloidal particles, granular media and glass slides have been treated, characterized and employed in deposition experiments in this research. Thus this chapter describes experimental and numerical procedures used and communicates results from characterization experiments. Specifically, coating techniques, counting procedures, electrokinetic measurements, filtration and flow cell experiments will be discussed.

5-1 Filtration Experiments

Packed-bed filtration experiments were conducted using granular media consisting of spherical glass beads, Ottawa sand or activated carbon to remove a variety of colloidal particles including silica, bacteria and viruses. In all cases, filters were charged from the top with aqueous colloidal dispersionss under laminar flow conditions using peristaltic pumps. Particulate feed solutions were diluted to concentrations ranging from parts per million to parts per thousand to minimize any particle-particle interactions and to avoid filter saturation, i.e. to operate in initial clean-bed stages.

5-1-1 Filter Configuration

The filter flow system was configured for the convenience of filling, rinsing, and sampling that are necessary for measuring filter coefficients for various physical and chemical conditions. Figure 5-1 shows a schematic of a single-column filtration system,

which allows the fluid to be pumped from the bottom or from the top using a single peristaltic pump. Filtration columns consisted of polymethylmethacrylate (PMMA) tubing (0.75 in ID/1.0 in OD) and 3 in cylinder end pieces as shown in Figure 5-2. End pieces consisted of a disc and a cylinder bolted together and secured to the column by sandwiching an o-ring between them, as shown in Figure 5-3. Fine steel screens (about 100 mesh) are secured at the end of the tube to prevent granular media from escaping from the column. To provide a means for attaching tubing, a thread (1/8 in. NPT) was tapped into the end piece. All solutions for filtration experiments were pumped through Masterflex Tygon® food grade tubing of 1/8 in. diameter with Masterflex peristaltic pumps, both of which were obtained from Cole-Parmer.

5-1-2 Filtration Procedure

Columns were gradually filled with granular media using a tap-and-fill methodology. Prior to adding granular media, the filtration system was completely assembled with the exception of the top end piece, and a few inches of water was charged into the bottom of the column. Then, approximately 10-20 ml of granular media was added to the top of the column, and the column was tapped until the media no longer settled or shifted; this procedure was repeated until the column was filled. The top end piece was then secured to the column, and water was pumped upward until all the air was removed from the column and tubing. Often, the flow direction had to be reversed to facilitate the removal of trapped air in the column and tubing. Once the column was filled and air removed from the lines, flow was directed downward through the column, and the flow rate was measured and adjusted as necessary. The source was then changed

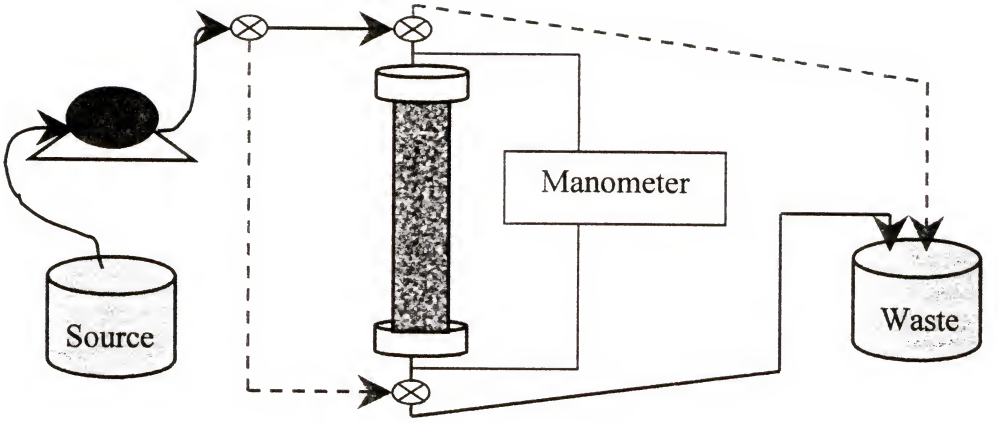

Figure 5-1. Schematic of packed-bed filtration system. Dotted lines represent path of fluid in the upward flow system.

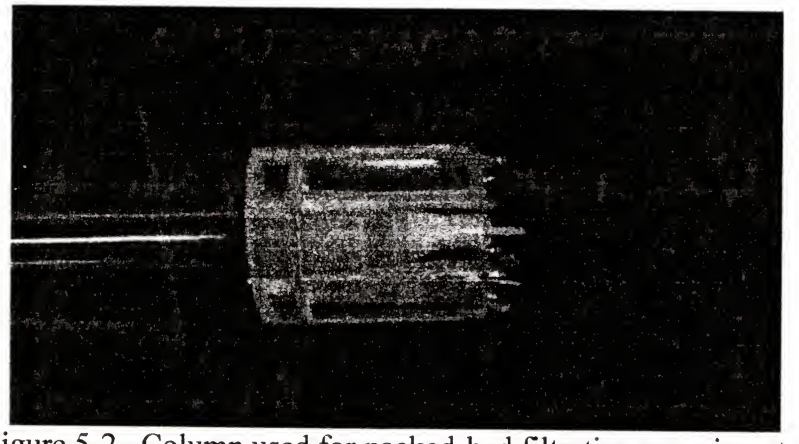

Figure 5-2. Column used for packed-bed filtration experiments.

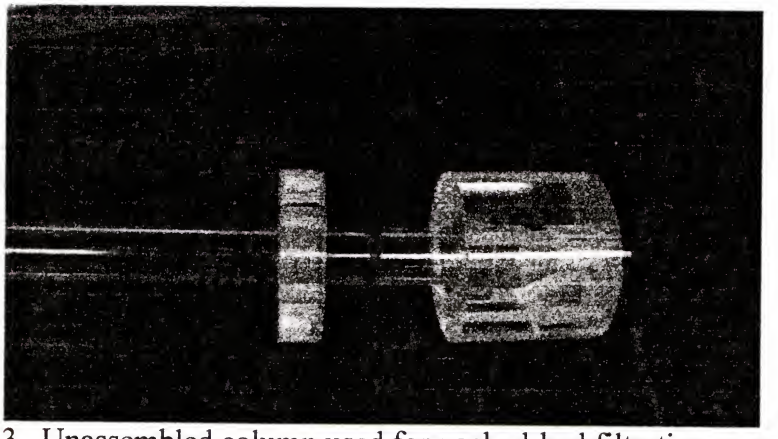

Figure 5-3. Unassembled column used for packed-bed filtration experiments.

from purified water to an aqueous hydrochloric acid solution of pH 2.6-3.0 to minimize pH fluctuations as recommended by Elimelech et al. (1995). The packed-bed was acid washed in this manner for about 15 minutes, after which the source was switched to a particle-free solution adjusted to the desired pH and salt concentration. To promote equilibrium in the column, this particle-free water was passed through the column for about 15 minutes prior to charging the solution with particles.

To obtain the desired particle concentration, typically a few milliliters of a concentrated solution would be added to about 2 liters of the electrolyte adjusted water. After particles were introduced into the system, some time was required for them to pass through the column and tubing. So, initially the effluent particle concentration was zero and increased to an equilibrium value until saturation of the column occurred. A plot of effluent concentration versus time, as seen in Figure 5-4, revealed that breakthrough can be confidently expected after two residence times. After this time, the samples were taken from the entrance and exit of the column, and the concentration was measured using a UV-vis spectrophotometer as described in section 5-3-2-2. Then the filter effluent was collected in a 2L Erlenmeyer flask for use as the influent in a second pass. A typical experimental run consisted of multiple concentration measurements from the entrance and exit of the column for two passes, each of which was operated for about 45 minutes to an hour.

5-1-3 Granular Media

A variety of granular media was employed in packed-bed filtration experiments to remove colloidal particles from aqueous streams. Soda-lime glass spheres of various sizes were obtained from Mo-Sci Corp, Ottawa sand was obtained from Fisher Scientific,

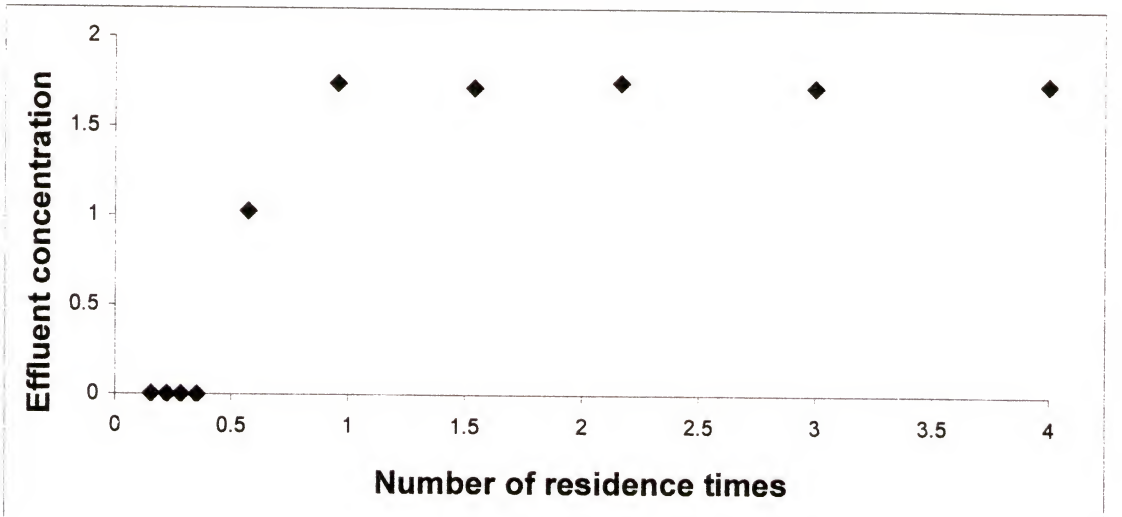

Figure 5-4. Typical breakthrough curve for filtration experiments.

and granular activated carbon was obtained from U.S. Filter brand cartridge filters. Before filtration, granular media was sieved to the desired size range, which was 25x30 mesh (0.6-0.7mm diameter) for most experiments. Once sieved, granules were soaked overnight in Chromerge acid solution and rinsed with deionized water in an aspirator until the pH of the effluent reached that of the water. The granules were then dried in an oven.

5-2 Parallel Plate Flow Cell Experiments

Computerized video microscopy was used to measure colloidal deposition kinetics in a parallel plate flow cell. The deposition of 0.5 and 1.0 μm diameter silica spheres in a parallel plate flow cell was directly measured using video microscopy. The video microscopy technique, which was originally used by Dabros and van de Ven (1998), provided a means of directly monitoring particle deposition under well-defined laminar flow conditions.

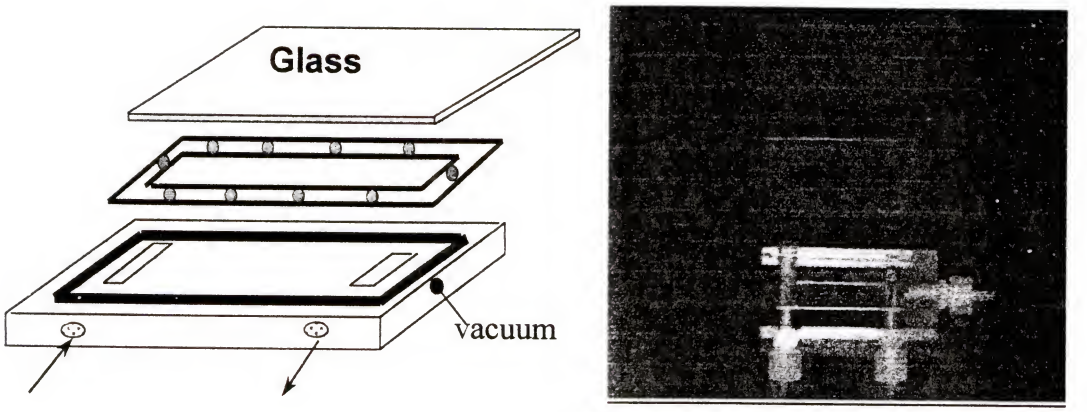

Figure 5-5. Parallel plate flow cell apparatus.

5-2-1 Equipment

The parallel plate flow cell obtained from CytoDyne consists of a Plexiglas base channeled for fluid flow, a glass slide onto which particles were deposited and a silicone gasket to separate the two as shown in Figure 5-5. The silicone gasket was placed over a groove through which a vacuum is pulled to hold the base and slide together. The dimensions of the flow domain in the cell are 8 mm (w), 37 mm (l) and 254 μm (h). The glass side of the flow cell was placed downward on the motorized stage of an inverted microscope, and images of deposited particles were taken at various positions and times and stored on a computer. A CCD camera was used to view images from the inverted Nikon microscope with a motorized stage that could be controlled with a joystick or with software. Optimas software package was used for controlling the stage, capturing images and counting particles. Ruta (1998) gives a detailed explanation of the automation and image analysis program Optimas and includes the codes written for automation and analysis.

5-2-2 Experimental Procedure

Immediately preceding deposition experiments, the flow cell, spacer gasket and glass slide were all rinsed with ethanol to minimize contamination. Two syringes were used as feeds to the flow cell. One syringe contained the desired particle solution, and the other contained a particle-free solution of the same pH and salt concentration. After the flow cell was assembled, a vacuum pump was used to secure the slide to the base, and the particle-free solution was pumped through the cell at full speed until all air bubbles were evacuated. This solution was then pumped through the flow cell at the desired flow rate for about 15 minutes to ensure equilibrium and to inspect the system through the microscope. The strength of the vacuum was adjusted to minimize water leakage into the pump trap while keeping an adequate seal. Finally, the source was switched to the desired colloidal suspension for deposition experiments.

Microscope objective lenses with magnifications of 40x and 100x were used to capture images for 1.0 and 0.5 μm diameter silica particles, respectively. Since small fields result in higher statistical uncertainty, objective lenses of the smallest magnification possible were used. Sample images taken at subsequent times of 1μm silica spheres using a 40x objective lens are shown in Figure 5-6. Initially, the lower right-hand corner of the cell was marked as the origin of the coordinate system. Several fields were then chosen and focused for image analysis. The software package was used to recursively scan the flow cell to capture images at several locations over time. Particle counts were seen to increase linearly in time as seen in Figure 5-7, and saturation was not reached during the course of the experiments. The deposition rate was determined

from a least squares fit of the slope, and the particle fluxes were obtained by dividing the slope by the field area.

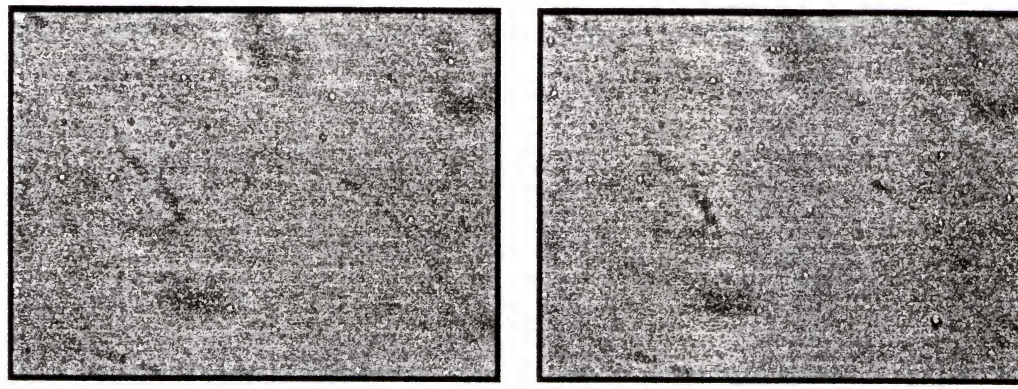

Figure 5-6. Examples of images taken for one-micron silica particles using a 40x objective lens.

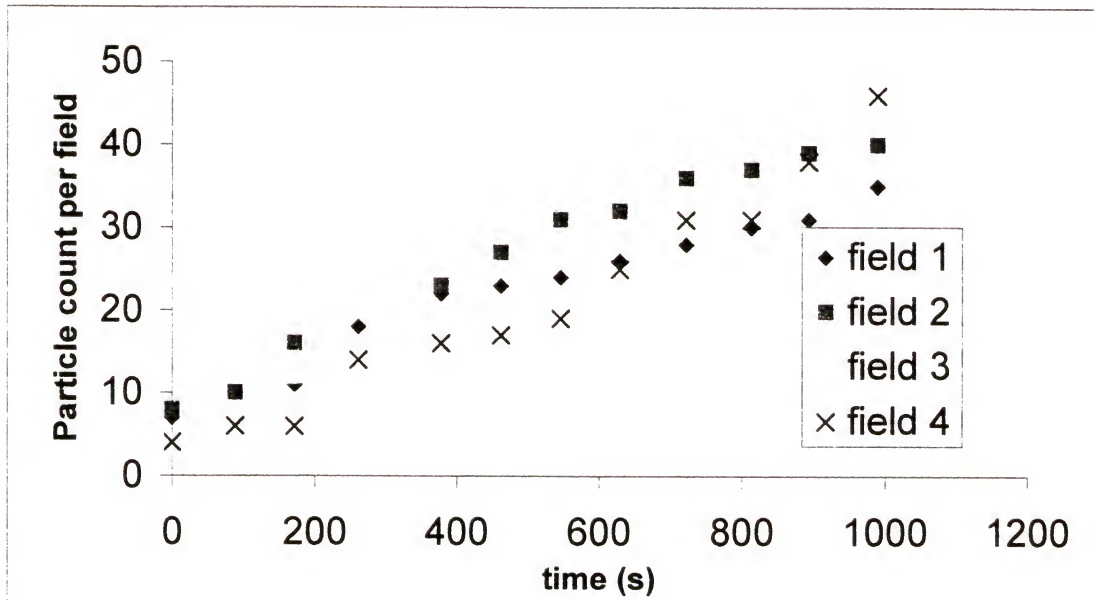

Figure 5-7. Typical particle counts taken at several locations over time.

5-3 Preparation and Counting of Particle Suspensions

Dilute colloidal dispersions were prepared for use in filtration and deposition experiments to verify a filtration model. Accurate particle counts of these dispersions were necessary to quantify experimental results and compare them to models. The procedures used for preparing and counting inorganic dispersions are described below, whereas the preparation and counting of biological suspensions are located in 6-1.

5-3-1 Dispersion Preparation

Colloidal dispersions were prepared at low concentrations to minimize any particle-particle interactions or agglomerate formations. Suspensions of 0.5 and 1.0 μm-diameter silica particles were prepared at concentrations ranging from 0.0001-0.01 percent by weight, depending on the physicochemical conditions of the dispersion and the nature of the experiments. Stock solutions of about 1% by weight were made to facilitate the preparation of desired suspension concentrations. The stock solutions were prepared by adding a known amount of dry particles to membrane-filtered water. Nanopure and Milli-Q membrane filtration systems yielded highly pure water with resistances of 18.2-18.3 MΩ. The water was passed through a 0.2 μm filter to further remove biological contamination. Prior to preparing desired suspensions, the stock solution was sonicated for at least four hours to disperse the particles and to break agglomerates. About one to three liters of membrane filtered water was adjusted to the desired salt concentrations and pH. Potassium chloride was used to adjust salt concentrations to the desired level, which was usually 1mM. The solution pH was adjusted using hydrochloric acid or sodium hydroxide as necessary. Most of the electrolyte-adjusted water was used to prepare dilute suspensions from concentrated stock

solutions, and the remainder was used for rinsing and bringing systems to equilibrium. Suspensions were sonicated for about one hour, just prior to experiments to ensure dispersion.

5-3-2 Counting Techniques

Reliable particle counting techniques were needed to measure deposition rates. An indirect method was used for filtration experiments, whereas a direct counting method was used for parallel plate flow cell experiments. Direct counting techniques are advantageous in that images of the surface can be stored for detailed analysis of coagulation, blocking, and transport behavior. Indirect counting techniques are faster and can be implemented for on-line analysis.

5-3-2-1 Direct particle counts

For parallel-plate flow cell measurements, absolute particle concentrations were needed since fluxes are dependent on the number of particles in the bulk. Particle counts were thus made directly under a microscope in a Petroff-Hauser counting chamber. The counting chamber consisted of a grooved glass plate topped with a microscope coverslip. Since the spacing in the groove was precisely known, two-dimensional particle counts were converted to suspension concentrations.

5-3-2-2 Indirect particle counts

In a packed-bed filter, particle concentrations were measured using an UV-Visible spectrophotometer since number counts were not required, and direct counting techniques were too tedious for the number of samples to be counted. A calibration curve, as in Figure 5-8, was constructed to determine the weight concentration of particles from absorbance measurements. Figure 5-8 shows a linear relationship between particle

concentration and light absorbance at low particle concentrations ($c<0.05$), as predicted by the Beer-Lambert law (Alberty and Silbey, 1995). When operating in this linear regime, relative particle concentrations were directly obtained from absorbance ratios. All experiments were conducted below about 0.03 weight percent to avoid calculating absolute concentrations, which are not needed for filtration experiments.

a)

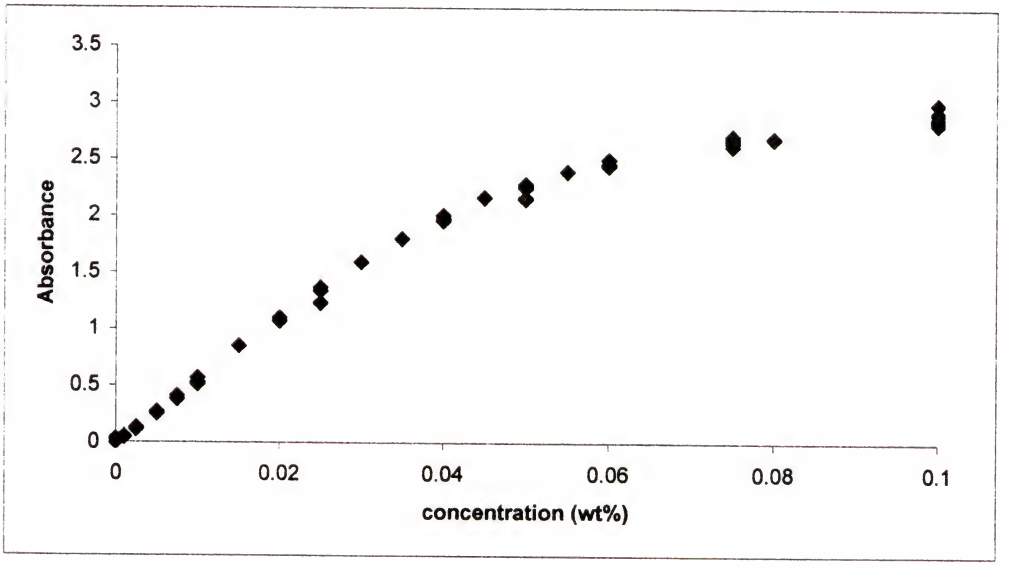

b)

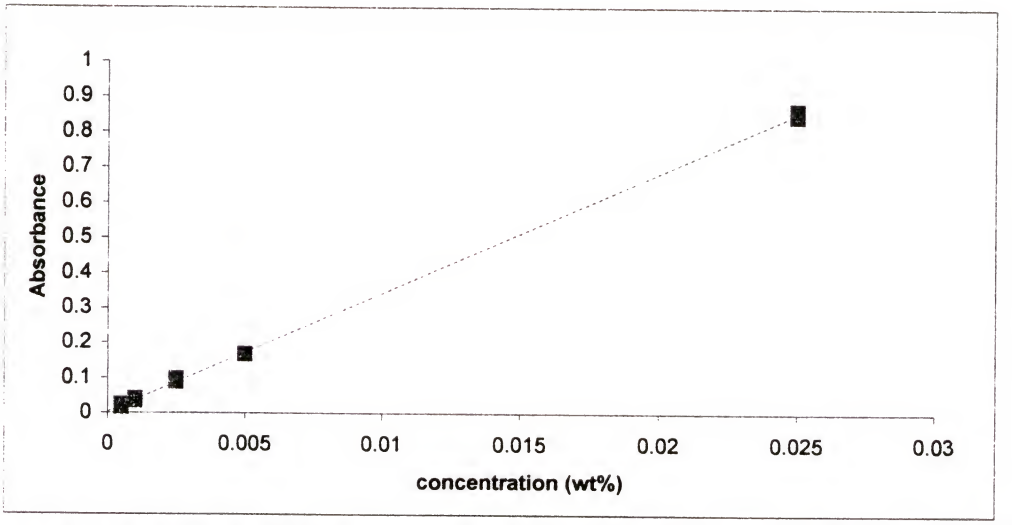

Figure 5-8. Absorbance of 350nm wavelength light for the desired concentration range: a) one micron diameter silica solutions show linear dependence on absorption for concentrations up to about 0.04%; b)absorbance for half micron diameter silica solutions.

5-4 Surface Modification

Various surface properties of particles and collectors can be tailored by physical or chemical modification of the surfaces, thereby altering colloidal interactions and deposition behavior. In this research, granular media have been coated by physical adsorption of metal hydroxides and chemical binding of quaternary ammonium siloxanes to alter surface properties of the media. Both types of coating were used to impart a positive charge on negatively charged filter media to enhance the capture of bacteria, viruses and silica, which are all negatively charged at natural pH.

5-4-1 Metal Hydroxide Coatings

Metal hydroxides precipitated onto granular media have been successfully used to enhance the removal of a wide range of microorganisms and metals (Lukasik 1998; Chen, 1998; Scott 2000). Lukasik (1998) investigated the efficacy of numerous metal mixtures and precipitation methods to enhance the capture of microorganisms. A combination of aluminum and ferric hydroxide proved to be the most effective and the procedure for precipitating this mixture was used in this work (Lukasik 1998). An aqueous mixture of 0.25 M ferric chloride and 0.5 M aluminum chloride were added to the granular media and heated to 60°C until dry. The media was mixed twice with 3N ammonium hydroxide and dried at 60°C to ensure a sufficient coating.

5-4-2 Quaternary Ammonium Siloxane Coatings

Chemical modification of silicates (e.g. glass and sand) via siloxane bridging can be advantageous to precipitation because the siloxanes can be readily functionalized and, in principle, are more stable than physically adsorbed materials. In this research, two types of quaternary ammonium siloxanes have been used to impart hydrophobicity and a

positive charge on the surface of glass, sand or silica. Both coatings were taken from commercial applications and are thus expected to be safe for use as a coating for filtration media. The first coating procedure is referred to as the Suhara coating and has been employed for cosmetics, and the second procedure yields a coating referred to as AEM 5700 and has been used commercially as an antimicrobial agent.

5-4-2-1 Suhara coating

The Suhara coating procedure is completed in a sequence of three steps as described by Suhara (1995a), and the reagent in the final reaction determines the length of the hydrocarbon chain on the quaternary ammonium group. The flexibility in hydrocarbon chain-length is desired as the chain-length determines, in part, the degree of the coating hydrophobicity. The chemical structures of the reagents and products for each reaction is shown in Figure 5-9, where the subscript m represents the number of carbon atoms. The procedure involves three distinct reactions: (1) polymerization of 2,4,6,8-tetramethylcyclotetrasiloxane (TMCTS) to form a coating of polymethylsiloxane (PMS), (2) hydrosilylation with chloromethylstyrene (CMS), and (3) introduction of a quaternary ammonium group by subsequent reaction with N,N-dimethyl-*n*-alklyamine. The details of each reaction are described below.

The first reaction (polymerization) was carried out either in a dry or an aqueous environment. For the dry reaction method, about 1% wt. of TMCTS was placed in a vessel with the glass beads and/or slides and cooked in an oven for about 20 hours with the container tightly sealed and about 10 hours with the container opened. The aqueous method was carried out in a 95% solution of ethanol adjusted to a pH of 4.5-5.5 with acetic acid. Then TMCTS was added to a concentration of about 2%. The solution was

a)

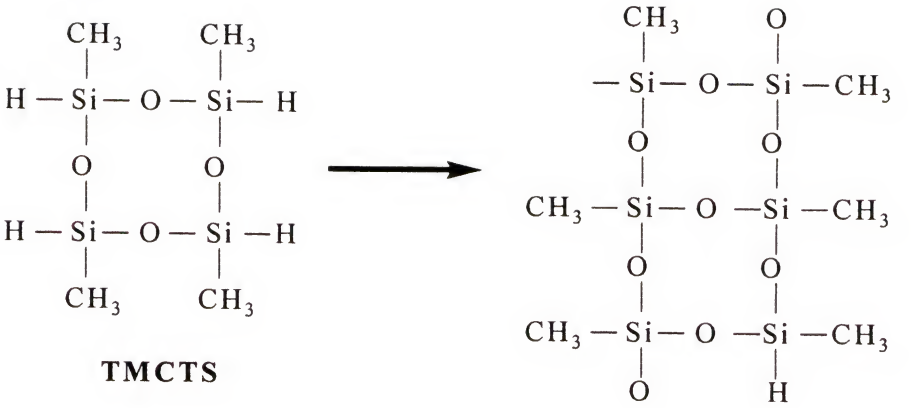

b)

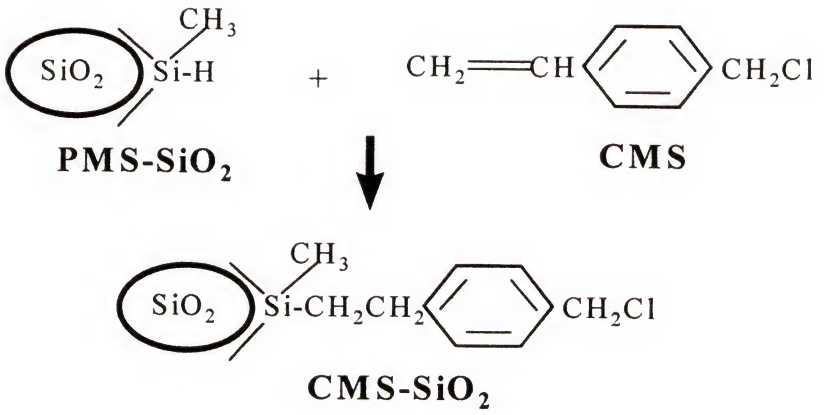

c)

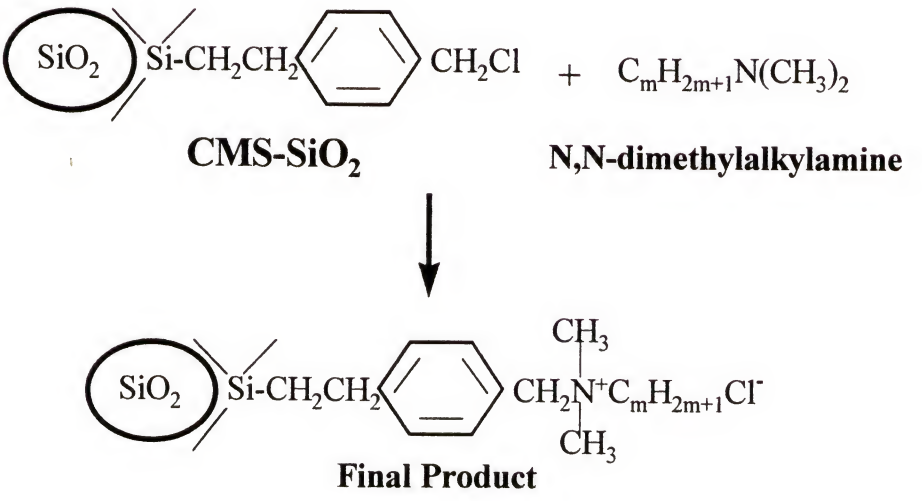

Figure 5-9. Three step Suhara coating procedure; a) reaction 1-Polymerization of TMCTS; b) reaction 2-hydrosylation of PMS-SiO_2; c) reaction 3-addition of quaternary ammonium group to CMS-SiO_2

stirred for about 5 minutes to allow hydrolysis to take place, and then the beads or slides were added. The reaction was carried out for about 2 or 3 minutes and subsequently rinsed with ethanol and left to dry at room temperature overnight.

For the second reaction (hydrosilylation), toluene was used as the solvent and tributylyamine and hydrogen hexachloroplatinate (IV) hydrate (platinic acid) as catalysts. The solvent, catalysts, chloromethylstyrene, and PMS coated glass beads and/or slides were refluxed in a sealed container at 110°C for about 4-6 hours and subsequently washed with toluene. The PMS-CMS coated beads were then left to dry overnight.

For the final reaction, glass beads coated with PMS and chloromethylstyrene were refluxed with N,N-dimethyl-*n*-alklyamine and acetonitrile at 65 °C for about 6 hours. The coated beads were then rinsed with acetonitrile and dried in vacuum at 110°C for about 12 hours. N,N-dimethylbutylamine, N,N-dimethyloctylamine and N,N-dimethyldodecylamine were used as reagents to yield hydrocarbon chain-lengths of 4, 8 and 12, respectively.

The Suhara coating procedure described is lengthy and tedious, and spectroscopic analysis is required to ensure each reaction occurs as expected. Therefore, a simpler procedure is desired to increase the likelihood of chemically binding a quaternary ammonium alkylamine to the surface.

5-4-2-2 AEM 5700 coating

Granular and colloidal particles, as well as glass slides, were coated with octadecyldimethyl(3-trimethoxysilyl-propyl)ammonium chloride, which is available commercially from Dow Chemical in an alcohol solution known as AEM 5700. The quaternary ammonium siloxane coated onto Ottawa sand, glass and silica is depicted in

Figure 5-10 and is referred to as AEM 5700 coating in this communication. A 1wt% aqueous solution of octadecyldimethyl(3-trimethoxysilyl-propyl)ammonium chloride was stirred at room temperature for about ten minutes to allow for hydrolysis and condensation prior to adding media. About 200 ml of granular media (or about 1 gram of colloidal particles) were then added and stirred in the coating solution for ten minutes. The coated media was removed, rinsed in a vacuum filtration system to remove any residual siloxane and dried overnight. Scanning electron micrographs reveal a non-uniform siloxane coating as shown in Figure 5-11.

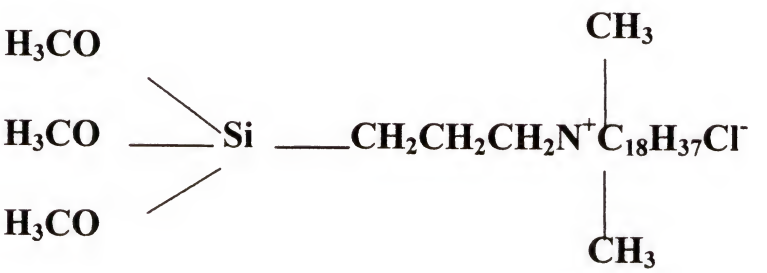

Figure 5-10. Structure of 3-(trimethoxysilyl)propyldimethyloctadecyl ammonium chloride (AEM 5700).

5-5 Characterization Techniques

Systems employed in filtration and deposition experiments were characterized to obtain necessary parameters for theoretical predictions. Zeta potential was measured for colloidal and granular particles, hydrophobicity was quantified for granular and flat substrates, the particle and collector size was measured, and the solution pH and conductivity were measured.

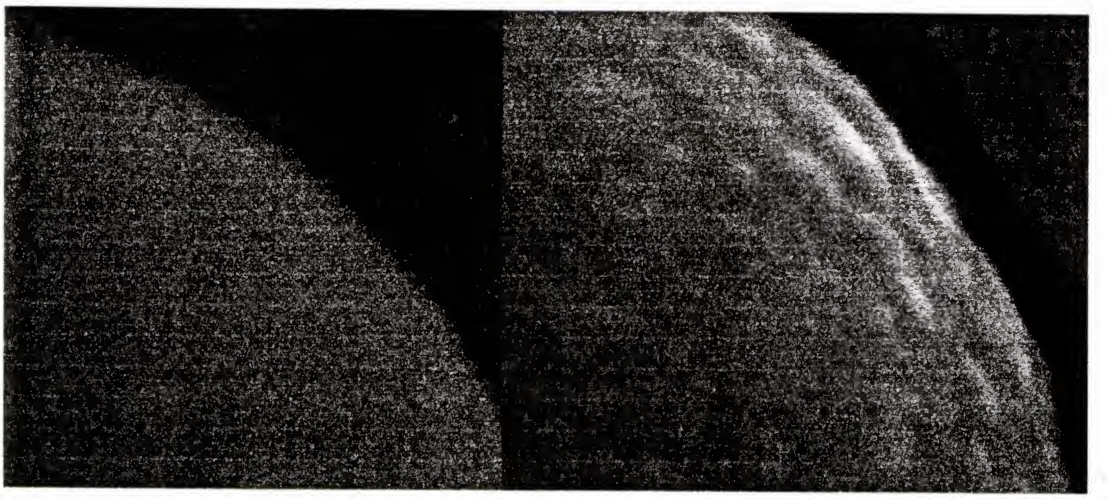

Figure 5-11. SEM micrograph of 1 micron-diameter bare silica (left) and siloxane coated silica (right).

5-5-1 Electrokinetic Measurements

Electrokinetic measurements performed to determine the zeta potential of granular and colloidal particles. Electrophoresis was used to measure the zeta potential with the commercially available Brookhaven Zeta Plus, and a streaming potential device was constructed to measure the zeta potential of granular media. Measured zeta potentials were used to evaluate coating procedures and to calculate colloidal interactions based on DLVO theory.

A streaming potential device was constructed using filtration columns adapted to include a silver mesh electrode as shown in Figure 5-12. The electrodes were made of 40 mesh silver gauze welded to 18 gauge silver wire. The electrodes were then electroplated in a 0.1 M hydrochloric acid solution by applying a 10 mA current for about 30-60 minutes using a copper cathode. The mesh electrodes also served to retain the granular media inside the column.

The zeta potential was measured by passing an electrolyte solution through the column at various pressure drops and measuring the response in voltage drop. Potassium chloride solutions were pumped through columns of about 20-40 cm in length using a peristaltic pump, and the pressure drop was measured using either a mercury manometer or an inverted water manometer. The voltage drops were measured using a handheld multimeter attached to electrodes at both ends of the column. The voltage drop was plotted against pressure drop, and the slope was used to calculate the zeta potential as

$$\zeta = (\Delta V\ \eta\ K)/(\Delta P\ \varepsilon_o\ \varepsilon_w), \qquad (5\text{-}1)$$

where η, K and ε_w are the viscosity, conductivity and dielectric constant of the electrolyte solution and ε_o is the permitivity of vacuum (Hunter, 1981; Van Wagenen and Andrade, 1989; Truesdail et al., 1998b).

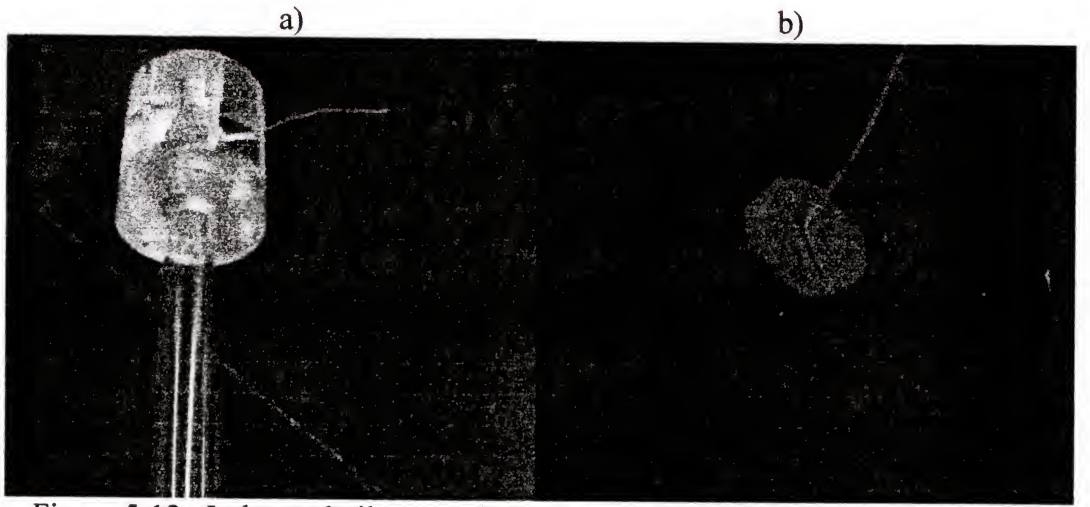

Figure 5-12. In-house built streaming potential device: a) column; b)electrode.

5-5-1-1 Unmodified media

The zeta potential of Ottawa sand in a 1 mM potassium chloride solution was measured over a pH range of 2.6-10.6. Figure 5-13 illustrates that the isoelectric point of the sand occurs at about pH 2.6, and the zeta potential of the sand becomes more negative as the pH is increased. Figure 5-14a shows the effect of pH on the measured zeta potential of glass spheres in a 1 mM KCl solution. The isoelectric point of glass beads was seen to be about 2.7. A quadratic equation was fitted to the data for interpolation of zeta potential values over a wide range of pH. Zeta potentials of 1 μm silica particles were measured by electrophoresis and are shown in Figure 5-14b. Zeta potential for silica particles was seen to be similar to those obtained using streaming potential measurements of glass.

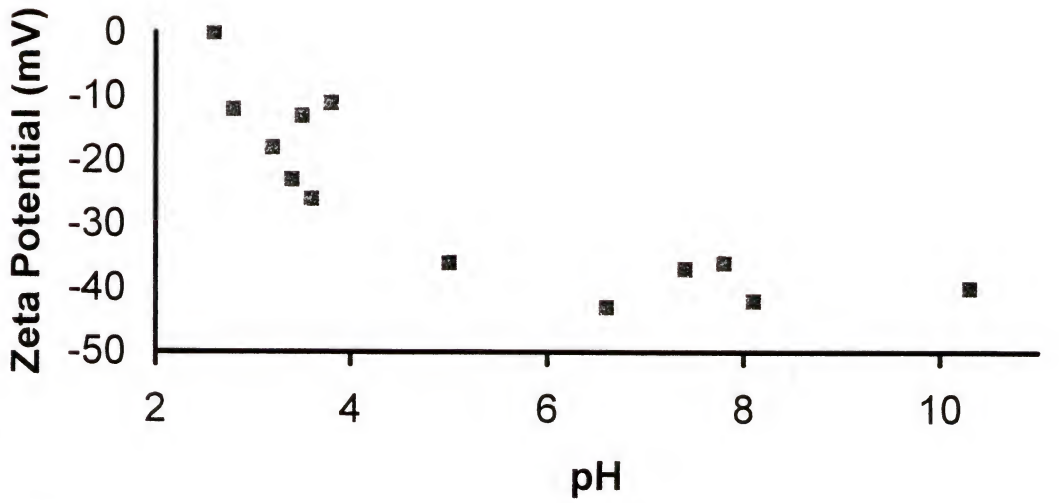

Figure 5-13. Zeta potential of Ottawa sand that has been soaked overnight in hydrochloric acid.

a)

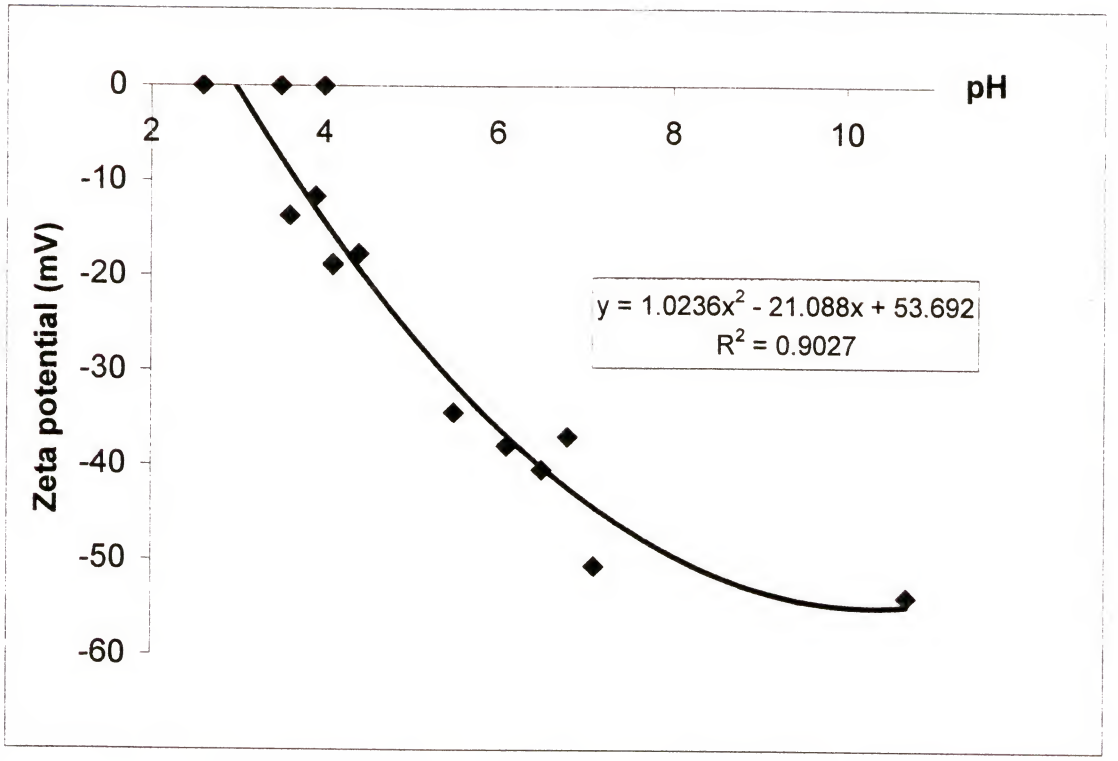

b)

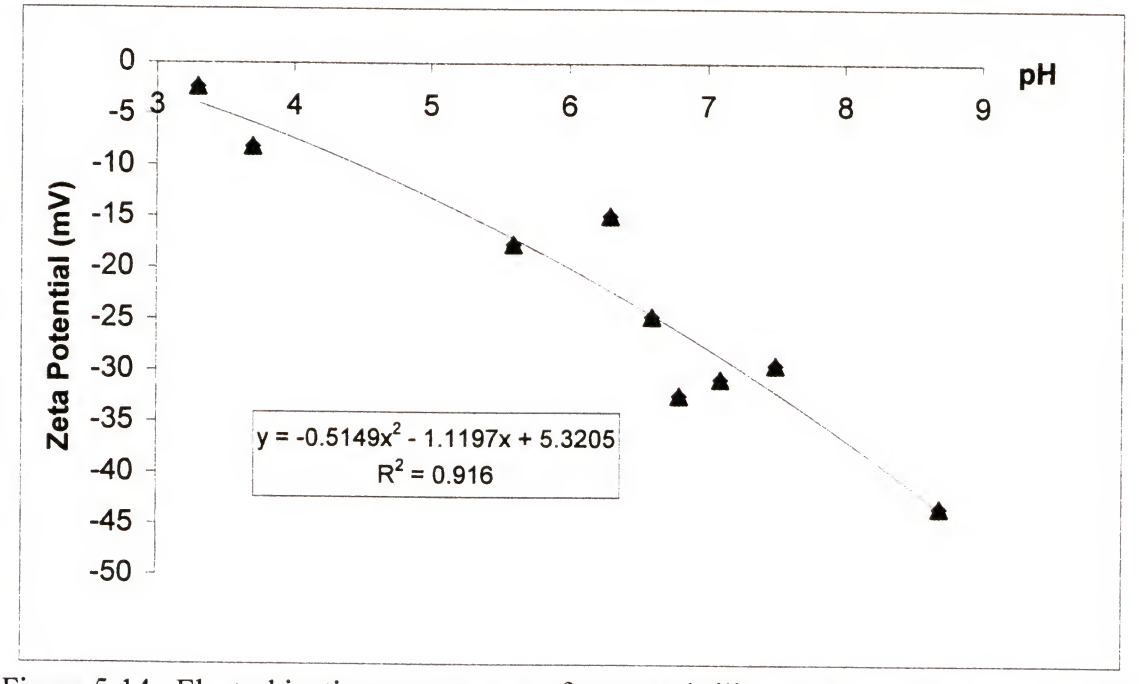

Figure 5-14. Electrokinetic measurement of uncoated silicates: a)streaming potential of soda-lime glass beads; b)electrophoresis of colloidal Stober silica.

5-5-1-2 Modified media

Streaming potential experiments were conducted to determine the zeta potential of Ottawa sand coated with metal hydroxides and AEM 5700. Figure 5-15 shows the measured zeta potential of aluminum and iron hydroxide coated sand between pH values of 4 and 10. The isoelectric point was determined to be about pH 8. The zeta potential of AEM 5700 coated sand was seen to be about 60 mV immediately after coating but quickly dropped and became negative after about 50 hours of washing as depicted in Figure 5-16. The reduction in zeta potential of quaternary ammonium siloxane coated media during washing has also been observed by Truesdail (1999).

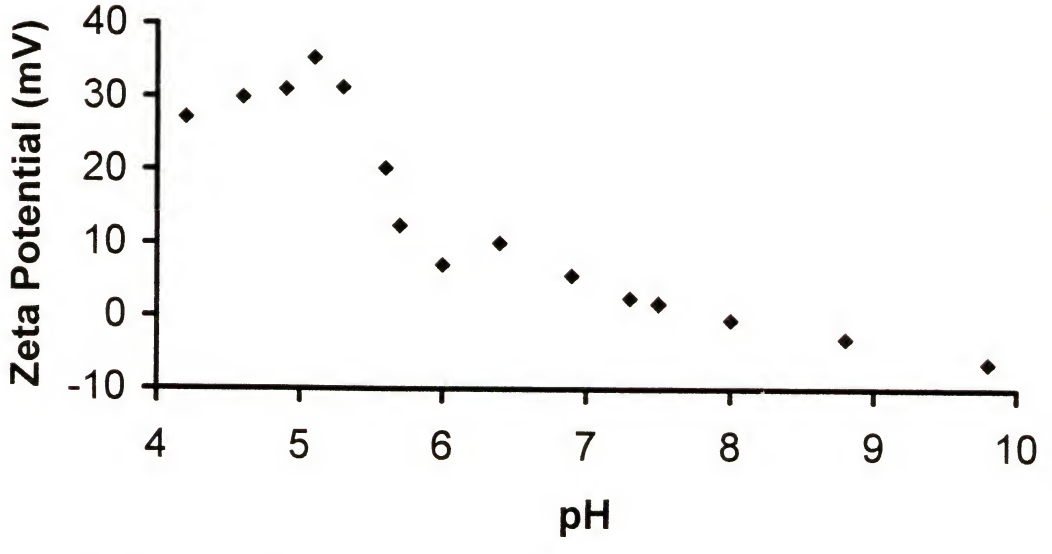

Figure 5-15. Zeta potential of metal hydroxide coated sand.

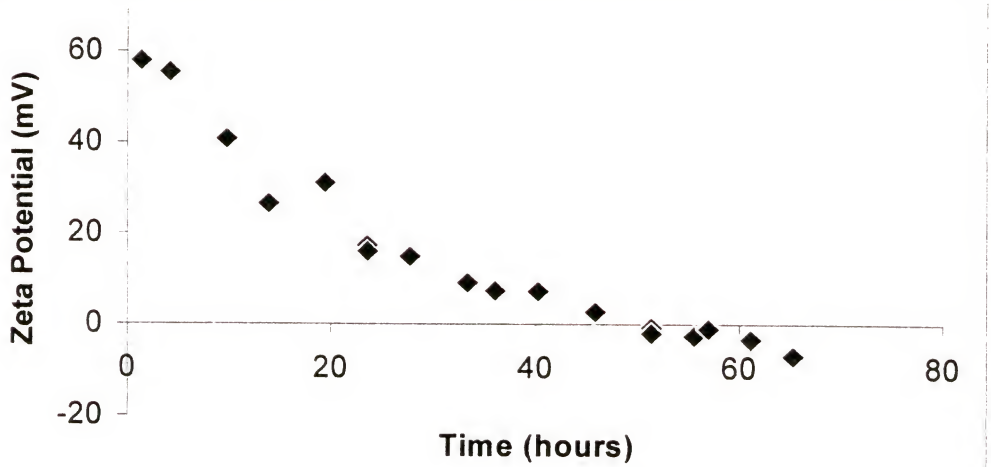

Figure 5-16. Zeta potential of AEM 5700 coated Ottawa sand as it is washed with deionized water. The coated media loses its positive charge quite rapidly.

5-5-2 Hydrophobicity

The hydrophobicity of glass slides and granular media was quantified by contact angle and capillary uptake measurements, respectively. Contact angles of water droplets on glass slides were determined using a contact angle goniometer. Large contact angles corresponded to a high degree of hydrophobicity. To quantify the hydrophobicity of granular media, capillary uptake experiments were performed in which granular media was packed in a glass tube and placed in a water bath, as depicted in Figure 5-17. The level of water inside the tube, relative to the water bath, was an indication of the hydrophobicity. Uptake heights were large for hydrophilic media and small for hydrophobic media. These two techniques appeared to give a good indication of the degree of hydrophobicity of glass beads and glass slides.

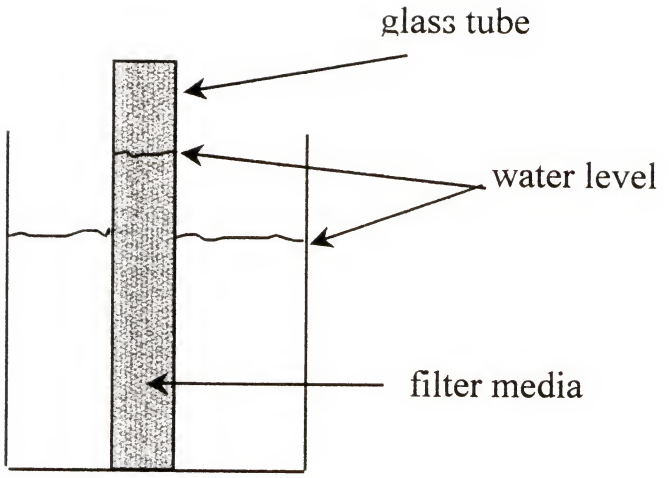

Figure 5-17. Capillary uptake experiments used to quantify hydrophobicity.

Glass beads and slides were coated with quaternary ammonium siloxanes of varying hydrocarbon chain lengths using the Suhara procedure described in 5-4-2-1. Figure 5-18 shows contact angle and capillary uptake measurements for coatings of varying hydrocarbon chain length. Both types of measurements indicate that longer chain lengths are more hydrophobic than shorter chain lengths.

5-5-3 Coating Stability

The longevity or stability of surface coatings is of practical and fundamental interests and directly affects the efficacy of the coatings to be employed in filtration processes. The zeta potential was measured over time as the media was washed with water. Hydrophobicity of the media was also measured for the hydrophobic siloxane coatings. Experiments have indicated that metal hydroxide coating lifetimes are on the order of months (Chen et al. 1998) and that siloxane coatings quickly lose their positive charge but not hydrophobicity.

a)

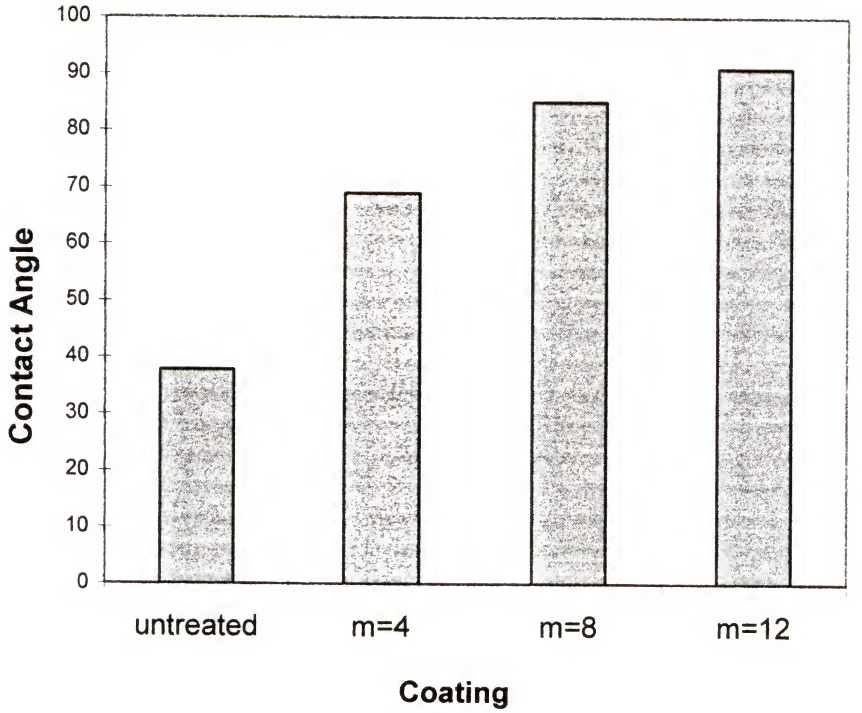

b)

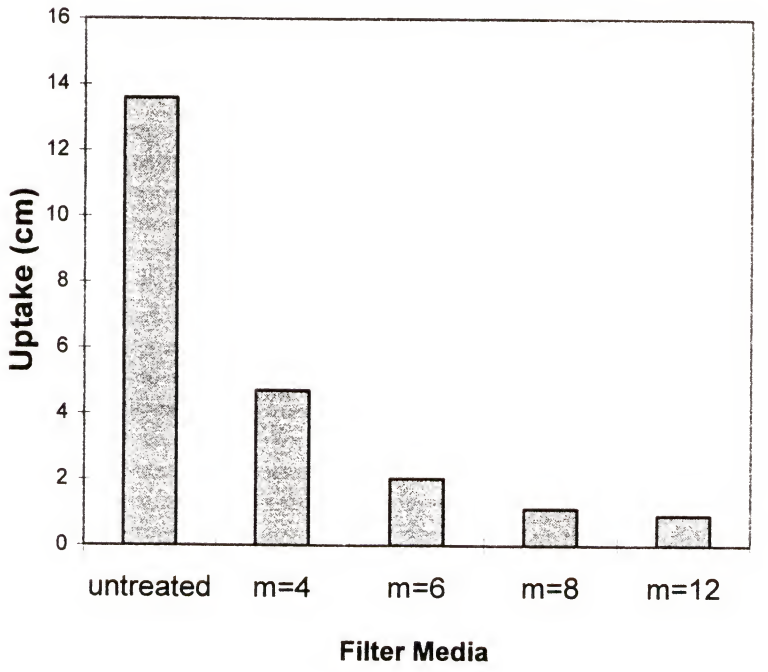

Figure 5-18. The relative hydrophobicity of glass substrates treated with quaternary ammonium siloxanes increases with hydrocarbon chain length. a) contact angle measurements of water on glass slides, and b) water uptake heights for glass beads in a 1cm glass tube.

a)

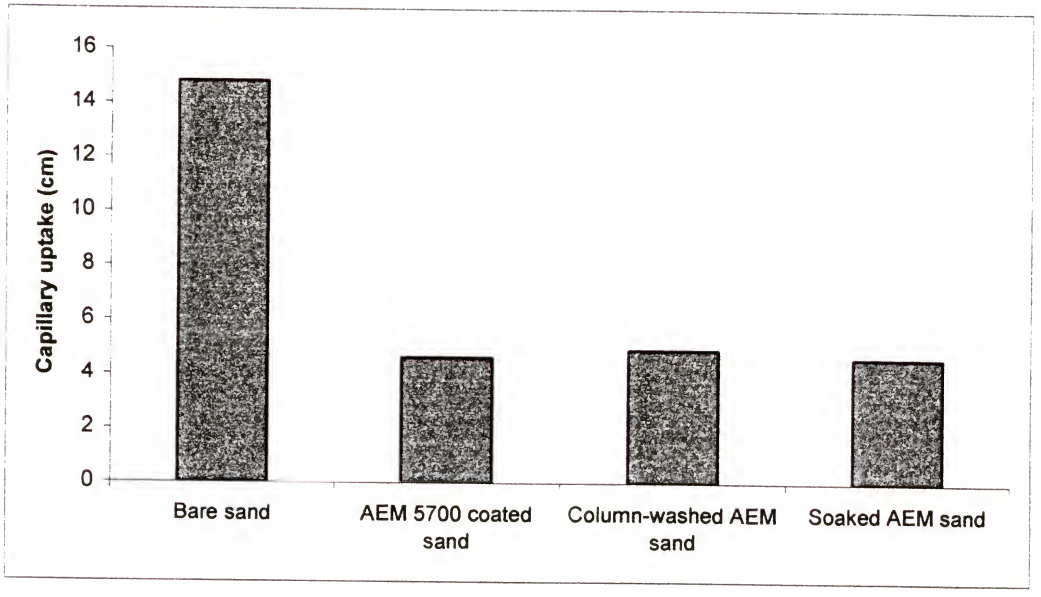

b)

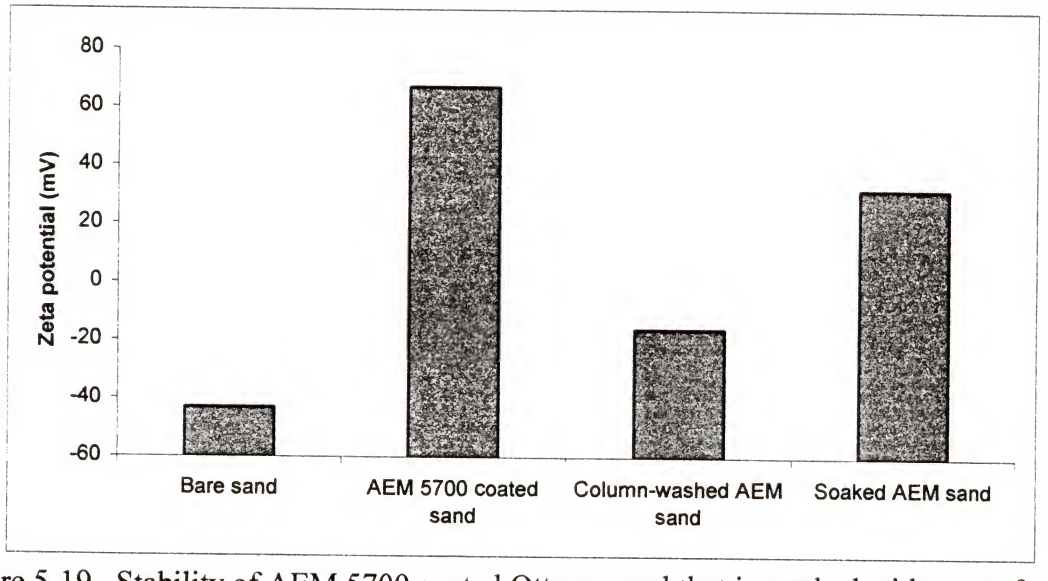

Figure 5-19. Stability of AEM 5700 coated Ottawa sand that is washed with water for one month in a column or soaked in water for two months: a) capillary uptake experiments show that the coated sand retains its hydrophobic behavior, while b) streaming potential measurements indicate the positive charge of the coated media is not retained.

The stability of metal hydroxide coatings was investigated by Chen (1998) and Chen et al. (1998) and found to be about 4 months. During this time the zeta potential

decreased from positive to negative, which correlated to deterioration in performance of the filter media. Electrokinetic measurements indicate that the zeta potential of AEM 5700 coated sand reverses much quicker than for metal hydroxide coated sand as shown in Figure 5-16. However, the coated media remained significantly more hydrophobic than uncoated media for the duration of the experiments, as seen in Figure 5-19, which compares the capillary uptake to zeta potential for AEM 5700 coated sand that has been washed.

5-6 Numerical Methods

Since an analytical solution to equations (3-18a-e) is not readily available, a numerical solution was sought to reduce the differential equations to algebraic ones. An implicit finite difference scheme known as the Crank-Nicolson method was used to simplify the calculation procedure without introducing large error terms. The calculation domain typically contained 10,000 by 10,000 calculation nodes. By using the Crank-Nicolson scheme, calculations were made for all positions of y at a single x position, based on the results from the previous x position, i.e. calculations were swept across the x-direction. The development of this convenient calculation scheme is discussed below, and more details can be found in Hoffman (1989).

The Crank-Nicolson calculation scheme employs central differencing approximations in both independent variables. The x-direction was divided into intervals of $(\Delta x/2)$, and the y-direction was divided into intervals of (Δy). Nodes in the y-direction are denoted by i, which ranges from 1 to I, and nodes in the x-direction are denoted by n, which ranges from 1 to N. Central differencing equations were written for both variables at nodal positions of i and $n + \frac{1}{2}$ resulting in error terms on the order of $(\Delta x)^2$ and $(\Delta y)^2$.

The difference equations for derivatives with respect to y were approximated by averaging about n and n+1 to eliminate the n + ½ node from the equations. The resulting system of linear algebraic equations readily conformed into systems of tridiagonal equations, which were decomposed into upper and lower diagonal matrices to further simplify calculations.

CHAPTER 6
FILTRATION AND INACTIVATION OF MICROORGANISMS

Removing microbial and chemical contaminants from municipal water supplies is a major public health concern all over the world. A 1998 USA Today special report on the dangers of drinking water cites a Centers for Disease Control and Prevention (CDC) record stating that 408,000 people became sick between 1993 and 1996 due to 52 confirmed waterborne illness outbreaks (Eisler, 1998). One of the outbreaks in 1993 was linked to 111 deaths and 403,000 illnesses in the Milwaukee area (Eisler, 1998). The article also cites a joint report from the Medical College of Wisconsin and the U.S. Environmental Protection Agency (EPA) that suggests 7.1 million people experience nausea or diarrhea and that as many as 1,200 people die each year in the U.S. from contaminated water (Eisler, 1998). While accurately confirming the statistics of illnesses and fatalities due to inadequately treated municipal water supplies is virtually impossible, the need for improved processes to provide clean, safe drinking water is clear.

Water treatment plants use a variety of methods, including chemical treatment and deep-bed filtration, to treat water (J. M. Montgomery, Inc., 1985). A number of investigations have been performed to improve the ability of packed-bed filters to remove microorganisms (Brown et al., 1974; Lukasik et al., 1996 and 1999; Chen, 1998; Truesdail, 1998a; Scott, 2000; Shaw et al., 2000). Granular filter media has been coated with peroxides (Scott, 2000), metal oxides (Lukasik et al., 1996 and 1999; Chen, 1998; Truesdail, 1998a; Scott, 2000; Shaw et al., 2000) and organosilicates (Fuchs, 1987) to

successfully enhance the adsorption or inactivation of a variety of microorganisms including protozoa, bacteria and viruses. For instance, Lukasik et al. (1996 and 1999) showed that virus removal rates were greater than 99% in columns packed with ferric and aluminum hydroxide coated sand, as compared to less than 30% removals in columns packed with uncoated sand. Here, the ability to enhance the removal of bacteria and viruses in column filtration and batch inactivation experiments was investigated for media coated with ferric and aluminum hydroxides and with quaternary ammonium siloxanes.

6-1 Materials Used for Microbe Adsorption Studies

Ferric and aluminum hydroxides were precipitated onto granular Ottawa sand and grade 1 diatomaceous earth (Sigma Chemicals Co., St. Louis, MO), and octadecyldimethyl(3-trimethoxysilyl-propyl)ammonium chloride (AEM 5700) was coated onto granular Ottawa sand and colloidal silica to investigate the ability of different coatings and media to adsorb or inactivate E. coli, MS-2 and PRD-1. Before coating, Ottawa sand was sieved to about 0.6-0.7 mm, which is a typical size used in large-scale municipal and industrial water filters (J. M. Montgomery, Inc., 1985). Granular activated carbon was taken directly from a CGAC Series U.S. Filter brand cartridge, sieved to remove fines and packed in columns for direct comparison to coated and uncoated sand-packed columns. Activated carbon was chosen as a control filter media because it is a standard component of point-of-use filtration systems (e.g., household faucet filters and water pitchers), which are becoming increasingly popular due to concern over microbiological qualities of water delivered by municipal utilities. Phages were assayed as plaque forming units (PFU) using agar overlay procedure: MS-2 (ATCC 15597-B1)

was assayed with Escherichia coli C-300 (ATCC 15597) as a host, and PRD-1 was assayed using Salmonella typhimurium (ATC 19585) (Scott, 2000). Escherichia coli (ATC 13706) was assayed as colony forming units (CFU) using a spread plate technique on MacConkey Agar (Scott, 2000).

6-2 Batch Inactivation of Bacteria and Viruses

Batch studies were carried out in which solutions of coated and uncoated colloidal and granular particles were charged with microorganisms, agitated and assayed for microbial activity. Ottawa sand that was unmodified, precipitated with ferric and aluminum hydroxides (as described in 5-4-1) or coated with AEM 5700 (5-4-2.2), spherical glass beads that were unmodified, coated with AEM 5700 or coated with PMS-CMS-nn-dimethyoctylamine (5-4-2.1), diatomaceous earth coated with ferric and aluminum hydroxides, and 1.5 μm-diameter silica that was unmodified or coated with AEM 5700 were each individually studied for their ability adsorb and/or inactivate MS-2 or E. coli. The particles were added to 10 ml of deionized water in a 50 ml centrifuge tube, and, for the case of colloidal silica, were gently sonicated in a water bath for 30 minutes to facilitate dispersion. The 10 ml of buffer, consisting of 0.02 M imidizole and 0.02 M glycine, were seeded with 10 μl of concentrated MS-2 or E. coli, and the solution was assayed to obtain original microbe counts. Then the microbe solution was added to the centrifuge tubes containing the granular or colloidal particles. The centrifuge tubes were mounted on a rocking shaker and agitated for 45-60 minutes. After agitation, silica solutions were settled by low-speed (1000 rpm) centrifugation for 5 minutes, and granular media was simply allowed to settle by gravity. The settled solutions were decanted, the supernatant was assayed for viable microbe counts. The number of

microbes in the supernatent, relative to the number originally added to the granular or colloidal particle solution, gave an indication of the number of viruses either inactivated or adsorbed to the particles. However, this assay could not distinguish whether the microbes were killed or simply adsorbed to the solids. Therefore, a 5 % beef extract solution was added to the solids in an attempt to elute any adsorbed microbes. The beef extract-particle mixtures were agitated for 10 minutes, and the supernatant was again assayed for viable microbes to determine if microorganisms may have been adsorbed but not inactivated. In addition, a mixture of deionized water and AEM 5700 coated silica solution, which was free of microorganisms, was agitated, and the supernatant was tested for its antimicrobial activity in a manner analogous to that described above.

Sand that was coated with metal hydroxides and AEM 5700, silica that was coated with AEM 5700 and diatomaceous earth that was coated with metal hydroxides all showed significant increase of MS-2 inactivation compared to controls, as seen in Figure 6-1. However, Figure 6-2 shows that AEM 5700 and metal hydroxide coated sand were not as effective in improving the inactivation of E. coli, but smaller particles (diatomaceous earth and silica) were able to significantly improve the inactivation of E. coli coated with either metal hydroxides or AEM 5700, respectively. Curiously, coated and uncoated spherical glass particles inactivated less MS-2 and E. coli than virtually any other media. The effect of substrate in creating a suitable antimicrobial surface seems to be significant but not well understood. Tables 6-1 and 6-2 illustrate that beef extract solutions were unable to elute significant numbers of MS-2 or E. coli from metal hydroxide or siloxane modified media, indicating that microbes were likely inactivated instead of simply adsorbed. The AEM 5700 supernatant control showed no antimicrobial

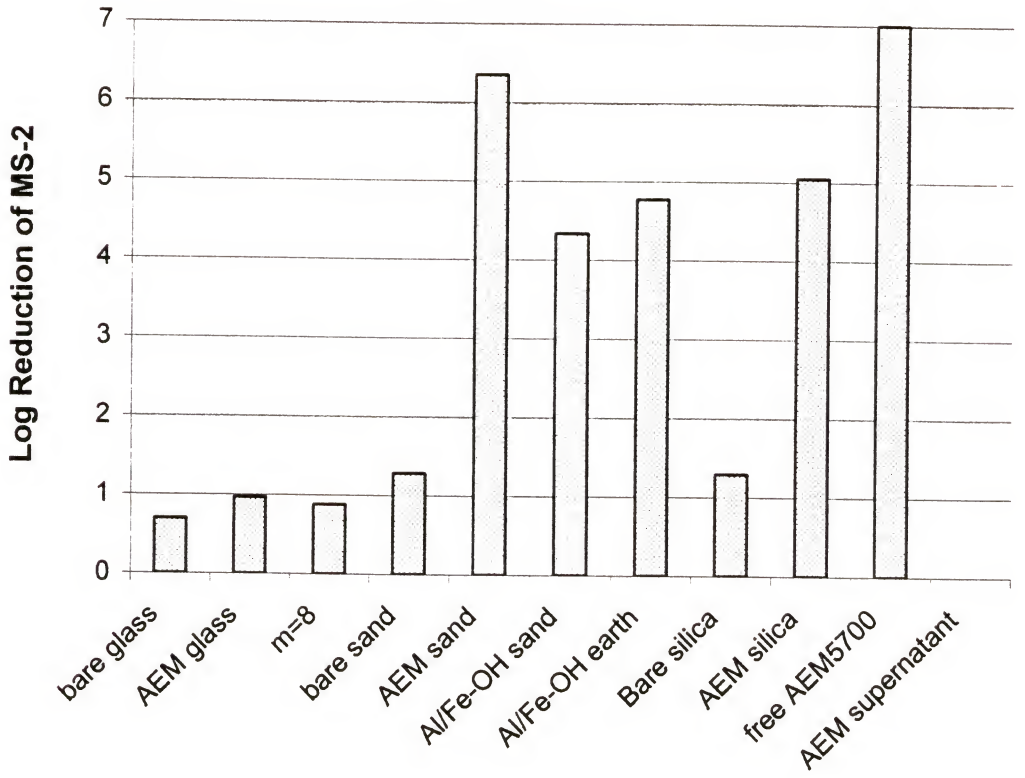

Figure 6-1. Batch inactivation of MS-2 by colloidal and granular particles. Metal hydroxide and AEM 5700 coated materials outperform uncoated media except in the case of coated glass beads. The last two items represent controls of unbound AEM 5700 added to MS-2 and rinsate of AEM 5700 coated particles, respectively.

activity, indicating that the siloxane was not leached from the surface, which was in keeping with previous studies (Clarkson and Evans, 1993; Isquith et al., 1972). Also, the unbound AEM 5700 that was combined with the microbes reveal that the quaternary ammonium siloxane itself has strong antimicrobial activity. The batch inactivation studies suggest that both the quaternary ammonium siloxane AEM 5700 and the mixture

of ferric and aluminum hydroxide are promising as coatings for promoting the filtration of bacteria and viruses.

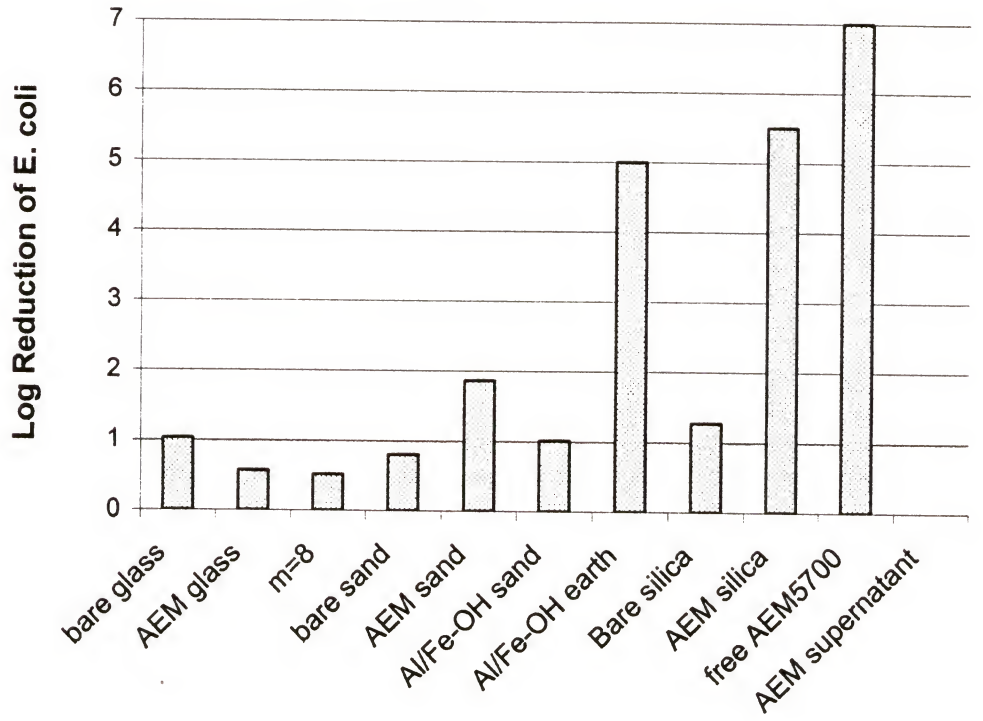

Figure 6-2. Batch inactivation of E. coli by colloidal and granular particles. Metal hydroxide coated diatemaceous earth and AEM 5700 coated silica and sand outperformed uncoated media. The last two items represent controls of unbound AEM 5700 added to E.coli and rinsate of AEM 5700 coated particles, respectively.

Table 6-1. Inactivation and subsequent elution of E. coli in batch tests.

Media	Initial Concentration (cfu/ml)	Supernatant Concentration	Eluant Concentration
AEM Coated Sand	$3.6x10^6$	$2.9x10^4$	$2.0x10^4$
Control Sand	$3.6x10^6$	$7.2x10^6$	None detected
AEM Coated Silica	$3.6x10^6$	None detected	None detected
Control Silica	$3.6x10^6$	$2.7x10^6$	$9.0x10^5$
Metal hydroxide diatomaceous earth	$6.1x10^5$	$2.4x10^2$	-
No particles*	$4.8x10^7$	$5.1x10^7$	-
AEM only**	$5.6x10^8$	-	-

* This represents the control group in which only the supernatnat from coated silica solution was charged with E. Coli.
** This control was for E. coli added to free AEM 5700.

Table 6-2. Inactivation and subsequent elution of MS-2 in batch tests.

Media	Initial Concentration (pfu/ml)	Supernatant Concentration	Eluant Concentration
Coated Sand	$2.9x10^8$	None detected	None detected
Control Sand	$2.9x10^8$	$2.5x10^5$	$2.2x10^5$
Coated Silica	$2.9x10^8$	$8.2x10^3$	$3.0x10^2$
Control Silica	$2.9x10^8$	$2.2x10^6$	$2.9x10^4$
Metal hydroxide diatomaceous earth	$7.1x10^7$	$1.2x10^3$	-
No particles*	$7.1x10^7$	$9.5x10^7$	-
AEM only**	$2.9x10^8$	-	-

* This represents the control group in which only the supernatnat from coated silica solution was charged with MS-2.
** This control was for E. coli added to free AEM 5700.

6-3 Column Filtration of Viruses

Four identical filtration columns, as described in 5-1, were filled with either Ottawa sand, AEM 5700 coated Ottawa sand, activated carbon or metal hydroxide coated Ottawa sand. Viral solutions were passed top-to-bottom through the columns at a superficial velocity of about 1 mm/s, which is typical of industrial and other water

treatment processes. The same stock solution was fed to all four columns. Pressure drops were measured in each of the four columns using a mercury manometer. Samples were taken for assay from the inlet and from the exit of each column periodically for about two hours or about 70 pore volumes, ensuring steady-state conditions. Virus removals for each column and organism were determined by viral assays, and corresponding filter coefficients are reported in Figure 6-3. Metal hydroxide coated sand was found to remove 52 $\pm$ 7% and 46 $\pm$ 9% of MS-2 and PRD-1, respectively, whereas unmodified sand columns were seen to remove –3 $\pm$ 4% and 6 $\pm$ 9%, respectively. A two-factor analysis of variance revealed a significant difference ($\alpha = 0.05$) in percent removals between different sand columns. Tukey's test was performed with $\alpha = 0.05$ to directly compare the percent removals of pairs of columns. Metal hydroxide coated

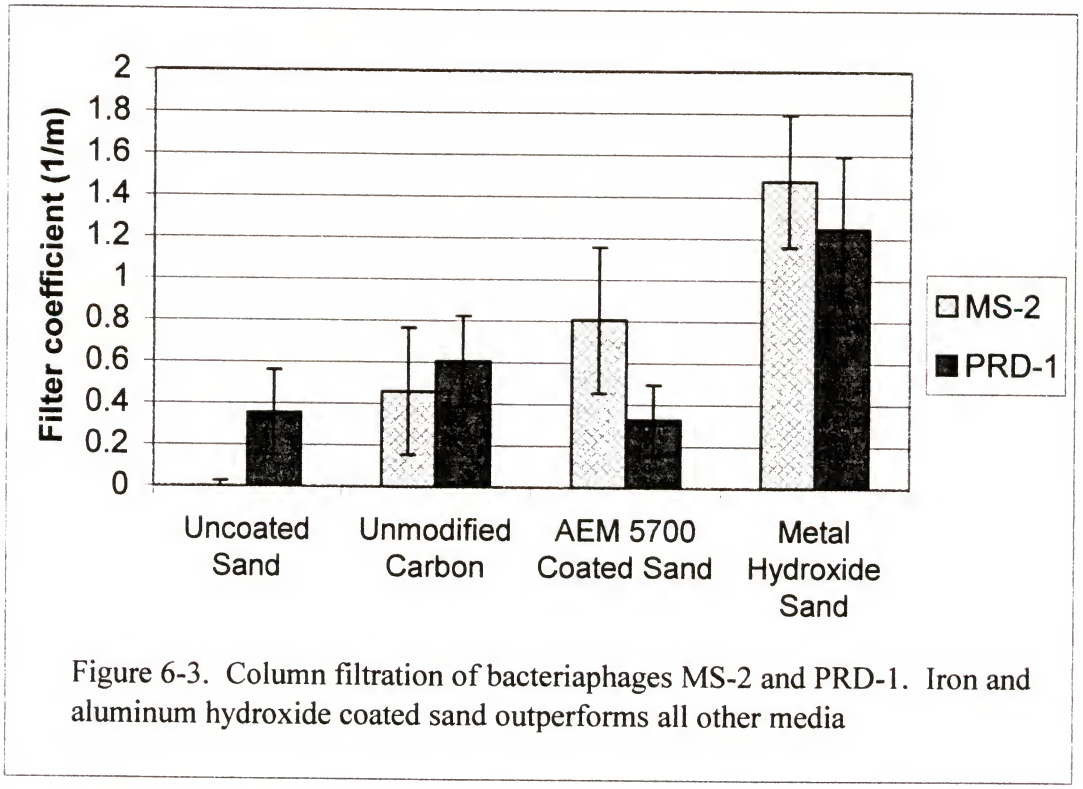

Figure 6-3. Column filtration of bacteriaphages MS-2 and PRD-1. Iron and aluminum hydroxide coated sand outperforms all other media

Ottawa sand removed more MS-2 and PRD-1 than both activated carbon and uncoated Ottawa sand and more PRD-1 than activated carbon and AEM5700 coated Ottawa sand. AEM5700 coated sand removed significantly more MS-2 than unmodified sand but not significantly more PRD-1, nor did AEM 5700 coated columns remove more viruses than activated carbon columns. The mediocre performance of AEM 5700 coated filter media is in contrast to its excellent performance in batch tests. One possible explanation for this discrepancy may be that the decline in positive zeta potential results in an electrostatic barrier between viruses and coated media. Another explanation is that the hydrophobic nature of the siloxane-coated media may affect the transport of the solution, perhaps resulting in fluid entrainment in the column.

6-4 Economic Feasibility of Metal Hydroxide Coated Filter Media

The chemical costs of coating filter media with iron aluminum hydroxides were estimated based on observed chemical requirements for coating media in the laboratory, together with costs of chemicals in bulk quantities (Table 6-3). The total coating cost for sand was 7.0 cents per kg, whereas the coating cost for activated carbon was 55 cents per kg. These costs were used in determining the added price to the consumer of water treated by coated filter media.

The lower of the mean percent removals (46% achieved with PRD1) was chosen to be representative of virus removals obtained by coated sand. Given this level of performance in a 0.5 m deep column, a corresponding removal of 70% may be expected in a 1.0 m deep column based on first-order removal (Tien, 1989). The cost of coating filter media to achieve this removal can be based on a unit cross-sectional area of 1.0 m^2

(normal to the downward flow direction of the water being treated). The chemical cost to coat the media contained in this unit area would be $120.57 (Table 6-4). The volume of water treated in 1 month by this unit area, based on a superficial velocity of 1.4 mm/s [2 gal/(ft^2 min)] and a 5% loss for backwashing, would be 3498 m^3. The unit chemical cost for water treatment with coated media is thus computed to be 3.4 cents per cubic meter. This compares to a typical delivered water price in U.S. municipal systems of 40 cents per cubic meter.

The cost of water treatment by a conventional household faucet filter as compared to the chemical cost of coating the activated carbon in such a filter is determined in Table 6-5. Based on a retail cost of $10 per filter, a lifetime of 1 month, and a daily throughput of 8 L, the unit cost of water treated by a faucet filter was estimated to be 4.1 cents per liter. Coating the activated carbon contained in one faucet filter would require 2.9 cents worth of chemicals, amounting to an additional cost of 0.01 cents per liter.

Table 6-3. Chemical costs of coating sand and activated carbon

		$FeCl_3 \cdot 6H_2O$	**$AlCl_3 \cdot 6H_2O$**	**NH_4OH[a]**	**Total**
Bulk chemical cost[b]		$0.33/kg	$1.76/kg	$0.25/kg	--
Amount used to coat 1 kg media	Sand	16.9 g	30.2 g	45 g	--
	Activated carbon	135 g	231 g	346 g	--
Cost in cents per kg media	Sand	0.5	5.3	1.2	7.0
	Activated carbon	4.4	41	9.5	55

[a]28-30% as NH_3 with a specific gravity of approximately 0.9

[b]Chemical Market Reporter (2001)

Table 6-4. Cost of using coated sand for municipal/industrial filtration

Filter coefficient	1.2 m^{-1}
Bed depth	1.0 m
Initial virus removal	70%
Porosity	0.35
Bed cross-sectional area	1.0 m^2
Bed depth	1.0 m
Bed volume	1.0 m^3
Media weight*	1722.5 kg
Unit coating cost	$0.07/kg
Coating cost for 1.0 m^3 bed	$120.57
Superficial velocity	1.4 mm/s
Volume treated in 1 month	3498 m^3
Unit cost	3.4 cents/m^3
Typical U.S. delivered municipal water cost (conventional filter media)	40 cents/m^3

*Specific gravity of sand = 2.65

The estimated chemical costs for coating sand and activated carbon, when expressed relative to the volume of water treated, are low relative to typical consumer costs for water. The chemical costs of coating would add approximately 10% to the cost of water delivered by municipal systems, whereas coating chemical costs would add less than 1% to the cost of water treated by faucet filters. It is thus clear that the improvement in virus removal performance gained by use of coated filter media provides a significant benefit

to the consumer in terms of increased microbiological quality at a negligible-to-modest increase in cost.

Table 6-5. Cost of using coated activated carbon in faucet filters

Media weight per filter	52 g
Initial virus removal	98%
Unit coating cost	$0.55/kg
Coating cost for 1 filter	2.9 cents
Daily water consumption	8 L
Volume treated in 1 month	243.5 L
Typical retail cost of conventional faucet filter	$10
Water cost for conventional faucet filter (assuming change-out after 1 month)	4.1 cents/L
Additional chemical cost for using coated media in faucet filter	0.01 cents/L

REFERENCE LIST

Adamczyk, Z., Dabros, T., Czarnecki, J., & van de Ven, T. G. M. (1983). Particle Transfer to Solid Surfaces. Advances in Colloid and Interface Science, 19, 183-252.

Adamczyk, Z., Siwek, B., Zembala, M., & Warszynski, P. (1989). Enhanced Deposition of Particles under Attractive Double-Layer Forces. Journal of Colloid and Interface Science, 130(2), 578-587.

Adamczyk, Z., & van de Ven, T. G. M. (1981). Deposition of Particles under External Forces in Laminar Flow through Parallel-Plate and Cylindrical Channels. Journal of Colloid and Interface Science, 80(2), 340-356.

Adamczyk, Z., Zembala, M., Siwek, B., & Czarnecki, J. (1986). Kinetics of Latex Particle Deposition from Flowing Suspensions. Journal of Colloid and Interface Science, 110(1), 188-200.

Adamson, A. W. (1990). Physical Chemistry of Surfaces (5th ed.). New York: John Wiley & Sons.

Alberty, R. A., & Silbey, R. J. (1995). Physical Chemistry (1st ed.). New York: John Wiley & Sons.

Bell, G. I., Dembo, M., & Bongrand, P. (1984). Cell Adhesion Competition between Nonspecific Repulsion and Specific Bonding. Biophysical Journal, 45, 1051-1064.

Bird, R. B., Stewart, W. E., & Lightfoot, E. N. (1960). Transport Phenomena. New York: John Wiley & Sons.

Bowen, B. D., & Epstein, N. (1979). Fine Particle Deposition in Smooth Parallel-Plate Channels. Journal of Colloid and Interface Science, 72(1), 81-97.

Brenner, H. (1961). The slow motion of a sphere through viscous fluid towards a plane surface. Chemical Engineering Science, 16, 242-251.

Brown, T. S., Malina, J. F., & Moore, B. D. (1974). Virus removal by diatomaceous earth filtration, part 1. Journal of the American Water Works Association, 66, 98-102.

Chandrasekhar, S. (1943). Stochastic Problems in Physics and Astronomy. Reviews of Modern Physics, 15(1).

Chang, Y.-I., & Whang, J.-J. (1997). Theoretical Simulation of the Collection Efficiencies of Brownian Particles. Colloids and Surfaces A: Physicochemical and Engineering Aspects, 125, 137-148.

Chang, Y.-I., & Whang, J.-J. (1998). Deposition of Brownian Particles in the Presence of Energy Barriers of DLVO Theory: Effect of the Dimensionless Groups. Chemical Engineering Science, 53(23), 3923-3939.

Chari, K., & Rajagopalan, R. (1985). Deposition of Colloidal Particles in Stagnation-point Flow. Journal of the Chemical Society. Faraday Transactions II, 81, 1345-1366.

Chen, J. (1998). Aging of metallic hydroxide-coated sand in particle filtration. Unpublished doctoral dissertation, University of Florida, Gainesville, FL.

Chen, J., Truesdail, S., Lu, F., Zhan, G., Belvin, C., Koopman, B., Farrah, S., & Shah, D. (1998). Long-term evaluation of aluminum hydroxide-coated sand for removal of bacteria from wastewater. Wat. Res., 32(7), 2171-2179.

Claesson, P. M., & Christenson, H. K. (1988). Very Long Range Attractive Forces between Uncharged Hydrocarbon and Fluorocarbon Surfaces in Water. J. Phys. Chem., 92, 1650-1655.

Clapp, A. R., & Dickinson, R. B. (2001). Direct Measurement of Static and Dynamic Forces between a Colloidal Particle and a Flat Surface Using a Single-Beam Gradient Optical Trap and Evanescent Wave Light Scattering. Langmuir, 17(7), 2182-2191.

Clarkson, N., & Evans, L. V. (1993). Evaluation of a potential non-leaching biocide using the marine fouling diatom amphora coffeaeformis. Biofouling, 7, 187-195.

Czarnecki, J., & Warszynski, P. (1987). The Evaluation of Tangential Forces Due to Surface Inhomogeneties in the Particle Deposition Process. Colloids and Surfaces, 22, 207-214.

Dabros, T., & van de Ven, T. G. M. (1982). Kinetics of Coating by Colloidal Particles. Journal of Colloid and Interface Science, 89(1), 232-244.

Dabros, T., & van de Ven, T. G. M. (1983). A Direct Method for Studying Particle Deposition onto Solid Surfaces. Colloid and Polymer Science, 261, 694-707.

Derjaguin, B. V., & Landau, L. D. (1941). Theory of the Stability of Strongly Charged Lyophobic Sols and the Adhesion of Strongly Charged Particles in Solutions of Electrolyte. Acta Physicochim URSS, 14, 733-.

Dickinson, R. B. (1997). A Dynamic Model for the Attachment of a Brownian Particle Mediated by Discrete Macromolecular Bonds. Journal of Colloid and Interface Science, 190, 142-151.

Ducker, W. A., Zhenghe, X., & Israelachvili, J. N. (1994). Measurements of Hydrophobic and DLVO Forces in Bubble-Surface Interactions in Aqueous Solutions. Langmuir, 10(9), 3279-3289.

Einstein, A. (1920). Investigations on the Theory of the Brownian Movement. New York, NY: E. P. Dutton and Company.

Eisler, P., Hansen, B., & Davis, A. (1998 October). Studies suggest millions of Americans could get sick each year. USA Today, pp. 15-24.

Elimelech, M. (1991). Kinetics of Capture of Colloidal Particles in Packed Beds under Attractive Double Layer Interactions. Journal of Colloid and Interface Science, 146(2), 337-352.

Elimelech, M. (1994). Effect of Particle Size on the Kinetics of Particle Deposition under Attractive Double Layer Interactions. Journal of Colloid and Interface Science, 164, 190-199.

Elimelech, M., Gregory, J., Jia, X., & Williams, R. (1995). Particle Deposition and Aggregation: Measurement, Modelling and Simulation. Oxford: Butterworth-Heinemann Ltd.

Farrah, S. R., Shah, D. O., & Ingram, L. O. (1981). Effects of Chaotropic and Antichaotropic Agents on Elution of Poliovirus Adsorbed on Membrane Filters. Proc. Natl. Acad. Sci. USA, 78(2), 1229-1232.

FitzPatrick, J. A. (1972). Mechanisms of Particle Capture in Water Filtration. Unpublished doctoral dissertation, Harvard University, Cambridge, Massachusetts.

Fitzpatrick, J. A., & Spielman, L. A. (1973). Filtration of Aqueous Latex Suspensions Through Beds of Glass Spheres. Journal of Colloid and Interface Science, 43(2), 350-369.

Frej, N. A., & Prieve, D. C. (1993). Hindred Diffusion of a Single Sphere Very Near a Wall in a Nonuniform Force Field. J. Chem. Phys., 98(9), 7552-7564.

Fuchs, A. E. (Inventor). (1987 July 28). I. H. H. N. Potters Industries (Assignee). Microbicidal Coated Beads. 4682992).

Goldman, A. J., Cox, R. G., & Brenner, H. (1967a). Slow viscous motion of a sphere parallel to a plane wall-I: Motion through a quiescent fluid. Chemical Engineering Science, 22, 637-651.

Goldman, A. J., Cox, R. G., & Brenner, H. (1967b). Slow viscous motion of a sphere parallel to a plane wall-II: Couette flow. Chemical Engineering Science, 22, 653-660.

Gregory, J. (1981). Approximate Expressions for Retarded van der Waals Interaction. Journal of Colloid and Interface Science, 83(1), 138-145.

Hamaker, H. C. (1937). The london-Van der Waals Attraction Between Spherical Particles. Physica IV, 10, 1058-1072.

Happel, J. (1958). Viscous Flow in Multiparticle Systems: Slow Motion of Fluids Relative to Beds of Spherical Particles. AIChE Journal, 4, 197-.

Happel, J., & Brenner, H. (1965). Low Reynolds Number Hydrodynamics. Englewood Cliffs, New Jersey: Prentice-Hall.

Hiemenez, P. C., & Rajagopalan, R.Principles of Colloid and Surface Chemistry. 3rd ed.,). New York, NY: Marcel Dekker.

Hoffman, K. A. (1989). Computational Fluid Dynamics for Engineers. Austin, Texas: Engineering Education System.

Hogg, R., Healy, T. W., & Fuerstenau, D. W. (1966). Mutual Coagulation of Colloidal Dispersions. Transactions of the Faraday Society, 62, 1638-1651.

Hull, M., & Kitchener, J. A. (1969). Interaction of Spherical Colloidal Particles with Planar Surfaces. Transactions of the Faraday Society, 65, 3093-3104.

Hunter, R. J. (1981). Zeta Potential in Colloid Science: Principles and Applications. New York: Academic Press Inc. (London) Inc.

Isquith, A. J., Abbott, E. A., & Walters, P. A. (1972). Surface-bonded antimicrobial activity of an organosilicon quaternary ammonium chloride. Applied Microbiology, 24(6), 859-863.

Israelachvili, J. N. (1992). Intermolecular & Surface Forces. London: Academic Press.

Israelachvili, J. N., & Adams, G. E. (1978). Measurement of Forces between Two Mica Surfaces in Aqueous Electrolyte Solutions in the Range 0-100 nm. Journal of the Chemical Society. Faraday Transactions I, 74, 975-1001.

J. M. Montgomery, Inc. (1985). Water Treatment Principles & Design. New York: John Wiley & Sons.

Kokkoli, E. (1998). Mapping Interactions Between Micropatterned Hydrophobic and Hydrophilic Surfaces by Atomic Force Microscopy. Unpublished doctoral dissertation, University of Illinois at Urbana-Champaign, Urbana, Illinois.

Kuwabara, S. (1959). The Force Experienced by Randomly Distributed Parallel Circular Cylinders or Spheres in a Viscous Flow at Small Reynolds Numbers. J Physics Soc. Japan, 14, 527-.

Levich, V. G. (1962). Physicochemical Hydrodynamics. Englewood Cliffs, NJ: Prentice-Hall.

Li, Y. (1998). Effective Medium Approximation and Deposition of Colloidal Particles In Fibrous and Granular Media. Unpublished doctoral dissertation, University of Florida.

Li, Y., & Park, C.-W. (2000). Effective Medium Approximation and Deposition of Colloidal Particles in Fibrous and Granular Media. Advances in Colloid and Interface Science, 87, 1-74.

Lukasik, J. (1998). The removal of microbial and chemical contaminants from aqueous solutions by particles coated with iron and aluminum hyroxy(oxides). Unpublished doctoral dissertation, University of Florida, Gainesville, FL.

Lukasik, J., Truesdail, S., Shah, D. O., & Farrah, S. R. (1996). Adsorption of microorganisms to sand and diatomaceous earth particles coated with metallic hydroxides. Kona Particle and Powder, 14, 87-91.

Lukasik, J., Cheng, Y.-F., Lu, F., Tamplin, M., & Farrah, S. R. (1999). Removal of Microorganisms from Water by Columns Containing Sand Coated with Ferric and Aluminum Hydroxides. Wat. Res., 33(3), 769-777.

Luthi, Y., Ricka, J., & Borkovec, M. (1998). Colloidal Particles at Water-Glass Interface: Deposition Kinetics and Surface Heterogeneity. Journal of Colloid and Interface Science, 206(314-321).

Marshall, J. K., & Kitchener, J. A. (1966). The Deposition of Colloid Particles on Smooth Slides. Journal of Colloid and Interface Science, 22, 342-351.

Meagher, L. (1992). Direct Measurement of Forces between Silica Surfaces in Aqueous $CaCl_2$ Solutions Using an Atomic Force Microscope. Journal of Colloid and Interface Science, 152, 293-295.

Meinders, J. M., & Busscher, H. J. (1993). Influence of ionic strength and shear rate on the desorption of polystyrene particles from a glass collector as studied in a parallel-plate flow chamber. Colloids and Surfaces A: Physicochemical and Engineering Aspects, 80, 279-285.

Meinders, J. M., Busscher, H. J., & Noordmans, J. (1992). Simultaneous Monitoring of the Adsorption and Desorption of Colloidal Particles during Deposition in a Parallel Plate Flow Chamber. Journal of Colloid and Interface Science, 152(1), 265-280.

Prieve, D. C., & Ruckenstein, E. (1976). Rates of Deposition of Brownian Particles Calculated by Lumping Interaction Forces into a Boundary Condition. Journal of Colloid and Interface Science, 57(3), 547-550.

Rabinovich, Ya. I., & Yoon, R.-H. (1994). Use of atomic force microscope for the measurement of hydrophobic forces. Colloids and Surfaces A: Physicochemical and Engineering Aspects, 93, 263-273.

Rajagopalan, R., & Kim, J. S. (1981). Adsorption of Brownian Particles in the Presence of Potential Barriers: Effect of Different Modes of Double-Layer Interaction. Journal of Colloid and Interface Science, 83(2), 428-448.

Ruckenstein, E., & Prieve, D. C. (1973). Rate of Deposition of Brownian Particles under the Action of London and Double-layer Forces. Journal of the Chemical Society. Faraday Transactions II, 69, 1522-1536.

Russel, W. B., Saville, D. A., & Schowalter, W. R. (1989). Colloidal Dispersions. New York, NY: Cambridge University Press.

Ruta, A. G. (1998). Quantitative Study of Mechanisms of Bacterial Adhesion to Surfaces. Unpublished doctoral dissertation, University of Florida.

Scott, T. M. (2000). Removal and recovery of microbial and chemical contaminants from water. Unpublished doctoral dissertation, University of Florida, Gainesville, FL.

Scott, T. M., Sabo, R. C., Lukasik, J., Boice, C., Shaw, K., Barroso-Giachetti, L., El-Shall, H., Farrah, S. R., Park, C., Moudgil, B., & Koopman, B. (2001). Performance and Cost-Effectiveness of Ferric and Aluminum Hydrous Metal Oxide Coating on Filter Media to Enhance Virus Removal. KONA.

Shapiro, M., Brenner, H., & Guell, D. C. (1990). Accumulation and Transport of Brownian Particles at Solid Surfaces: Aerosol and Hydrosol Deposition Processes. Journal of Colloid and Interface Science, 136(2), 552-573.

Shaw, K., Walker, S., & Koopman, B. (2000). Improving Filtration of Cryptosporidium. Journal AWWA, 103-111.

Shaw, K., Walker, S., & Koopman, B. (2000). Improving filtration of Cryptosporidium. Journal AWWA, 103-111.

Sjollema, J., & Busscher, H. J. (1989). Deposition of Polystyrene Latex Particles toward Polymethylmethacrylate in a Parallel Plate Flow Cell. Journal of Colloid and Interface Science, 132(2), 382-394.

Sjollema, J., & Busscher, H. J. (1990). Deposition of Polystyrene Particles in a Parallel Plate Flow Cell. 1. The Influence of Collector Surface Properties on the Experimental Deposition Rate. Colloids and Surfaces, 47, 323-336.

Sjollema, J., & Busscher, H. J. (1990). Deposition of Polystyrene Particles in a Parallel Plate Flow Cell. 2. Pair Distribution Functions Between Deposited Particles. Colloids and Surfaces, 47, 337-352.

Song, L., Johnson, P. R., & Elimelech, M. (1994). Kinetics of Colloid Deposition onto Heterogeneously Charged Surfaces in Porous Media. Evironmental Science Technology, 28, 1164-1171.

Spielman, L. A. (1977). Particle Capture From Low-Speed Laminar Flows. Ann. Rev. Fluid Mech., 9, 297-319.

Spielman, L. A., & Friedlander, S. K. (1974). Role of the Electrical Double Layer in Particle Deposition by Convective Diffusion. Journal of Colloid and Interface Science, 46(1), 22-31.

Suhara, T., Kanemaru, T., Fukui, H., & Yamaguchi, M. (1995). Fine silica powder modified with quaternary ammonium groups: reactivity and characteristics. Colloids and Surfaces A: Physicochemical and Engineering Aspects, 95, 1-9.

Tien, C. (1989). Granular Filtration of Aerosols and Hydrosols. Boston, MA: Butterworth Publishers.

Tobiason, J. E. (1987). Physicochemical Aspects of Particle Deposition in Porous Media. Unpublished doctoral dissertation, The Johns Hopkins University, Baltimore, Maryland.

Tobiason, J. E., & O'Melia, C. R. (1988). Physicochemical Aspects of Particle Removal in Depth Filtration. American Water Works Association, 80, 54-64.

Truesdail, S. E. (1999). Fundamental Forces Important to the Enhancement of Biological Colloid Removal. Unpublished doctoral dissertation, University of Florida, Gainesville, FL.

Truesdail, S. E., Lukasik, J., Farrah, S. R., Shah, D. O., & Dickinson, R. B. (1998a). Analysis of Bacterial Deposition on Metal (Hydr)oxide-Coated Sand Filter Media. Journal of Colloid and Interface Science, 203, 369-378.

Truesdail, S., Westermann-Clark, G. B., & Shah, D. O. (1998b). Apparatus for Streaming Potential Measurements on Granular Filter Media. Journal of Environmental Engineering, 124(12), 1228-1231.

Vaidyanathan, R. (1986). Hydrosol Deposition in Granular Beds. Unpublished doctoral dissertation, Syracuse University, Syracuse, New York.

Vaidyanathan, R., & Tien, C. (1991). Hydrosol Deposition in Granular Media under Unfavorable Surface Conditions. Chemical Engineering Science, 46, 967-983.

van de Ven, T. G. M. (1989). Colloidal Hydrodynamics. San Diego, CA: Academic Press Inc.

van de Ven, T. G. M. (1998). The Capture of Colloidal Particles on Surfaces and in Porous Material: Basic Principles. Colloids and Surfaces A: Physicochemical and Engineering Aspects, 138, 207-216.

Van Wagenen, R. A., & Andrade, J. D. (1980). Flat Plate Streaming Potential Investigation: Hydrodynamics and Electrokinetic Equilavency. Journal of Colloid and Interface Science, 76(2), 305-314.

Verwey, E. J. W., & Overbeek, J. T. G. (1948). Theory of the Stability of Lyophobic Colloids. Amsterdam, Netherlands: Elsevier.

Wilson, K. (2000). The Sedimentation and Rheological Behavior of Colloidal Suspensions. Unpublished doctoral dissertation, University of Florida, Gainesville, FL.

BIOGRAPHICAL SKETCH

Ronald Charles Sabo, Jr. was born on September 16, 1975, to Rita Faye Ford and Ronald Charles Sabo in Tazewell, Tennessee, where he lived until 1981 when he moved to Houston, Texas, with his family. He comes from a supportive family of three siblings: Michael Dwayne Sabo, Sean Christopher Liles and Lori Denise Liles. Ronald spent much of his childhood in Houston until he moved back to Tennessee with his mother while in the eighth grade. For about a year and a half, he attended Halls High School, and the remainder of his high school education was obtained at Central High School in Harrison, Tennessee, where he graduated with highest honors. Ron spent the next four years at Vanderbilt University where he graduated magna cum laude with a Baccalaureate of Engineering in chemical engineering and mathematics in 1997. He then moved to Gainesville, Florida, to pursue a Doctor of Philosophy in chemical engineering from the University of Florida.

I certify that I have read this study and that in my opinion it conforms to acceptable standards of scholarly presentation and is fully adequate, in scope and quality, as a dissertation for the degree of Doctor of Philosophy.

Chang-Won Park, Chair
Professor of Chemical Engineering

I certify that I have read this study and that in my opinion it conforms to acceptable standards of scholarly presentation and is fully adequate, in scope and quality, as a dissertation for the degree of Doctor of Philosophy.

Richard B. Dickinson
Associate Professor of Chemical Engineering

I certify that I have read this study and that in my opinion it conforms to acceptable standards of scholarly presentation and is fully adequate, in scope and quality, as a dissertation for the degree of Doctor of Philosophy.

Spyros Svoronos
Professor of Chemical Engineering

I certify that I have read this study and that in my opinion it conforms to acceptable standards of scholarly presentation and is fully adequate, in scope and quality, as a dissertation for the degree of Doctor of Philosophy.

Ben Koopman
Professor of Environmental Engineering Sciences

This dissertation was submitted to the Graduate Faculty of the College of Engineering and to the Graduate School and was accepted as partial fulfillment of the requirements for the degree of Doctor of Philosophy.

December 2001

Pramod P. Khargonekar
Dean, College of Engineering

Winfred M. Phillips
Dean, Graduate School